NAVAL POSTGRADUATE SCHOOL
Monterey, California

THESIS

**HUMAN DISORIENTATION AS A FACTOR IN
SPACECRAFT CENTRIFUGE DESIGN**

By

Christopher E. Howse

September, 2002

Thesis Advisor: Stephen A. Whitmore
Second Reader: Sherif Michael

Approved for public release; distribution is unlimited.

THIS PAGE INTENTIONALLY LEFT BLANK

REPORT DOCUMENTATION PAGE		*Form Approved OMB No. 0704-0188*

Public reporting burden for this collection of information is estimated to average 1 hour per response, including the time for reviewing instruction, searching existing data sources, gathering and maintaining the data needed, and completing and reviewing the collection of information. Send comments regarding this burden estimate or any other aspect of this collection of information, including suggestions for reducing this burden, to Washington headquarters Services, Directorate for Information Operations and Reports, 1215 Jefferson Davis Highway, Suite 1204, Arlington, VA 22202-4302, and to the Office of Management and Budget, Paperwork Reduction Project (0704-0188) Washington DC 20503.

1. AGENCY USE ONLY *(Leave blank)*	2. REPORT DATE September 2002	3. REPORT TYPE AND DATES COVERED Master's Thesis	
4. TITLE AND SUBTITLE: Human Disorientation As A Factor In Spacecraft Centrifuge Design		5. FUNDING NUMBERS	
6. AUTHOR: LT Christopher E. Howse, USNR			
7. PERFORMING ORGANIZATION NAME(S) AND ADDRESS(ES) Naval Postgraduate School Monterey, CA 93943-5000		8. PERFORMING ORGANIZATION REPORT NUMBER	
9. SPONSORING / MONITORING AGENCY NAME(S) AND ADDRESS(ES) NASA Dryden Flight Research Center Edwards CA 93523		10. SPONSORING / MONITORING AGENCY REPORT NUMBER	

11. SUPPLEMENTARY NOTES The views expressed in this thesis are those of the author and do not reflect the official policy or position of the Department of Defense or the U.S. Government.

12a. DISTRIBUTION / AVAILABILITY STATEMENT Distribution Statement A. Approved for public release; distribution is unlimited.	12b. DISTRIBUTION CODE

13. ABSTRACT *(maximum 200 words)*

Weightlessness is the major contributing factor behind the degradation of bone mass, muscle tone, and aerobic capacity during long-term space missions. With the loss of bone mass progressing at up to two percent per month, long duration and interplanetary missions shall remain the sole duty of robotic explorers until sufficient countermeasures are developed.

Several countermeasures are either in use, or under development to alleviate this problem. Exercise is currently used to reduce the severity of bone loss and muscle atrophy. Exercise has proven ineffective despite the fact two hours of daily exercise together with elaborate apparatus have been devoted to simulating the load of Earth's gravity. Drug therapy and other, more exotic, countermeasures are also under consideration, but the side-effects of these other treatments and the fact that they do not directly address the root cause of the negative effects of weightlessness means that they may only reduce, not cure, those problems. Only artificial gravity addresses the root cause, weightlessness itself.

This thesis addresses the need to balance the effects of Coriolis on human disorientation with the engineering costs of constructing a centrifuge for human occupation in space.

14. SUBJECT TERMS: Artificial Gravity, Centrifuge Model, Centrifuge Simulator, Human Disorientation, Human Factors, Spacecraft Centrifuge, Vestibular Model, Vestibular Simulator			15. NUMBER OF PAGES 146
			16. PRICE CODE

17. SECURITY CLASSIFICATION OF REPORT Unclassified	18. SECURITY CLASSIFICATION OF THIS PAGE Unclassified	19. SECURITY CLASSIFICATION OF ABSTRACT Unclassified	20. LIMITATION OF ABSTRACT UL

NSN 7540-01-280-5500

Standard Form 298 (Rev. 2-89)
Prescribed by ANSI Std. 239-18

THIS PAGE INTENTIONALLY LEFT BLANK

HUMAN DISORIENTATION AS A FACTOR IN SPACECRAFT CENTRIFUGE DESIGN

Christopher E. Howse
Lieutenant, United States Naval Reserve
B.S., U.S. Merchant Marine Academy, 1994

Submitted in partial fulfillment of the
requirements for the degree of

MASTER OF SCIENCE IN SPACE SYSTEMS OPERATIONS

from the

NAVAL POSTGRADUATE SCHOOL
September, 2002

Author:

Christopher E. Howse

Approved by:

Dr. Stephen A. Whitmore, PhD, Thesis Advisor

Dr. Sherif Michael, PhD, Second Reader

Dr. Rudy Panholzer, PhD, Chairman
Space Systems Academic Group

THIS PAGE INTENTIONALLY LEFT BLANK

ABSTRACT

Weightlessness is the major contributing factor behind the degradation of bone mass, muscle tone, and aerobic capacity during long-term space missions. With the loss of bone mass progressing at up to two percent per month, long duration and interplanetary missions shall remain the sole duty of robotic explorers until sufficient countermeasures are developed.

Several countermeasures are either in use, or under development to alleviate this problem. Exercise is currently used to reduce the severity of bone loss and muscle atrophy. Exercise has proven ineffective despite the fact two hours of daily exercise together with elaborate apparatus have been devoted to simulating the load of Earth's gravity. Drug therapy and other, more exotic, countermeasures are also under consideration, but the side-effects of these other treatments and the fact that they do not directly address the root cause of the negative effects of weightlessness means that they may only reduce, not cure, those problems. Only artificial gravity addresses the root cause, weightlessness itself.

This thesis addresses the need to balance the effects of Coriolis on human disorientation with the engineering costs of constructing a centrifuge for human occupation in space.

THIS PAGE INTENTIONALLY LEFT BLANK

TABLE OF CONTENTS

LIST OF FIGURES

LIST OF TABLES

THIS PAGE INTENTIONALLY LEFT BLANK

ACKNOWLEDGMENTS

THIS PAGE INTENTIONALLY LEFT BLANK

I. INTRODUCTION

A. NEGATIVE EFFECTS OF LONG TERM SPACE FLIGHT

Long Term Space Flight carries with it numerous negative effects upon the human body. The micro-gravity environment experienced by astronauts in space imparts a weakening of muscles, bone structure, and a redistribution of bodily fluids. Effective countermeasures have been developed against fluid redistribution and muscular atrophy to mitigate their adverse effects upon the astronaut's return to Earth. However, effective countermeasures have not been developed to overcome the weakening of the body's bones in space as shown in Figure 1.[1]
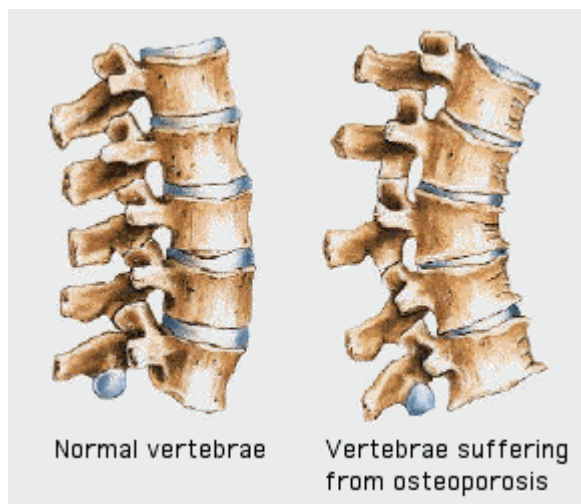
Figure 1: A Comparison of Normal Vertebrae and Vertebrae Effected By Osteoporosis[2]

1. Bone Loss Associated with Space Flight

As a result, bone loss is one of the greatest obstacles to Long Duration Manned Space Flight. Osteoporosis, a well-publicized disease that is normally associated with

---

[1] Julie Moberly, "Human Physiology Research and the ISS: Staying Fit Along the Journey," Space Research, March 2002, pp. 6-11 and 25

[2] Scott M. Smith, "Calcium Kinetics During Spaceflight," 19 April 2002, Nutritional Biochemistry Laboratory, NASA Johnson Space Center, http://www.jsc.nasa.gov/sa/sd/facility/labs/nutritionalbl/currentproj/cal_kin.htm

advanced age and menopause, occurs when the body's natural process of bone renewal, called remodeling, breaks down. Remodeling is effected by a complex interplay of many hormones, the pull of muscles, and gravity[3]. Although there are no documented cases of Osteoporosis caused by space flight, bone loss occurs at a significant rate in space:

> "When you remove gravitational loading, bones no longer sense the stresses and strains that are normally experienced here on Earth. As a result, astronauts are subjected to an accelerated rate of bone loss, losing between a half of 1 percent and 2 percent of their bone mass per month,"[4].

> "Weakening of the bones due to the progressive loss of bone mass is a potentially serious side-effect of extended spaceflight. Studies of cosmonauts and astronauts who spent many months on space station Mir revealed that space travelers can lose (on average) 1 to 2 percent of bone mass each month."[5]

Without some means of preventing or reducing space flight bone loss, astronauts on a theoretical two year mission to Mars could lose up to 24% of their bone mass.

2.   Methods to Counter Bone Loss During Space Flight

A complex interplay of physiology, exercise, and environment serve to maintain the body's fluid distribution, muscle tone, and bone mass. Because our bodies evolved on Earth, they are designed to resist the constant pull of gravity. In space our body's natural process of maintenance and repair works to expel fluids displaced by the absence of gravity, muscles atrophy from disuse, and the remodeling process slowly degrades bone mass due to the absence of gravity[6]. There are three basic means of counteracting the detrimental effects of space flight: exercise, drug therapy, and artificial gravity.

---

[3] "Boning Up on Osteoporosis", September 1996 (Revised September 2001), FDA Consumer, U.S. Food and Drug Administration, 25 June 2002, http://www.fda.gov/fdac/features/796_bone.html

[4] Ted Bateman, BioServe Space Technologies, Principal Investigator and Director of Biomedical Research, http://spaceresearch.nasa.gov/general_info/issphysiology.html

[5] Doug Hullander, Patrick L. Barry, "Space Bones," 1 Oct. 2001, Science@NASA, NASA Marshall Space Flight Center, 14 Sept. 2002, http://science.nasa.gov/headlines/y2001/ast01oct_1.htm

[6] Moberly

a. Exercise

Aerobic exercise can reduce the effect of some of the physiological problems associated with space flight. Astronauts receive individualized exercise prescriptions before and during their missions that are designed to maintain their aerobic capacity, bone density, and muscle mass as much as possible[7]. However, reducing the effects of muscle atrophy currently requires about two hours of exercise per day with the aid of 'exotic devices' to reproduce the effects of Earth's gravity. Unfortunately, exercise has proven ineffective as a countermeasure to bone and muscle loss[8].

Figure 2: An Astronaut Exercising on a Shuttle Treadmill.
Image courtesy of NASA Johnson Space Center[9]

b. Drug Therapy

The remodeling process manages the development and maintenance of bone health. In mature adults, the remodeling process maintains the structure of normal bone tissue (pictured in Figure 3) through an equilibrium between the activity of osteoblasts (bone forming cells) and osteoclasts (bone absorbing cells). In the astronauts

---

[7] Moberly, pp. 6 and 8

[8] Patrick L. Barry, "Good Vibrations," Science@NASA, 2 Nov. 2001, NASA Marshall Space Flight Center, 14 Sept. 2002, http://science.nasa.gov/headlines/y2001/ast02nov_1.htm

[9] Exercise In Space, 22 April 1998, Exercise Countermeasures Project, NASA Johnson Space Center, 14 Sept. 2002, http://www.jsc.nasa.gov/sa/sd/sd3/exl/spacephoto.htm

and the elderly, osteoblast activity is inhibited while osteoclast activity remains constant. The resulting loss in bone mass eventually leads to osteoporosis.[10]

Drug therapy could potentially reduce the amount of bone loss experienced by astronauts during space flight. Alendronate Sodium (Fosamax), for example, inhibits the resorption of bone by inhibiting osteoclast activity, reducing or potentially reversing the progression of osteoporosis. However, this drug is poorly absorbed following oral administration. It must be administered separately from other medications and cannot be administered with food or caffeine. It also increases the risk of GI problems if any Non-Steroidal Anti-inflammatory Drugs (NSAIDs) are used[11].
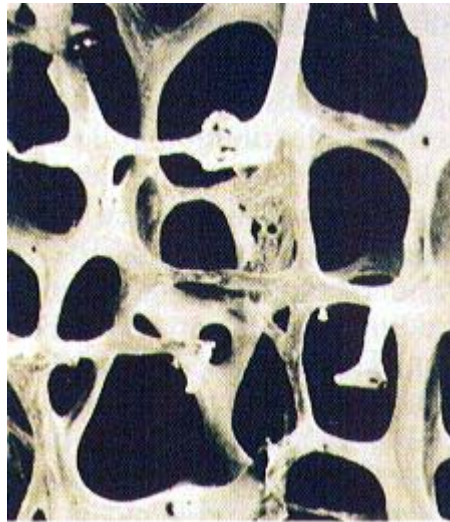
Figure 3: The Structure Of Normal Bone Tissue, Image Courtesy of NASA Quest[12]

In addition to Alendronate Sodium, there are several other drugs on the market that are used to treat Osteporosis. Risedronate (Actonel), like Alendronate Sodium, alters the remodeling process by inhibiting osteoclast activity, with a similar list of precautions and side effects.[13] Raloxifene (Evista) works like estrogen in post-

---

[10] Moberly, p. 10

[11] Judith H. Deglin, April H. Vallerand, Davis's Drug Guide for Nurses, 5th Ed., Philadelphia: F. A. Davis, 1997, pp. 21-23

[12] Barry

[13] "Risendronate," WebMD, 2 June 2000, Ver. 4.01, Multum Information Services, 14 Sept. 2002, http://my.webmd.com/content/article/4046.1450

menopausal women to prevent osteoporosis.[14] Finally, Calcitonin (Calcimar, Miacalcin) is a naturally occurring hormone that helps to regulate calcium levels and is involved in the bone building part of the remodeling process.[15]

Of the currently marketed drugs, only calcitonin would be useful to astronauts. Raloxifene is intended for women who choose not to take estrogen or other medications.[16] Alendornate Sodium and Risedronate is intended for patients that can remain upright for at least 30 minutes and then eat after taking the medication to prevent heartburn[17,18,19], (impossible in a micro-gravity environment).

In addition to the existing FDA approved osteoporosis drugs, research is ongoing with Osteoprotegerin, another naturally occurring protein that is involved in the remodeling process.

c.   *Other Countermeasures*

Other, more exotic, countermeasures are under development to reduce the effects of long-term space flight. One such countermeasure makes use of vibrating plates. Connecting an astronaut to a plate which is gently vibrating at 90 hz for 10 to 20 minutes may stimulate osteoblasts into generating new bone. Such vibrations have produced near normal bone formation rates in studies where animals were prevented from bearing weight in certain limbs. The control animals exhibited a 92% reduction in bone formation when not exposed to the vibrations and were prevented from bearing weight in the same limbs. Though promising, vibrating plates do not address the issues of muscle atrophy and degradation of aerobic capacity.[20,21]

---

[14] Kathleen M. Ariss, "Raloxifene for osteoporosis," WebMD, 2002, Healthwise Inc., 14 Sept. 2002, http://my.webmd.com/encyclopedia/article/1829.50935

[15] Ariss, "Calcitonin for osteoporosis," WebMD, 2002, Healthwise Inc., 14 Sept. 2002, http://my.webmd.com/encyclopedia/article/1829.50940

[16] Ariss, "Raloxifene for osteoporosis"

[17] Deglin, Vallerand, p. 23

[18] Ariss, "Alendronate for osteoporosis," WebMD, 2002, Healthwise Inc., 14 Sept. 2002, http://my.webmd.com/encyclopedia/article/1829.50937

[19] Ariss, "Risendronate for osteoporosis," WebMD, 2002, Healthwise Inc., 14 Sept. 2002, http://my.webmd.com/encyclopedia/article/1829.50935

[20] Barry

[21] "Astronaut osteoporosis," BBCi, 15 May 2002, British Broadcasting Corporation, 23 Sept. 2002, http://www.bbc.co.uk/science/tw/2002/may15osteoporosis.shtml

Another countermeasure that is under development is known as Lower Body Negative Pressure (LBNP). An LBNP device consists of a partial vacuum chamber that encompasses the legs, feet, and pelvis, which seals at the waist. A vacuum of 30 to 50 mmHg is pulled in the chamber resulting in a footward force, which through design, can be the equivalent of 1 G. Exercise equipment, such as a treadmill, can be incorporated within and around the LBNP device to allow an astronaut to exercise in the equivalent of a 1 G environment. Exposing the body to a vacuum carries with it the associated risks of petechiae (minute hemorrhages resulting from burst capillaries[22]), hernia, and syncope (brief unconsciousness). Furthermore, what are the medical risks of long term, daily exposure of the lower extremities to partial vacuum?

d. *Artificial Gravity*

Using a centrifuge to provide astronauts with artificial gravity in space goes to the root of the problem, weightlessness.[23] The Centrifugal Force provided by a rotating environment simulates the presence of gravity. This rotating environment provides the best means of stimulating the natural processes that maintain the body's fluid distribution, muscle tone, and bone mass. A 'normal' exercise routine could be enjoyed on 'normal' exercise equipment. A normal lifestyle could be enjoyed versus specialized astronaut food and sponge baths.

Additionally, research could be conducted on the long-term effects of 'fractional-G' on the human body. How much gravity is necessary for a person to maintain physical fitness and the reformation process? Would gravity exposure at scheduled times as part of the astronaut's daily routine be sufficient to maintain their health? Outside of drop-tubes and parabolic flight paths that simulate the microgravity environment for a few seconds, research into artificial gravity at levels of centrifugal force less than 1 G is not possible on Earth. The installation of a centrifuge aboard a spacecraft is the only means by which such research can be conducted.

---

[22] "Petechia," <u>The American Heritage Dictionary</u>, 2nd College Ed., Boston: Houghton-Mifflin Co., 1985, p. 927

[23] Hullander, Barry

B.   WHY MODEL A SPACE FLIGHT CENTRIFUGE?

Human beings are not designed to live in a rotating environment. A positive side effect of a rotating environment is known as a somatogravic illusion: a false-perception of attitude due to prolonged angular motion.[24] Through this illusion, an astronaut will not perceive the rotation of the centrifuge, only the force of its artificial gravity. However, when there is a change in angular velocity, or the astronaut changes his radial position, a "Coriolis Illusion" is generated that contains an element of rotation in the plane of the head movement.[25] The causes and effects of the "Coriolis Illusion" will be discussed in a later section.

The use of a centrifuge in space bears associated costs and risks. More to the point, can a centrifuge be constructed and put in space at a cost that would make its realization feasible? The engineering behind such a centrifuge is nothing new, the International Space Station (ISS) when finished will have a centrifuge as part of the Centrifuge Accommodation Module (CAM). The human factor, however, is not so well understood. In other words, what is the best balance between centrifuge size (cost) and an astronaut's ability to tolerate the rotational environment such a centrifuge would impose? Such costs and benefits must be weighed not only in dollars, but also in terms of health, time, and welfare of the astronauts it would benefit. For example, suppose that the ISS 3 man crew were able to gain 4.5 man-hours every day by reducing aerobic exercise requirements from 2 hours daily to 30 minutes daily[26] through the use of a centrifuge to maintain their health. What would that extra time be worth?

Construction of a centrifuge in space large enough for human occupation is currently in the realm of science fiction. The cost and risk inherent to space flight make such an endeavor too costly to consider in the near-term. However, a smaller centrifuge, being developed for the purpose of performing experiments with animal subjects is being

---

[24] John Ernsting, A.N. Nicholson, D.J. Rainford, Aviation Medicine, 3rd Ed., Oxford: Butterworth-Heinemann, 1999, p. 438

[25] Ernsting, Nicholson, Rainford, p. 434

[26] "ACSM Guidelines For Healthy Aerobic Activity," 11 Sept. 2000, American College of Sports Medicine, American College of Sports Medicine, 14 Sept. 2002, http://www.ascm.org/pdf/Guidelines.pdf

developed for the ISS. The CAM, which will be small enough to be carried aboard the Space Shuttle, will be large enough to allow experiments on small animals.

The usefulness in a Centrifuge Simulation becomes apparent when one considers the need for artificial gravity during long-term space flight, the magnitude of undertaking involved in building a human sized centrifuge in space, and the need to design experiments for the ISS Centrifuge that will most accurately reproduce the desired human experience for its test subjects.

The purpose of this thesis is to allow the user to conduct a unified simulation of the engineering cost of a centrifuge versus an astronaut's ability to tolerate the rotational environment that such a centrifuge would impose.

II. THESIS

A. HUMAN DISORIENTATION AS A FACTOR IN SPACECRAFT CENTRIFUGE DESIGN

1. Why Is Human Disorientation Such an Important Factor?

Disorientation is manifested when the Visual and Vestibular System receives a provocative stimulus.[27] In other words, the eyes are reporting something different than the sense of orientation. This sensory conflict leads to feelings that range from general malaise, disorientation, nausea, and can cause emesis (vomiting[28]) and incapacitation.

The Vestibular System consists of the Semi-Circular Canals that detect changes in angular velocity, and the Otoliths that detect linear acceleration. These provocative stimuli can be specified according to the sensory systems that are involved. A visual-vestibular conflict occurs when the eyes and the vestibular receptors report incompatible information. An intravestibular conflict occurs when there is a mismatch in the information reported from the semi-circular canals and the Otoliths.[29]

The physical characteristics of the semi-circular canals are well known and have been derived through dynamic analysis.[30] The three canals are firmly coupled to the skull in order to experience the same accelerations as the head.[31] As shown in Figure 4, each canal contains a fluid, endolymph, which rotates within the canal whenever the skull rotates in space. The endolymph, flowing through a smooth bore, enjoys laminar flow making the flow resistance linearly dependent on velocity. Movement of the endolymph deflects the Cupula, a hair-cell transducer, within the ampulla. The Cupula also acts as a weak spring and will restore itself to zero deflection in the angular velocity is at a steady state. Deflection of the Cupula produces a neural signal that informs the brain of change

---

[27] Ernsting, Nicholson, Rainford, p. 459-461

[28] "Emesis," The American Heritage Dictionary, p. 448

[29] Ernsting, Nicholson, Rainford, p. 459-461

[30] Milsum, p. 186

[31] Ernsting, Nicholson, Rainford, p. 434

in the person's spatial orientation.[32,33] The mathematical properties of this system are laid out in Appendix C.
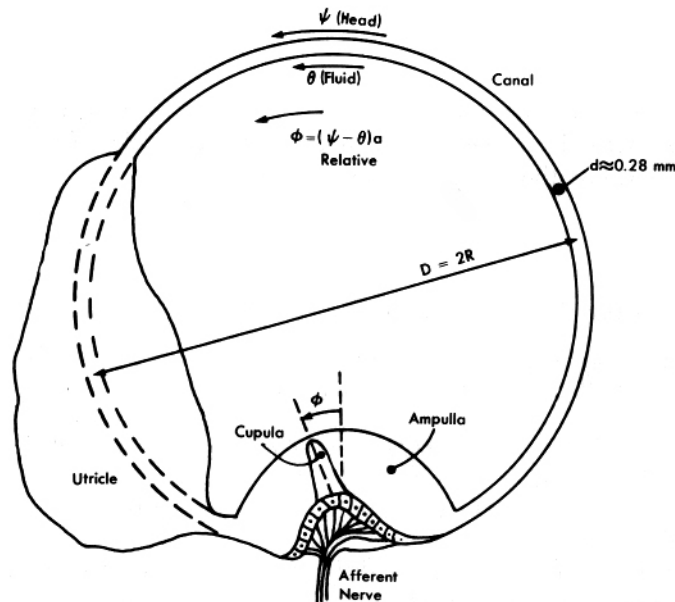
Figure 4: Diagram Of A Semi-Circular Canal[34]

Of particular interest to this thesis is the special case of a Cross-Coupled, or Coriolis, Stimulation where the individual is being rotated about a particular axis and then moves the head in a manner that produces a change in angular velocity. The result of Coriolis Stimulation is to produce an erroneous signal of a turn about an axis that does not accord with either the axis of rotation, or the axis of movement. This erroneous signal persists after the movement has been completed due to the fact the Cupula requires 10 seconds or more to return to equilibrium. During this time the Otoliths sense the correct attitude of the individual with relation to apparent gravity. This mismatch produces a potent stimulus for inducing motion sickness to which all individuals with an intact Vestibular System may succumb if the angular velocity of the rotating environment and amplitude of head movement are high enough, and there are a sufficient number of

---

[32] Milsum, p. 186

[33] Ernsting, Nicholson, Rainford, p. 426

[34] John H. Milsum, Biological Control System Analysis, New York: McGraw-Hill, 1966, p. 186

repetitions.[35] Seasickness is a classic example of this effect, particularly on small boats in rough seas.

The disorientation resulting from radial translation in a rotating environment could potentially cause a great deal of disorientation and discomfort, which could inhibit an astronaut's ability to perform normal functions. Movements that on the ground that are taken for granted such as moving from a sitting to a standing position, walking, exercise, and climbing a ladder would become extremely burdensome and uncomfortable.

2.   Modeling Engineering Cost Versus Coriolis

Due to the expense of placing objects in orbit, there will be a strong temptation to keep the size of a centrifuge for use by astronauts to a minimum. However, as discussed in the previous section, Coriolis Stimulus can have a profound effect on an individual. Therefore, if a centrifuge were to be employed in a long term mission in space, the effect of Coriolis must be balanced with cost in the design process so that astronaut will be able to function with an acceptable level of discomfort.

To appropriately model Engineering Cost and Coriolis two competing models must be designed. For Engineering Cost, a model of the external characteristics of a centrifuge, namely its size and power requirements, must be designed. The mathematical rigor behind the development of the Centrifuge Model is shown in Appendix A. For Coriolis, a model of the internal characteristics of a centrifuge and the semi-circular canals, namely Centrifugal Force, Coriolis Force, and the dynamic response of the Cupula, must be designed. The mathematical rigor behind the development of the Human Disorientation model is shown in Appendices B and C.

a.   *Centrifuge Model*

The construction, assembly, and flight of a centrifuge for use in space is not a trivial exercise. The development of a computer model that considers centrifuges of various sizes must take into account the effect such a centrifuge would have on the spacecraft of which it would be a vital component. However, a sizable centrifuge has not

---

[35] Ernsting, Nicholson, Rainford, p. 461-462

yet been flown in space. The only example is the proposed design for the ISS Centrifuge the characteristics of which are shown in Table 1.

Description	Specification
Location	Centrifuge Accomodation Module
Mass	2700 kg
Rotating Radius	1.25 m
Habitat Size	19 in W× 28 in H× 24 in D
Habitat Mass	116 kg
Habitat Quantity	2
Apparent Gravity	0.01-2 G (0.01 G increments)
Spin-Up Time	5-60 min

Table 1: International Space Station Centrifuge Specifications[36]
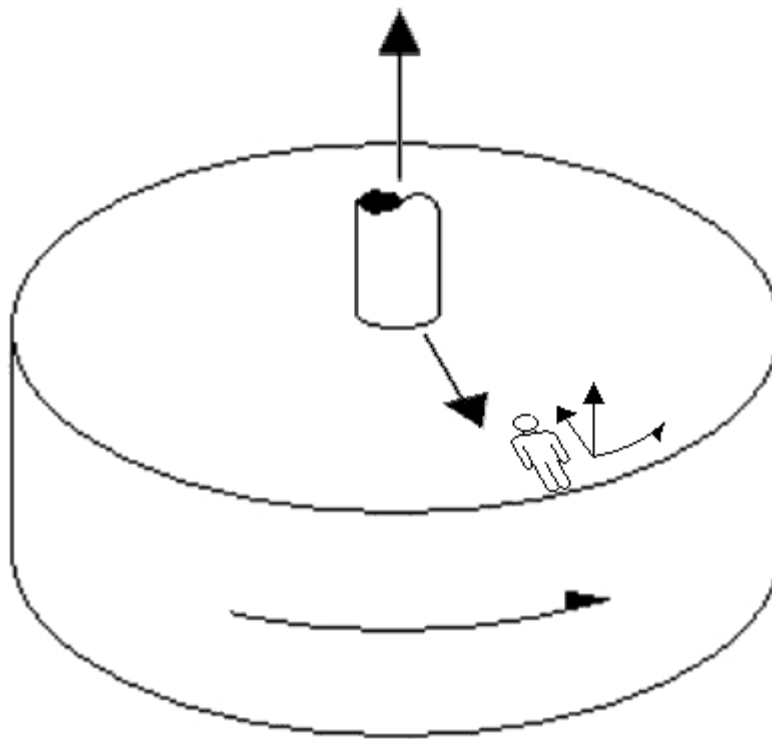
Figure 5: Diagram Of An Annular Centrifuge

---

[36] "Centrifuge," 2 July 2002, Space Station Biological Research Project, NASA Ames Research Center, 6 July 2002, http://brp.arc.nasa.gov/GBL/centriTC.html

Although the ISS Centrifuge has not been flown yet, it does provide a baseline. This baseline can be used to determine the effect similar centrifuges of various sizes would have on a potential spacecraft. The model constructed from this baseline would assume that the centrifuge would be a rotating cylinder, as shown in Figure 1, designed to reproduce the dimensional, mass, apparent gravity, and spin-up characteristics of the ISS Centrifuge. This model would be scalable to test the characteristics of cylindrical centrifuges of various sizes. The outputs of this model will be mean power cost and graphs of angular velocity, current, and power vs. time.

This thesis only considers cylindrical centrifuges rotating as shown in Figure 5. Some futurists and visionaries have also discussed alternative centrifuge architectures such as radial-arm and tethered centrifuges. A radial arm centrifuge would consist of two or more modules mounted at the end of rigid spokes connected to a central hub about which the entire apparatus would spin. A tethered centrifuge would consist of two or more modules connected by a cable that would be held rigid by the centrifugal force of the spinning bodies.[37] These alternate centrifuge architectures present different technical characteristics and were considered to be beyond the scope of this thesis.

b. *Human Disorientation Model*

Consider an astronaut within a centrifuge operating at a constant angular velocity. If the astronaut is stationary relative to his surroundings he feels gravity as if he was on Earth. This artificial gravity is the result of a somatogravic illusion of normal gravity generated within a centrifuge because the apparent gravitoinertial force vector is normal to the floor on which he is standing, as in Figure 6. A somatogravic illusion is a phenomenon of the Vestibular System that produces a false perception of actual gravitational force due to prolonged exposure to an atypical force vector.[38] This means that the astronaut only feels the centrifugal force, not the angular velocity.

As shown in Equation (B.14) from Appendix B, movement by the astronaut in the axial plane (a change in position along the axis of rotation) has no effect on the astronaut. Movement in the angular plane (a change in position around the axis of

---

[37] Theodore W. Hall, "After Skylab, 1973-1991," The Architecture of Artificial-Gravity Environmentsfor Long-Duration Space Habitation, Ann Arbor: University of Michigan, 1994, 24 Sept. 2002, http://www0.arch.cuhk.edu.hk/~hall/ag/Dissertation/1_4.htm

[38] Ernsting, Nicholson, Rainford, p. 437

13

rotation) produces a Coriolis Force that has the effect of increasing or decreasing the apparent gravitational force. Movement in the radial plane (change in distance from the axis of rotation) produces a Coriolis Force that has the effect of both a shear force in the angular plane and a torque in the axial plane. Previous studies conducted where human test subjects were placed into a slowly rotating room underscored the detrimental effects of translation in the radial plane of a rotating environment.[39]
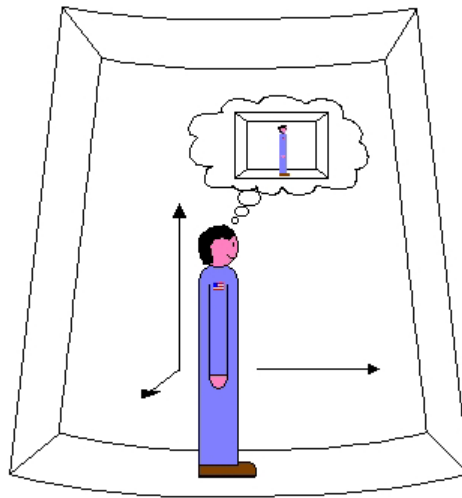
Figure 6: An Astronaut's Perception Of The Rotating Environment

When the astronaut moves in the radial plane, he receives a Coriolis Stimulation and detects a change in angular velocity with his semi-circular canals.[40] The two sets of semi-circular canals reside on each side of the head in the inner ear (illustrated in Figure 7 and Figure 8). Each semi-circular canal is capable of detecting angular acceleration in three dimensions via the anterior vertical, posterior vertical, and lateral canals; labeled "pv," "av," and "l" in Figure 8. The brain processes the information from each semi-circular canal and is able to accurately sense the plane, direction, and magnitude of any change in angular motion within certain limits. Although the semi-circular canals are not aligned with the pitch, roll, and yaw axes the brain processes the information from both canals as a unified model of the body's angular motion.

---

[39] Percival McCormack, Personal Interview, 7 Feb. 2002

[40] Ernsting, Nicholson, Rainford, p. 425

Therefore, the alignment of the semi-circular canals is trivial and only head alignment should be considered.[41]
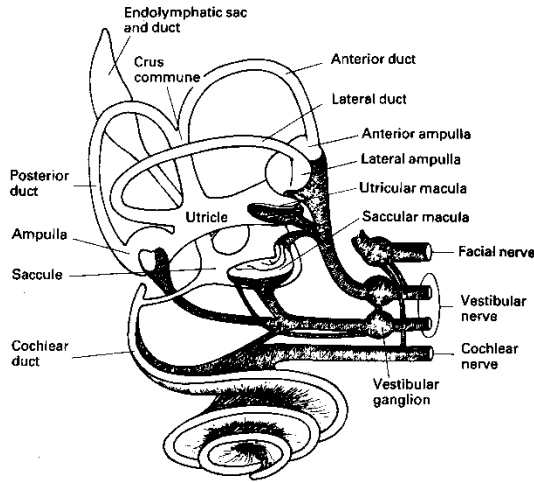
Figure 7: The Inner Ear[42]
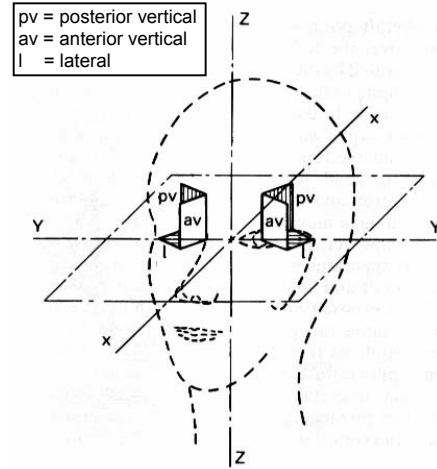
Figure 8: Semi-Circular Canal Orientation[43]

As shown in equation (B.14), in Appendix B, Coriolis Stimulation due to radial translation only occurs in one plane. Therefore, only one semi-circular canal needs to be modeled. The effects of linear acceleration due to Coriolis are not considered in this paper because they are assumed to be predictable and astronauts should be able to adapt to them easily.

B.   COMPUTER MODELS

Placing objects in orbit is extremely expensive. As a result there will be a strong temptation to keep the size of any centrifuge considered for use in space by astronauts to a minimum without consideration of the profound effect Coriolis Stimulation can have on an individual. In an effort to promote the use of a centrifuge in long-term missions in space, two competing models were designed, appropriately modeling Engineering Cost and the effect of Coriolis. In order for the use of a centrifuge in space to be effective, a

---

[41] Ernsting, Nicholson, Rainford, p. 426

[42] Ernsting, Nicholson, Rainford, p. 424

[43] Ernsting, Nicholson, Rainford, p. 426

balance must be struck between its Engineering Cost and the effect of Coriolis on its occupants must be balanced in the design process so that an astronaut will be able to function with an acceptable level of discomfort.

1.   Building a Computer Model Using LabView

National Instruments LabView 6.0 was selected as the program within which the necessary models were to be developed. Its advantages were its graphical interface, its stability, the modularity of its components, ease in debugging, the portability of the programs developed using it to multiple platforms, and its ability to run on the several platforms of various capabilities.

2.   Dual Analysis

The equations of motion, as developed in the appendices, were solved using two different mathematical approaches. First, a check case was developed using a step inputs and Laplace Transforms to achieve an analytical solution of the model as a function of time.   Second, each model was written in state-variable form, discretized and programmed in LabView to allow numerical solutions for arbitrary input conditions. Each analysis was compared using separate computer programs developed in LabView to determine if each analysis was producing the same numerical results.

3.   Experimental Validation

A simple validation experiment was conducted to get a 'seat-of-the-pants' feel for the results of the Human Disorientation Model.   Using a Merry-Go-Round was the simplest means to determine how radial movement of the head feels in a rotating environment roughly the size of the ISS Centrifuge. A 7 ft. 6.5 in. Merry-Go-Round, pictured in Figure 9, was found on the Former Fort Ord in Marina, CA near the Naval Postgraduate School; the outer radius of which was within 10 cm of the rotating radius of the ISS Centrifuge. The experiment was designed to be run with a small number of people of various military backgrounds who were colleagues of the author in the Space Systems Operations Curriculum at the Naval Postgraduate School. The experiment was also designed to be run at levels of Centrifugal Force that could be withstood by a person sitting on a Merry-Go-Round.

Experiment Run	Centrifugal G
10 RPM	0.13
20 RPM	0.52

Table 2: Centrifugal Force Produced During Each Run

The experiment consisted of two runs per test subject. The first run would be conducted at 10 RPM, and the second at 20 RPM. The angular velocities were selected to keep the centrifugal force at a level that could be managed by an individual sitting on an open platform Merry-Go-Round as shown in Table 2.

Figure 9: The Apparatus Used In The Validation Experiment

Figure 10: Test Subject's Perspective

Each run was then divided into three phases for the purposes of recording the amount of disorientation. The first phase consisted of the spin-up acceleration and first 60 seconds of steady state angular velocity. The second phase consisted of 10 seconds of cyclical head movement at about 0.5 Hz through 10 cm. The third phase consisted of the final 60 seconds and the spin-down acceleration. Additionally, the test subjects were instructed to stare at the yellow surveyor's flag directly across from them so that any oculogyral illusions around that fixed point could be recorded as shown in Figure 10. An arbitrary scale of disorientation, shown in Table 3, was devised to quantify the disorientation felt by the test subjects. Time was kept using a stopwatch and angular velocity was maintained by counting the seconds on the stopwatch between passes of the yellow surveyor's flag shown in Figure 9.

Disorientation Level	Associated Feeling
1	Normal
2	Slightly Dizzy
3	Dizzy
4	Nauseated
5	Imminent Emesis

Table 3: Qualitative Disorientation Scale

4.   Expected Results

The computer models, combined with the results of the validation experiment should show: (1) that disorientation is felt when the head is moved in the radial plane of a rotating environment, (2) that the disorientation felt is related to a feeling of twisting in the axial plane of a rotating environment, and (3) that the feeling of disorientation is directly related to centrifuge radius and angular velocity. The validation experiment allows for a calibration of predicted Cupula Velocity to be related to an arbitrary level of discomfort. Additionally, this thesis should show that a centrifuge for providing astronauts artificial gravity without significant discomfort due to disorientation is feasible

and could be a future upgrade to the International Space Station, part of a future space station, or a component of a spacecraft for a manned interplanetary flight.

THIS PAGE INTENTIONALLY LEFT BLANK

III. COMPUTER MODEL

A. COMBINED SIMULATION

The ability to develop a dynamic model of a centrifuge and its effect on human disorientation resides in the mathematical understanding of the two systems. Because this thesis seeks to produce a unified analysis of two different systems; a user interface was developed that allows the simultaneous input of parameters and display of results. This overview of the two models is called the Centrifuge Front Panel.

FRONT PANEL	Centrifuge Front Panel.vi
STATE SPACE	Centrifuge State Space.vi
STATE SPACE	Human Disorientation State Space.vi

Table 4: Major Components Of The Centrifuge Front Panel

The Centrifuge Front Panel is a computer program written using *LabVIEW 6i[44]*. This "virtual instrument," or VI , as shown in Table 4, incorporates the Centrifuge Dynamic Model, the Human Disorientation Model, and their various sub-components to display the engineering costs of an arbitrary centrifuge together with the physical response of a human semi-circular canal. The block diagram shown in Figure 11 details the relationships between the various VIs utilized in this thesis.

1. Combined Simulation User Interface

The user interface (known as the front panel) of the combined simulation, shown below in Figure 12, is designed to allow the user to input the specific parameters of a centrifuge and the person occupying it via controls with the results displayed on indicators. The individual parameters (known as controls) are available for user manipulation when up and down arrows are depicted next to the numerical readout. These parameters are grouped into 'clusters' of related data such as Simulation Parameters, Electric Parameters, Centrifuge Dimensions, and Human Parameters. The

---

[44] LabView, CD-ROM, Ver. 6i, Austin Texas: National Instruments Corp., 2000

output paramters, known as indicators, of the simulation took the form of plots or numerical readouts. Every control, cluster, or indicator is represented on a diagram, which is where *LabVIEW* programs are written.
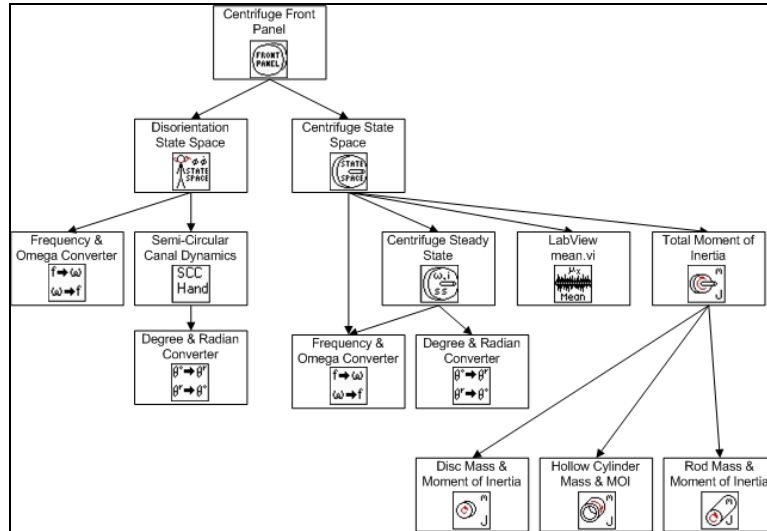
Figure 11: Block Diagram of the Centrifuge Front Panel
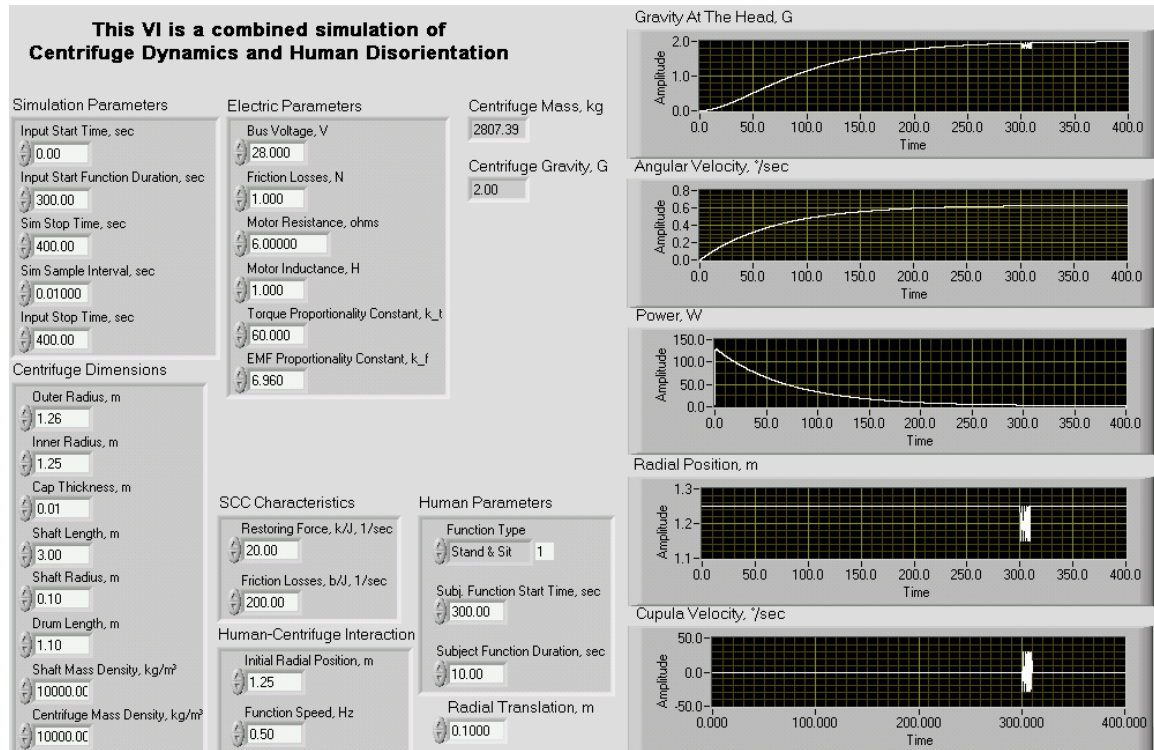
Figure 12: Centrifuge Front Panel

22

2.   Diagram

   a.   Centrifuge Dynamic Model

The diagram of the Centrifuge Front Panel contains a Sequence Structure that consists of two frames. The first frame, pictured below in Figure 13, collects the user's inputs for the Centrifuge Dynamics Model. Those inputs are the Electric Parameters, Centrifuge Dimensions, and Simulation Parameters clusters. Wiring the clusters from the front panel of this VI into a linked VI, in this case Centrifuge State Space, has the effect of reproducing the user's inputs in similarly structured control clusters in the linked VI. One output, Angular Velocity (a one-dimensional array indexed with respect to time) is wired to a Sequence Local that passes that data to any subsequent frames for later use. The remaining outputs; scalars representing Centrifuge Gravity and Mass and vectors representing Power vs. Time and Angular Velocity vs. Time are connected to their corresponding display indicators.
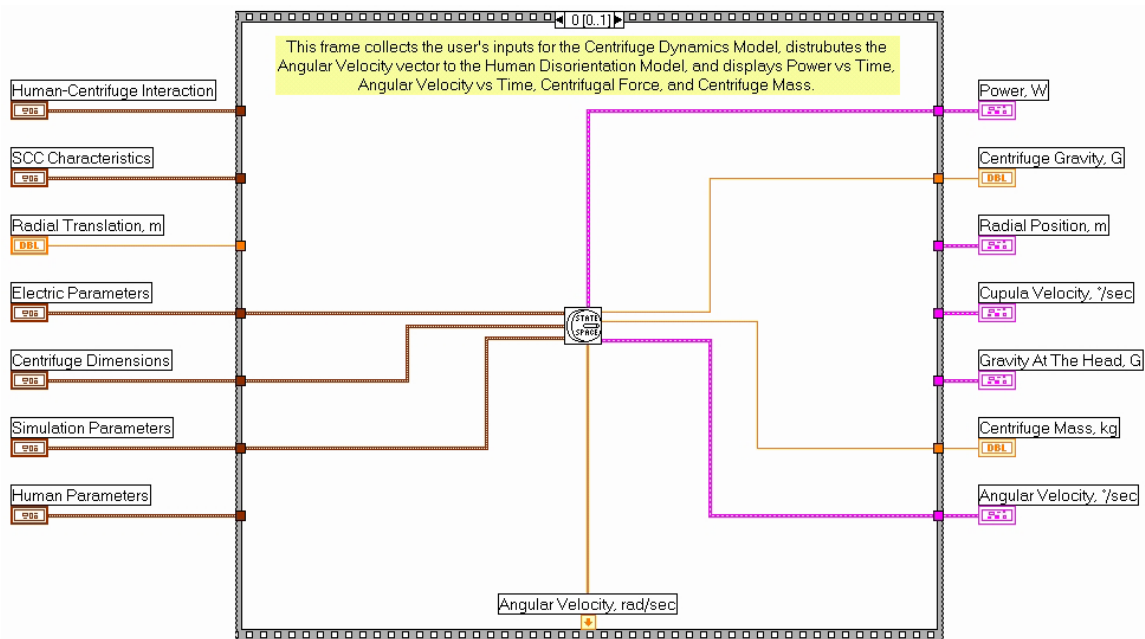
Figure 13: Front Panel Interaction With The Centrifuge Dynamic Model

   b.   Human Disorientation Model

The second frame, pictured in Figure 14, collects the inputs for the Human Disorientation Model.   Those inputs are the Human-Centrifuge Interaction, SCC

23

Characteristics, Simulation Parameters, and Human Parameters clusters together with the Radial Translation scalar and the Angular Velocity array from the Centrifuge Dynamics Model. The inputs are wired to their counterpart controls in the linked VI, in this case Human Disorientation State Space. The outputs are vectors representing Radial Position vs. Time, Cupula Velocity vs. Time, and Gravity At The Head vs. Time are connected to their corresponding display indicators.
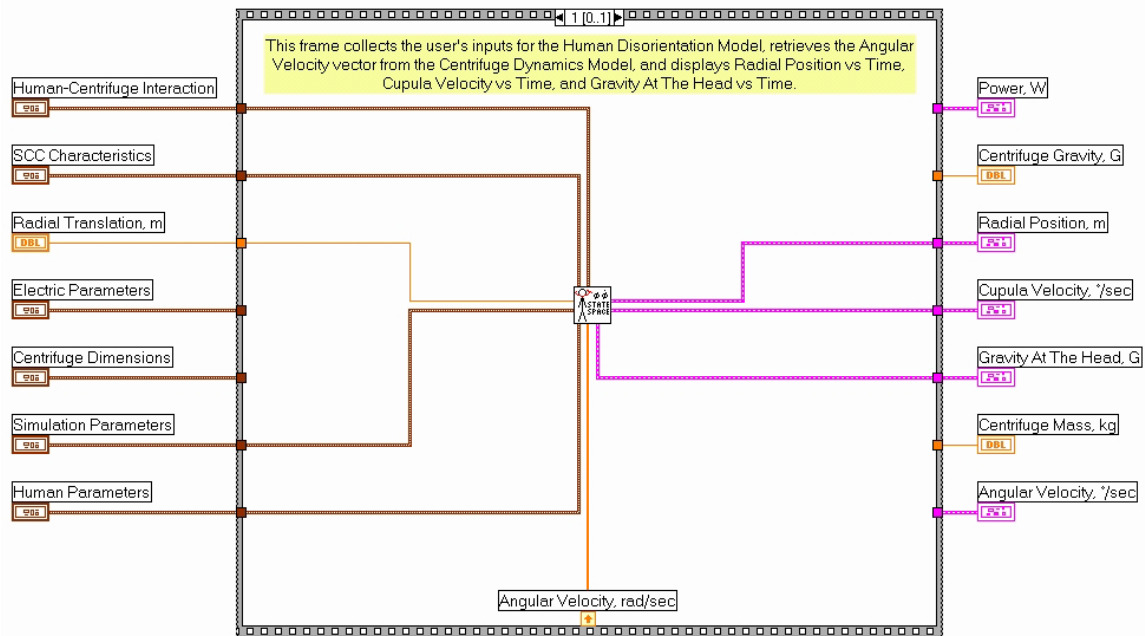
Figure 14: Front Panel Interaction With The Human Disorientation Model

STATE SPACE	Centrifuge State Space.vi
ω,i ss	Centrifuge Steady State.vi
f→ω ω→f	Freq and Omega 2 way Converter.vi
μx Mean	Mean.vi
J	Total Moment of Inertia.vi

Table 5: Major Components Of The Centrifuge Dynamic Model

24

The details of the construction of the Centrifuge Dynamic Model and the Human Disorientation Model VIs will be detailed in the proceeding sections.

B.   CENTRIFUGE DYNAMICS MODEL

Because the VIs listed in Table 5 deal specifically with the dynamics of a centrifuge, more information can be displayed in the user interface. The Control Clusters of this VI are structured so that the model can be run independently, or as component of the combined simulation.
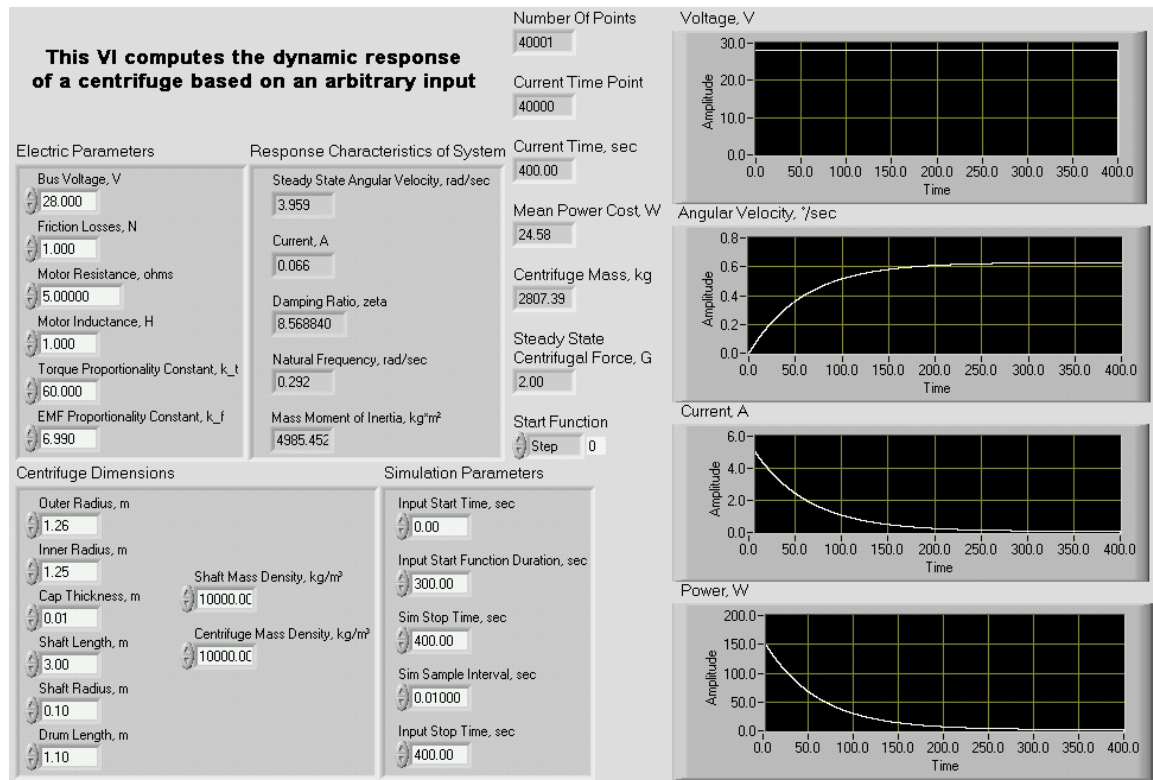
1.   Front Panel

Figure 15: Centrifuge Dynamic Model User Interface

The front panel of the Centrifuge Dynamics Model, shown in Figure 15, is structured so that the user can not only control the simulation (as when running the combined simulation), but can also vary the start-up dynamics so that different means of reducing the power required to start the centrifuge can be examined. The different start-

up functions are: Unit-Step, Ramp, Two-Step, and Three-Step. Additional indicators are utilized to show specific facets of the centrifuge's engineering cost, specifically: Mean Power Cost, Voltage vs. Time, and Current vs. Time.

2. **Diagram**

a. *Centrifuge Natural Response Characteristics*

The diagram of the Centrifuge Dynamic Model contains a Sequence Structure that consists of four frames. The first frame, pictured in Figure 16, collects the user's inputs and determines the Centrifuge Steady State Response. Those inputs are the Electric Parameters, Centrifuge Dimensions, and Simulation Parameters clusters can be entered directly by a user or linked from a superior VI. The Centrifuge Dimension cluster of this VI is wired into the linked VI, Total Moment of Inertia and the Formula Node for determining Steady State Centrifugal Force. The Electric Parameters cluster, together with the output of the Total Moment of Inertia VI, is rebundled into the Physical Parameters control cluster of the linked Centrifuge Steady State Response VI. The output of the Centrifuge Steady State Response VI is rebundled, together with the Total Mass Moment of Inertia, into the Response Characteristics indicator cluster. Steady State Angular Velocity is separately unbundled from the Response Characteristics cluster to provide an input to the Formula Node for computing Steady State Centrifugal Force. Total Moment of Inertia is wired to a Sequence Local, and the Formula Node returns Steady State Centrifugal Force for its corresponding indicator on the Front Panel.

The following formula, based on Equation (B.18) in Appendix B, is used to compute the Steady State Centrifugal Force:

$$G = \frac{r\omega^2}{g_0}$$
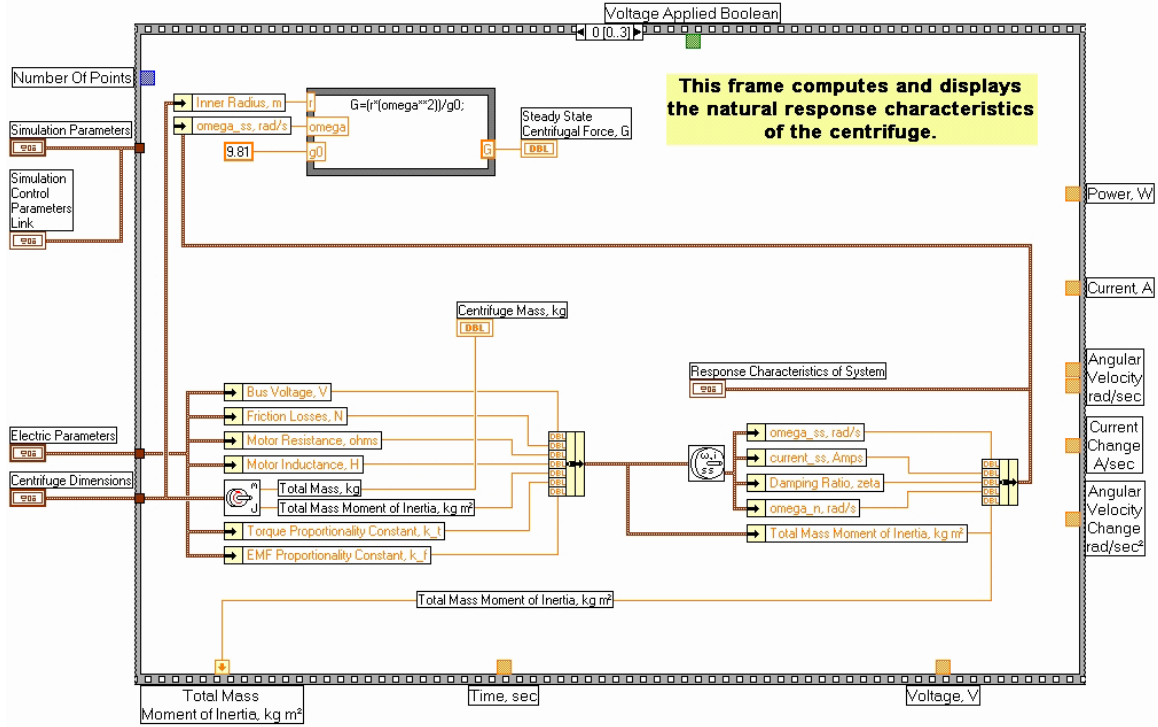
Figure 16: Determination Of The Centrifuge's Natural Response Characteristics

b.   *Unit Step Function Start-Up Response*

Logic	Case Response
Input Stop Time > Current Time Input Start Time > Current Time	False
Input Stop Time > Current Time Input Start Time <= Current Time	True
Input Stop Time <= Current Time Input Start Time <= Current Time	False

Table 6: Start-Up Voltage Case Logic

The second frame, pictured in Figure 17, collects the user's inputs and computes voltage with respect to the start-up function. Those inputs are the Electric Parameters and Simulation Parameters clusters. The start-up function is determined through the use of a Ring Control. The first, and default, selection of the Ring Control is

the Unit Step Function. The Ring Control is not designed to be manipulated from a superior VI, therefore when the Centrifuge Dynamic Model is linked within another VI, it will generate its responses using the Unit Step Function which means that the voltage instantaneously changes from zero to its steady state value.
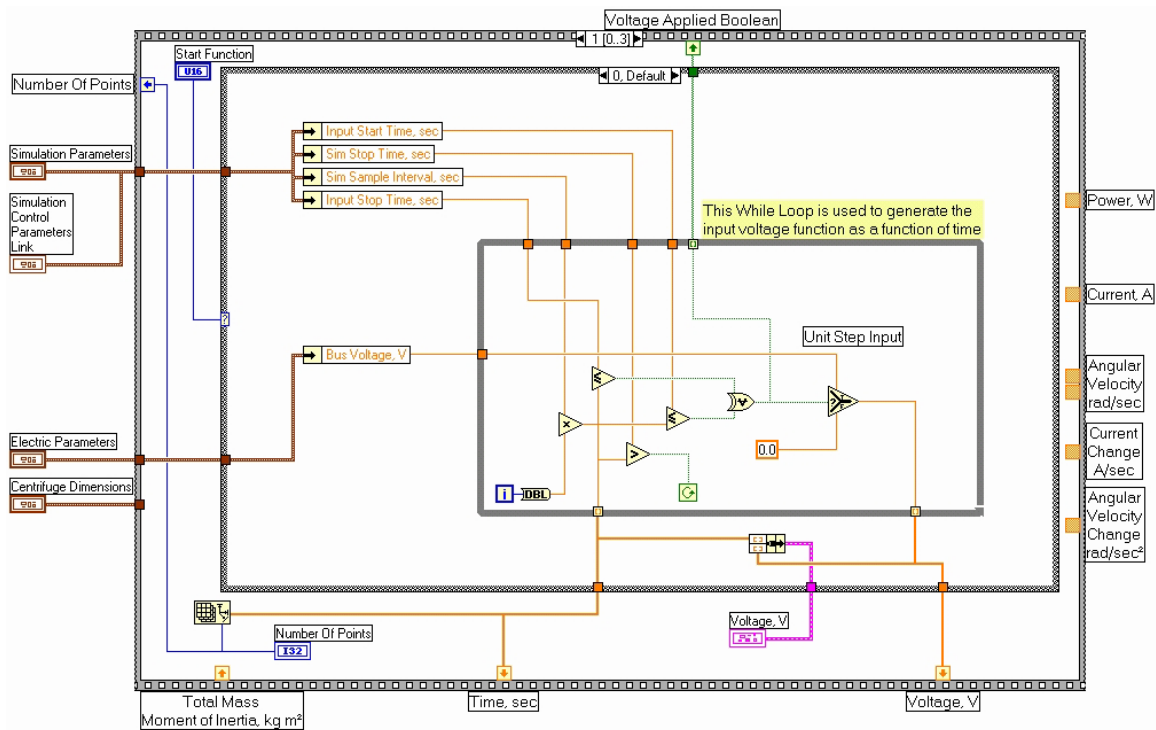
Figure 17: Centrifuge Dynamic Start-Up Response to a Unit-Step Function

For each case, a simple logic tree, shown in Table 6, and Case Structure is used to determine when to apply the designated start function. Voltage, Time, and a Voltage Applied Boolean are indexed into one-dimensional arrays and connected to Sequence Locals for later use.
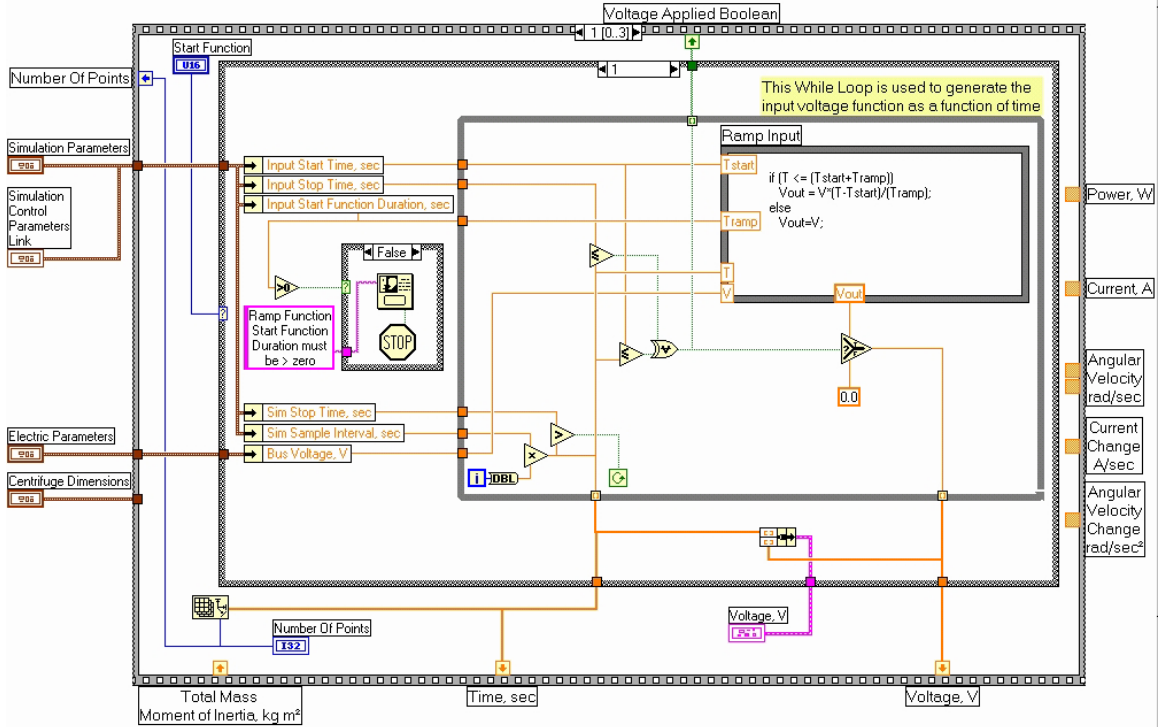
Figure 18: Centrifuge Dynamic Start-Up Response To A Ramp Function

c. Ramp Function Start-Up Response

The second case, pictured in Figure 18, uses a Ramp Function to compute the start-up voltage. The Ramp Function utilized is shown below:

$$V_{start-up} = V_{final}\left(\frac{t - t_{start}}{t_{function}}\right)$$

d. Two-Step Function Start-Up Response

The third case, pictured in Figure 19, uses a Two-Step Function to compute the start-up voltage. This case assumes some electronic means is used to halve the voltage for the duration of the start-up function. The Two-Step Function utilized is shown below:

$$V_{start-up} = \frac{1}{2}V_{final}$$

29

Figure 19: Centrifuge Dynamic Start-Up Response to a Two-Step Function

e. Three-Step Function Start-Up Response

The fourth case, pictured in Figure 20, uses a Three-Step Function to compute the start-up voltage. This case assumes some electronic means is used to step the voltage by thirds for the duration of the start-up function. The first half of the Three-Step Function utilized is shown below:

$$V_{start-up} = \frac{1}{3}V_{final}$$

The second half of the Three-Step Function is:

$$V_{start-up} = \frac{2}{3}V_{final}$$

30

Figure 20: Centrifuge Dynamic Start-Up Response to a Three-Step Function

f.   *Initial Prediction of Current and Angular Velocity*

The third frame, pictured in Figure 21, consists of a nested Sequence Structure that has three frames. The first nested frame takes user inputs and the current state of angular velocity and current to compute the change in current and angular velocity and predict the new state in angular velocity and current. The user inputs are the Electric Parameters and Simulation Parameters clusters. Moment of Inertia, Voltage, Time, and the Voltage Applied Boolean are brought forward into this frame using Sequence Locals. The Voltage Applied Boolean is used to determine whether or not voltage is being applied.

The formulae used in Figure 21 are based on the State Space Analysis found in Equation (A.123) in Appendix A. Change in current is predicted by:

$$\hat{\dot{i}} = -\frac{R}{L}i - \frac{k_f}{L}\omega + \frac{V}{L}$$

31

Change in angular velocity is predicted if voltage is applied by:

$$\hat{\dot{\omega}} = \frac{k_t}{J} i - \frac{B}{J} \omega$$

Otherwise, the change in angular velocity without voltage is:

$$\hat{\dot{\omega}} = -\frac{B}{J} \omega$$
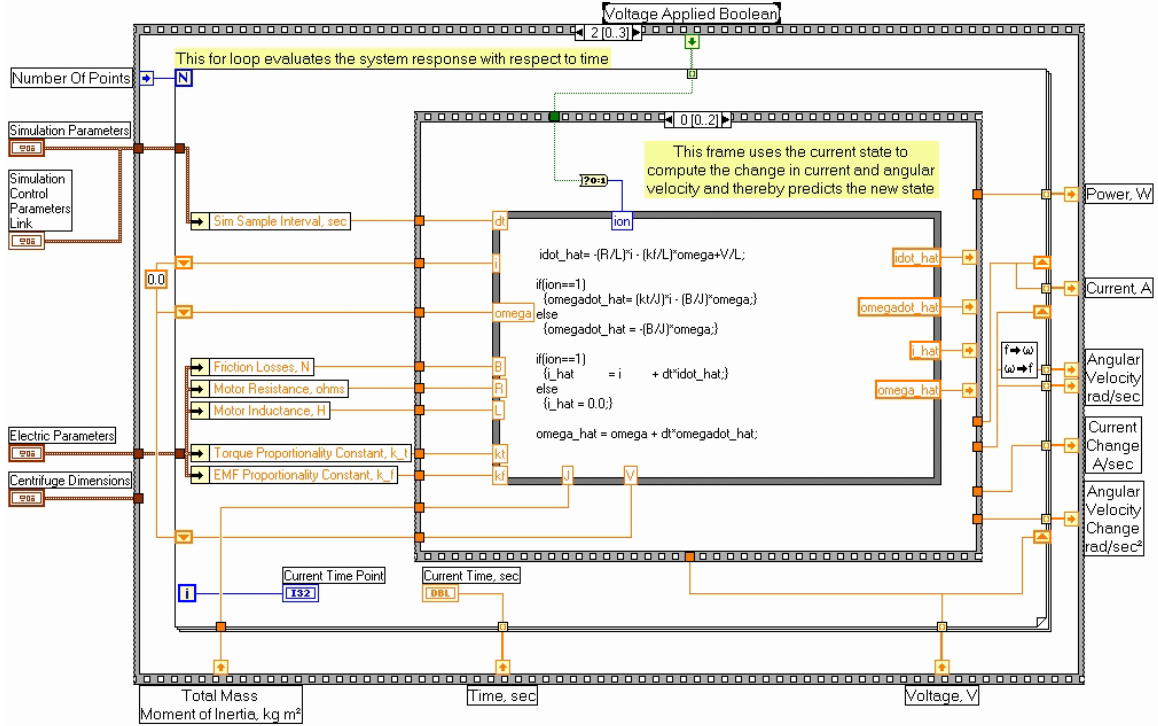
Figure 21: State Space Prediction of Current and Angular Velocity

The predicted current when voltage is applied:

$$\hat{i} = i + \hat{\dot{i}} \Delta t$$

Otherwise, without voltage the predicted current is zero. Predicted angular velocity is determined by:

$$\hat{\omega} = \omega + \hat{\dot{\omega}} \Delta t$$

The results of the above formulae: $\hat{i}$, $\hat{\dot{i}}$, $\hat{\omega}$, and $\hat{\dot{\omega}}$ are passed to the next frame using Sequence Locals.

32

g. *Correction of Predicted Current and Angular Velocity*

The second nested frame takes user inputs and the predicted state of angular velocity and current to correct the predicted state of change in current and angular velocity and produce the new state of angular velocity and current. Again, the user inputs are the Electric Parameters and Simulation Parameters clusters. Moment of Inertia, Voltage, Time, and the Voltage Applied Boolean are brought forward into this frame using Sequence Locals. Additionally, the predicted states are passed into this frame using Sequence Locals. The Voltage Applied Boolean is used to determine whether or not voltage is being applied.
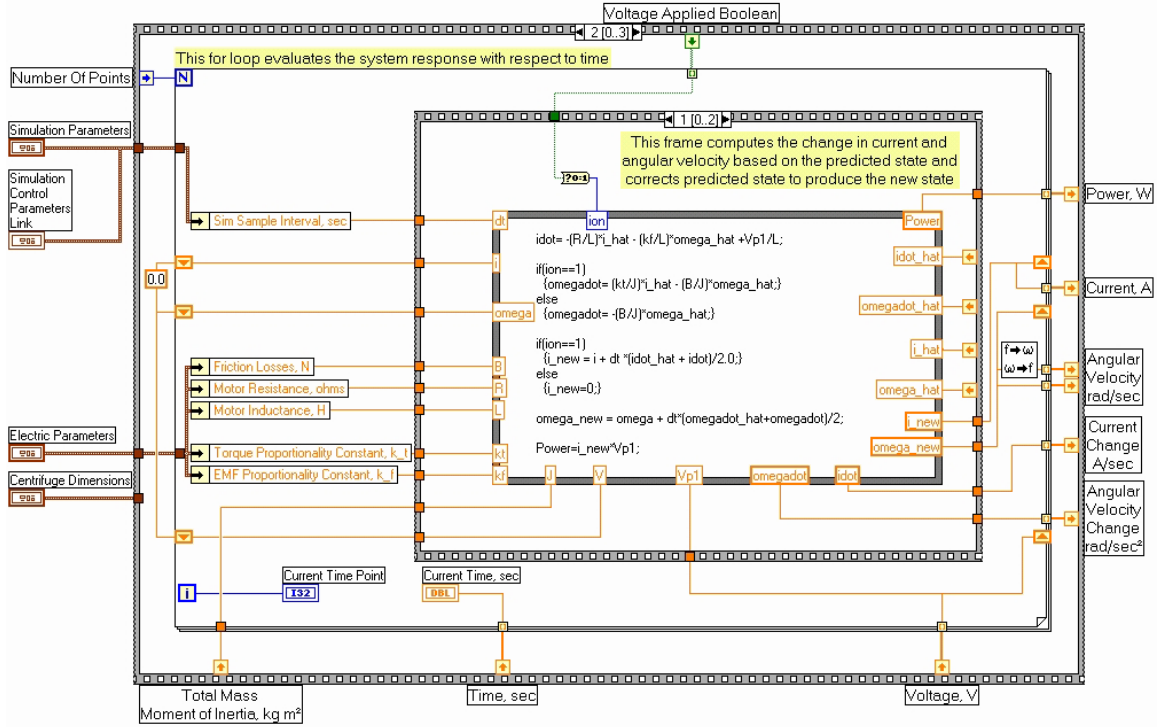
Figure 22: Correction of Predicted State to Produce New State

The formulae used in Figure 22 are based on those found in Equation (A.123) in Appendix A. Change in current is:

$$\dot{i} = -\frac{R}{L}\hat{i} - \frac{k_f}{L}\hat{\omega} + \frac{\hat{V}}{L}$$

Change in angular velocity is when voltage is applied:

$$\dot{\omega} = \frac{k_t}{J}\hat{i} - \frac{B}{J}\hat{\omega}$$

Otherwise, the change in angular velocity without voltage is:

$$\dot{\omega} = -\frac{B}{J}\hat{\omega}$$

The corrected prediction of current when voltage is applied:

$$i_{t+\Delta t} = i_t + \left(\frac{\hat{i} + i}{2}\right)\Delta t$$

Otherwise, without voltage the predicted current is zero. The corrected prediction of angular velocity is determined by:

$$\omega_{t+\Delta t} = \omega_t + \left(\frac{\hat{\dot{\omega}} + \dot{\omega}}{2}\right)\Delta t$$

In addition to the current and angular velocity predictions, instantaneous power is computed in this frame:

$$P = i_{t+\Delta t}\hat{V}$$

The results of the computations conducted within this frame: Power, Current, and Angular Velocity are wired outside of the nested Sequence Structure, indexed versus time into one-dimensional arrays, and connected to Sequence Locals for use in a later frame.

h.   *Display of Results*

In the final frame of the Centrifuge Dynamic Model, the results of the State Space Analysis: Power, Current, and Angular Velocity are bundled with a one-dimensional Time array and plotted on the Front Panel. Additionally, Mean Power Cost is computed using *mean.vi*[45] and displayed as a scalar together with Outer Radius. A one-dimensional of the Angular Velocity results is connected to a hidden indicator for linking to the Human Disorientation Model.

---

[45] "mean.vi", CD-ROM, LabVIEW 6i, Austin Texas: National Instruments Corp., 2000
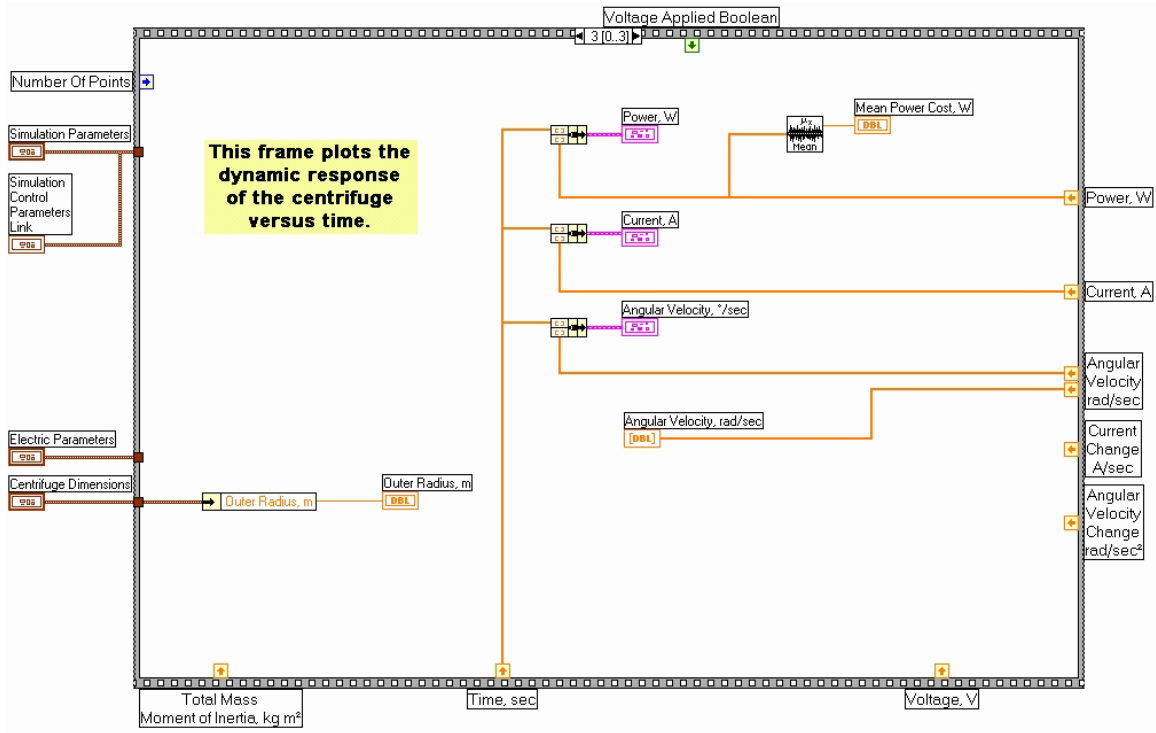
Figure 23: Display of Centrifuge Dynamic Model Results

C. CENTRIFUGE STEADY STATE RESPONSE

1. Front Panel

	Centrifuge Steady State.vi
	Freq and Omega 2 way Converter.vi
	Degrees and Radians 2 way Converter.vi

Table 7: Major Components of the Centrifuge Steady State Model

The front panel of the Centrifuge Steady State Response, shown in Figure 24, is not designed for direct user manipulation. Rather, this VI is designed to be a subordinate VI nested within the Centrifuge State Space VI. The variables within the input Control Cluster, Physical Parameters, are linked from the Centrifuge Dynamic Model providing the information necessary to compute the steady state characteristics of a centrifuge in

motion.   The output Indicator Clusters: Steady State Parameters and Response Characteristics link the results of this VI to the Centrifuge Dynamic Model.   The major components of this VI are listed in Table 7.

This VI Computes the steady state response and damping chacteristics of the system

Physical Parameters

Bus Voltage, V
28.000

Friction Losses, N
1.000

Motor Resistance, ohms
100.000

Motor Inductance, H
10.000

Mass Moment of Inertia, kg*m²
100.000

Torque Proportionality Constant, k_t
1.000

EMF Proportionality Constant, k_f
1.000

Steady State Parameters

Steady State Angular Velocity, deg/sec
15.884

Steady State Angular Velocity, rad/sec
0.277

Steady State Angular Velocity, hz
0.044

Steady State Angular Velocity, RPM
2.647

Steady State Current, A
0.028

Response Characteristics

Steady State Angular Velocity, rad/sec
0.277

Steady State Current, A
0.028

Damping Ratio
0.173

Natural Frequency, rad/sec
31.780

Figure 24: Centrifuge Steady State Model User Interface

2.   **Diagram**

a.   *Steady State Angular Velocity*

The diagram of the Centrifuge Steady State Response contains a Sequence Structure that consists of five frames. The first frame, pictured in Figure 25, collects the linked inputs and determines the Centrifuge's Steady State Angular Velocity. The Steady State Angular Velocity computed in this frame is wired into a Sequence Local for use in

36

later frames. The fifth frame, not pictured, converts Steady State Angular Velocity into four commonly used units (rad/sec, deg/sec, hz, and RPM) all of which are bundled for display in the Steady State Parameters Indicator Cluster. The formula used in this frame is based on Equation (A.15) in Appendix A:

$$\omega_{ss} = \left[\frac{k_\tau}{\left(RB + k_\tau k_f \right)} V_{ss} \right]$$
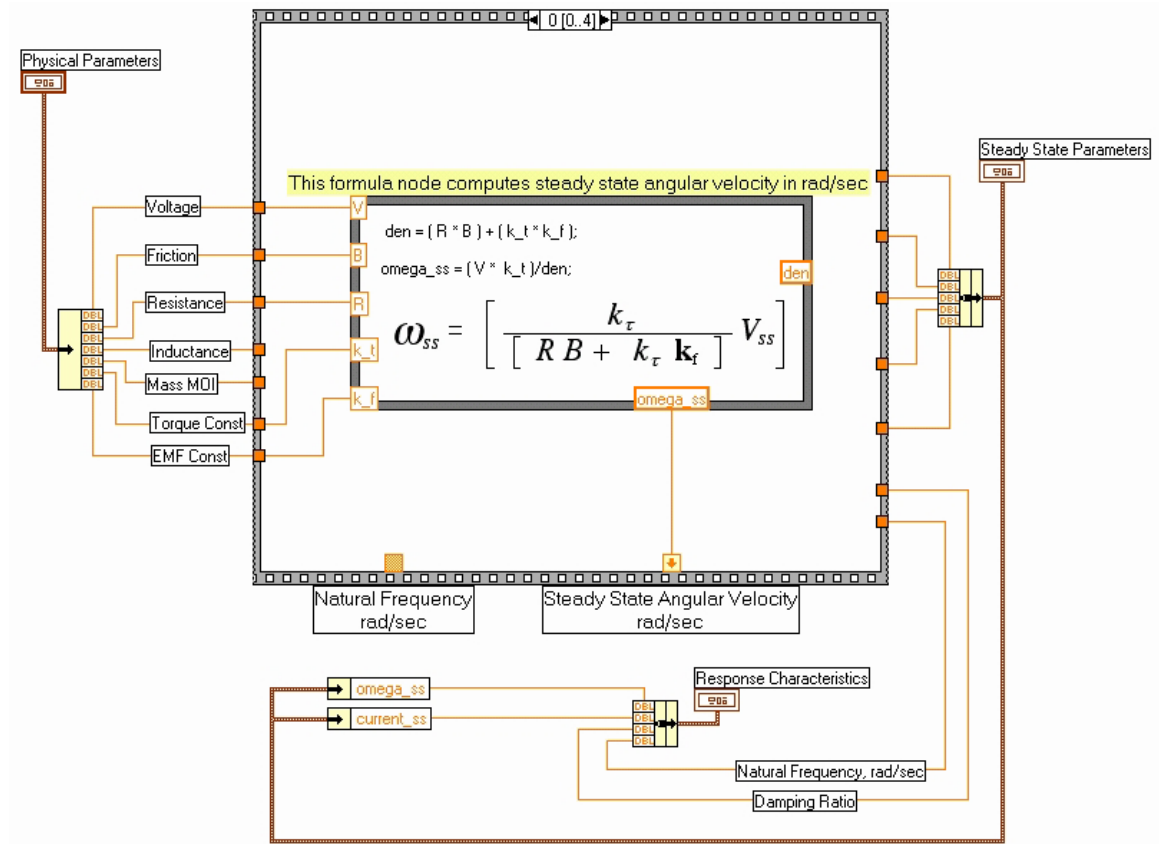
Figure 25: Determination Of Centrifuge Steady State Angular Velocity

b.   *Steady State Current*

The second frame, pictured in Figure 26, collects the linked inputs and determines the Centrifuge's Steady State Current. The Steady State Current computed in this frame is wired into a bundle for display in the Steady State Parameters Indicator Cluster. The formula used in this frame is based on Equation (A.17) in Appendix A:

$$i_{ss} = \left[\frac{B}{\left(RB + k_\tau k_f \right)} V_{ss} \right]$$
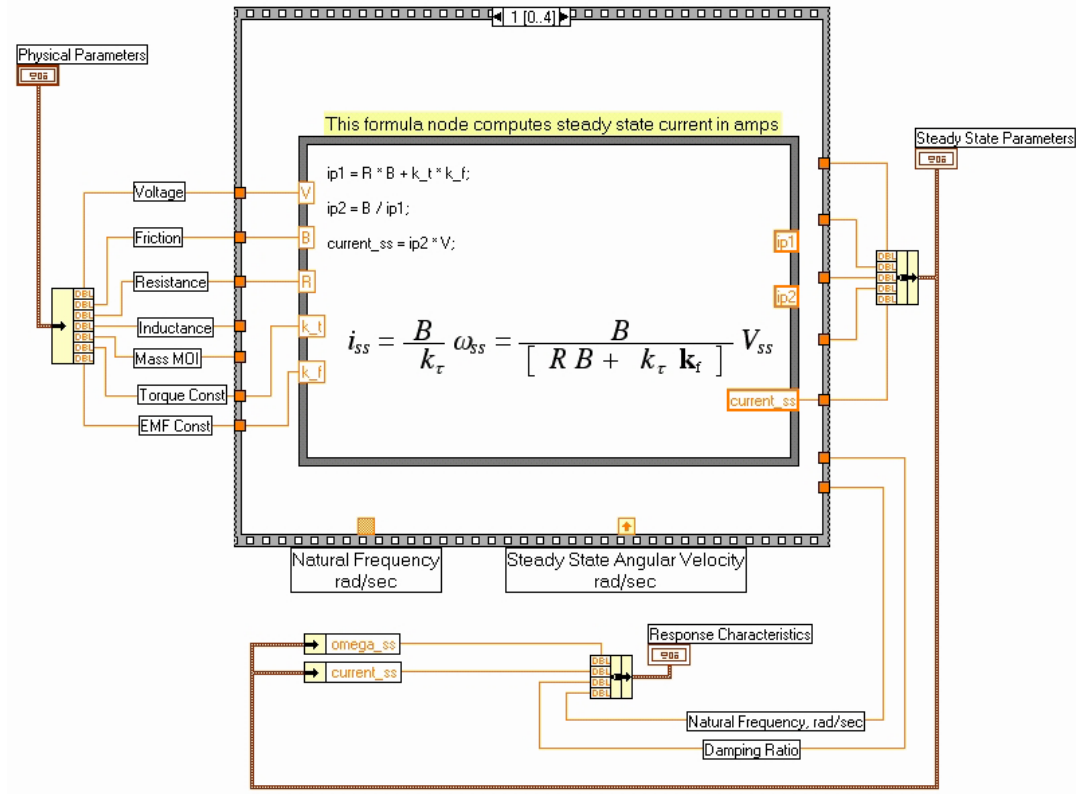
Figure 26: Determination of Steady State Current

c.   Natural Frequency

The third frame, pictured in Figure 27, collects the linked inputs and determines the Centrifuge's Natural Frequency. The Natural Frequency computed in this frame is wired into a bundle for display in the Response Characteristics Indicator Cluster. The formula used in this frame is based on Equation (A.25) in Appendix A:

$$\omega_n = \sqrt{\left(\frac{BR + k_\tau k_f}{LJ} \right)}$$
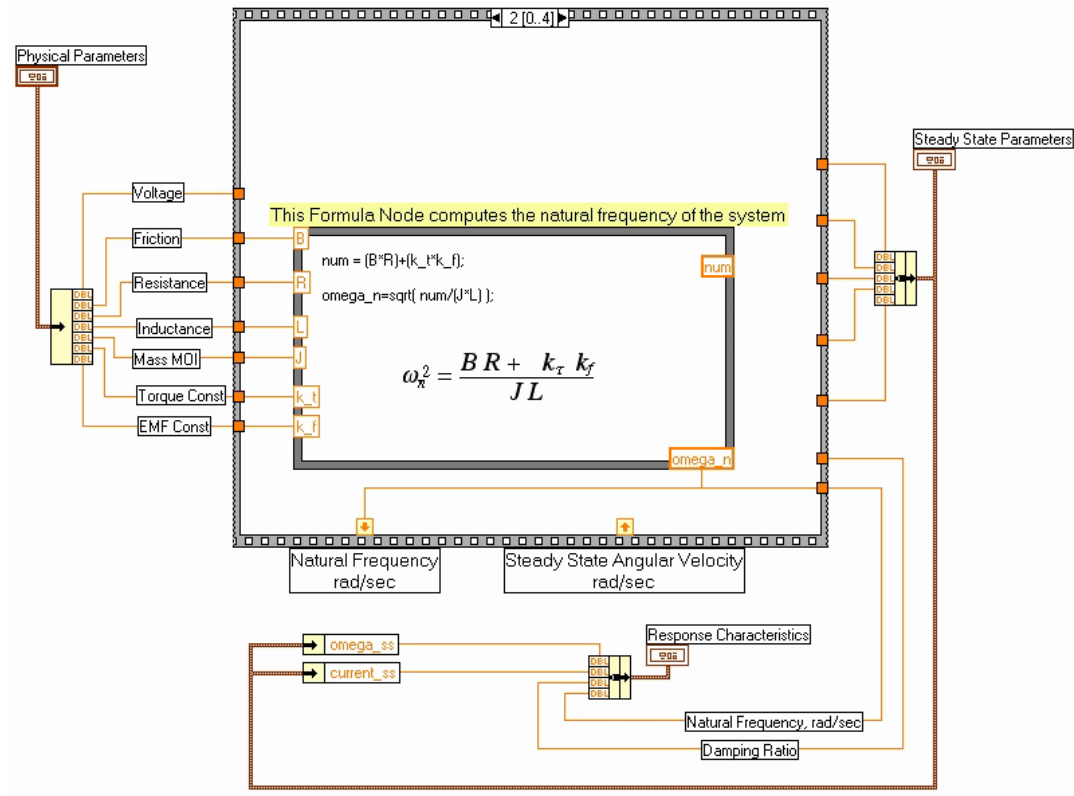
Figure 27: Determination of Natural Frequency

d.   Damping Ratio

The fourth frame, pictured in Figure 28, collects the linked inputs and determines the Centrifuge's Damping Ratio. The Damping Ratio computed in this frame is wired into a bundle for display in the Response Characteristics Indicator Cluster. The formula used in this frame is based on Equation (A.25) in Appendix A:

$$\omega_n = \sqrt{\left(\frac{BR + k_\tau k_f}{LJ}\right)}$$
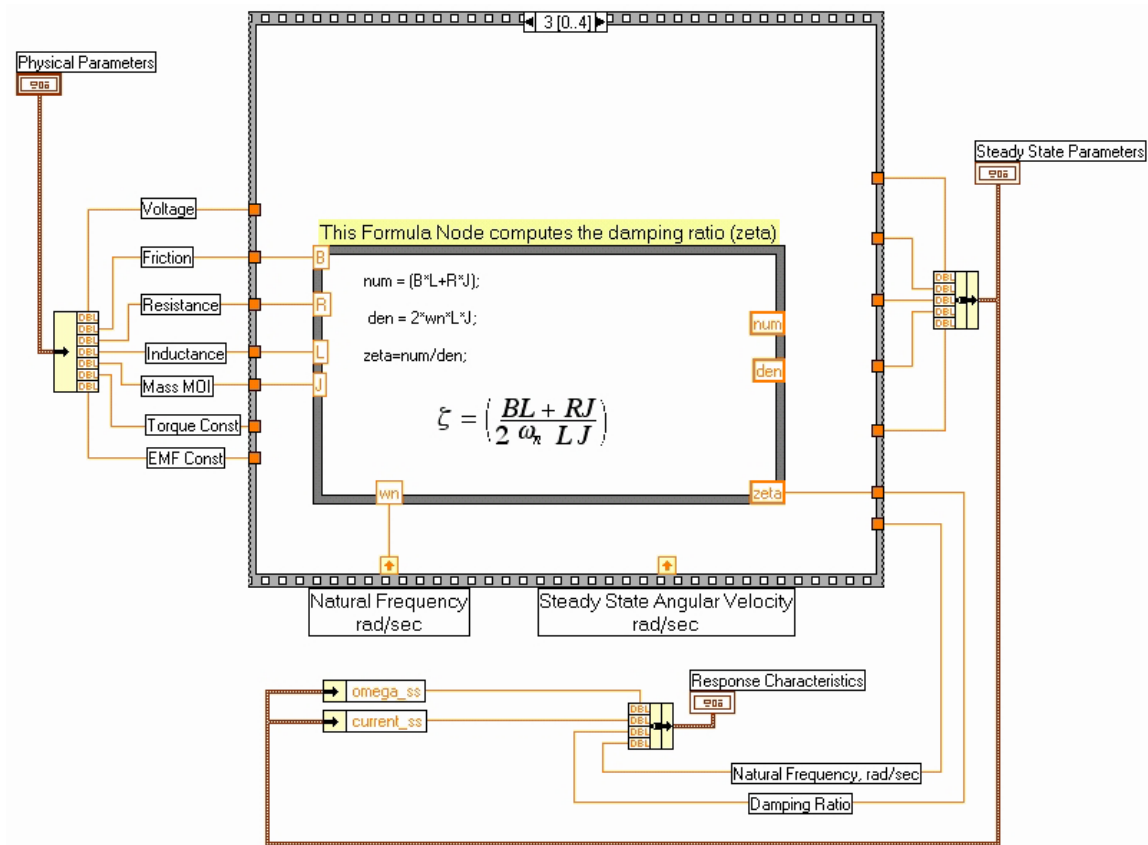
Figure 28: Determination of Damping Ratio

D.   HUMAN DISORIENTATION MODEL

State Space icon	Human Disorientation State Space.vi
f→ω ω→f icon	Freq and Omega 2 way Converter.vi
SCC Hand icon	SCC Hand Math.vi

Table 8: Major Components of The Human Disorientation Model

As with the Centrifuge Dynamic model, the VIs listed in Table 8 deal specifically with the dynamics of a Semi-Circular Canal, more information can be displayed in the user interface. The Control Clusters of this VI are structured so that the model can be run independently, or as component of the combined simulation.
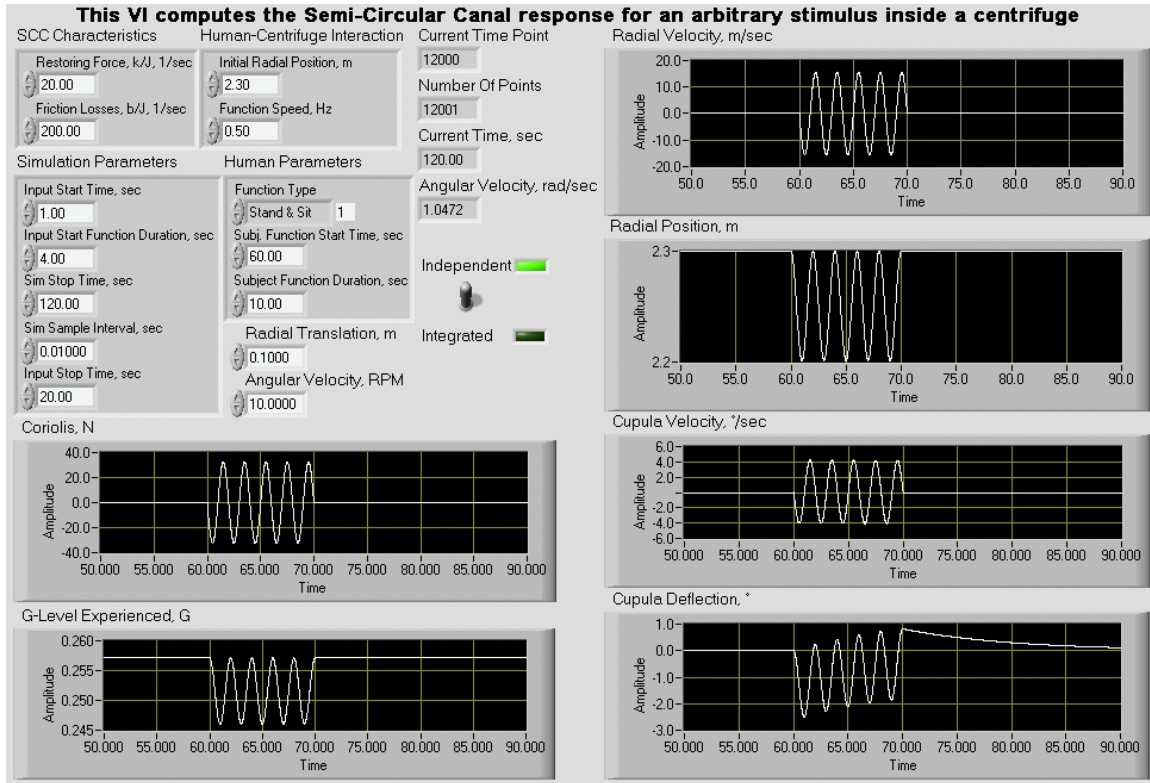
1. Front Panel

Figure 29: Human Disorientation Model User Interface

The front panel of the Human Disorientation Model, shown in Figure 29, is structured so that the user can not only control the simulation (as when running the combined simulation), but can also employ various radial motion functions of the test subject so that different types of motion can be tested. The motion functions are: At-Rest, Stand & Sit, Up Ladder, and Down Ladder. Additional indicators are utilized to show specific facets of the human disorientation, specifically: Cupula Deflection vs. Time, Radial Velocity vs. Time, and Coriolis vs. Time. Finally, a toggle switch is employed to allow the user to change the model between independent and integrated modes. The independent mode allows user manipulation of Centrifuge Angular Velocity as a scalar from the front panel. The default, integrated mode allows the input of a one-dimensional time indexed array of Angular Velocity linked from the Centrifuge Dynamic

41

Model. Visual feedback is employed to test the logic, aid in troubleshooting, and verify the toggle switch position.

2. **Diagram**

a. ***Radial Velocity of a Subject At-rest***

Logic	Case Response
Function Start > Current Time Function Duration + Function Start > Current Time	False
Function Start > Current Time Function Duration + Function Start <= Current Time	True
Function Start <= Current Time Function Duration + Function Start <= Current Time	False

Table 9: Motion Case Logic
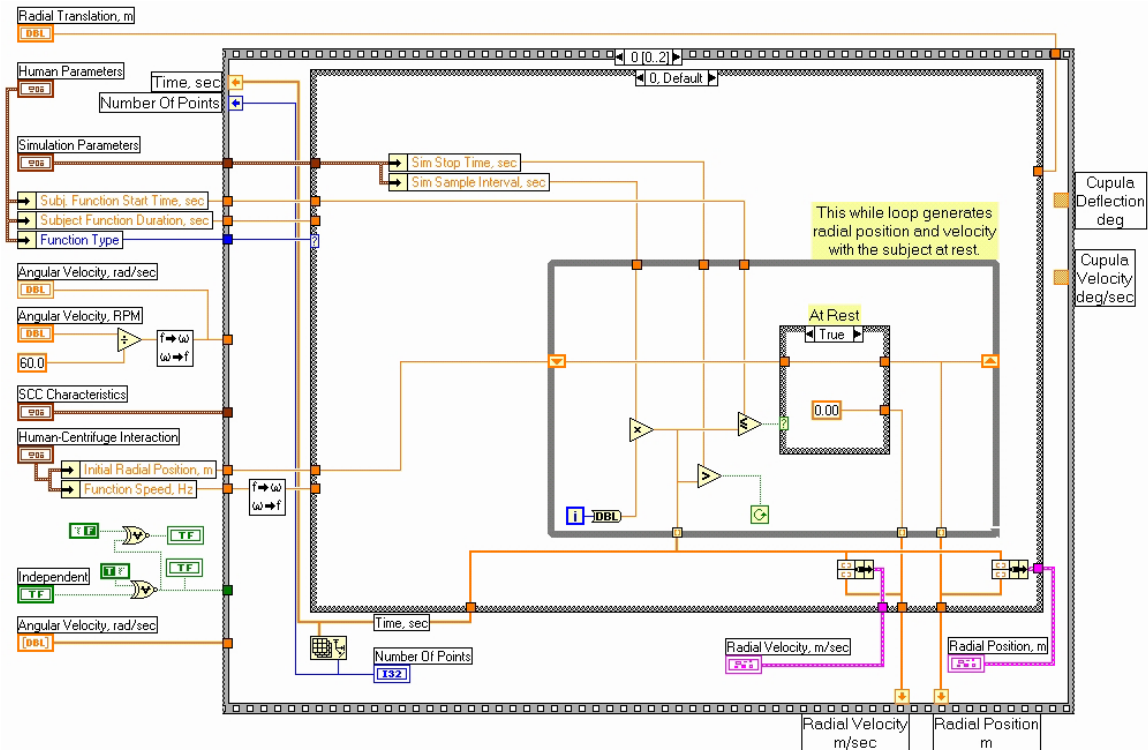
Figure 30: Determination of Subject Radial Velocity when At Rest

The diagram of the Human Disorientation Model contains a Sequence Structure that consists of three frames. The first frame, pictured in Figure 30, collects the user's inputs and computes radial velocity with respect to the motion function. Those inputs are Radial Translation and Angular Velocity scalar controls and the Human Parameters, Human-Centrifuge Interaction, and Simulation Parameters clusters. The motion function is determined through the use of a Ring Control. The default selection of the Ring Control is the Stand & Sit Function. The Ring Control is not designed to be manipulated from a superior VI, therefore when the Centrifuge Dynamic Model is linked within another VI, it will generate its responses using the Stand & Sit Function which means that the subject will stand and sit alternately in a manner determined by the user. In the case of a subject at rest, as shown in Figure 30, the radial velocity will be zero and the radial position will not change.

For each case, a simple logic tree, shown in Table 9, and Case Structure is used to determine when to apply the designated motion function. Radial Position, Radial Velocity, and Time are indexed into one-dimensional arrays and connected to Sequence Locals for later use, bundled with one-dimensional Time arrays, and plotted versus Time on the Front Panel.

b.   *Radial Velocity of a Subject Alternately Standing and Sitting*
The second case, pictured in Figure 31, uses a sine function to generate the motion of a person sitting and standing. The user input, Radial Translation, becomes the amplitude of the sine function. The following equations were utilized:

$$\dot{r} = (1.55\Delta r)\sin(f\Delta t)$$

$$v = \frac{\dot{r}}{\Delta t}; r_{t+\Delta t} = r_t + \dot{r}\Delta t$$
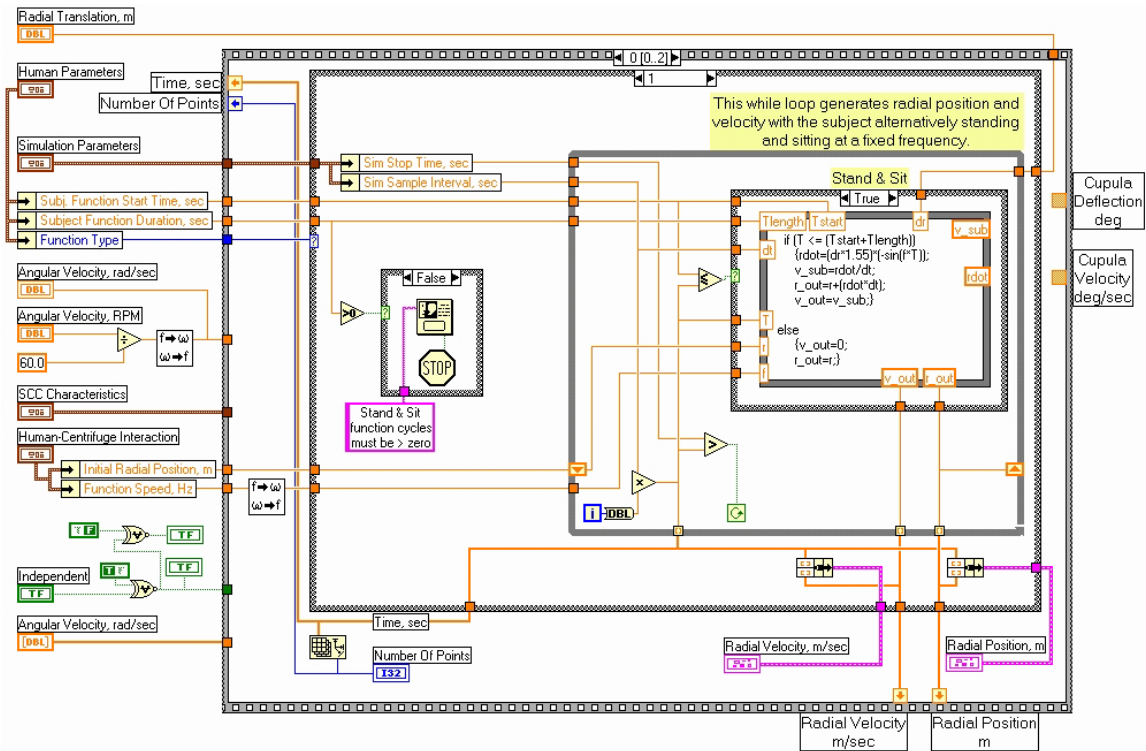
Figure 31: Determination of Subject Radial Velocity when Alternately Standing and Sitting
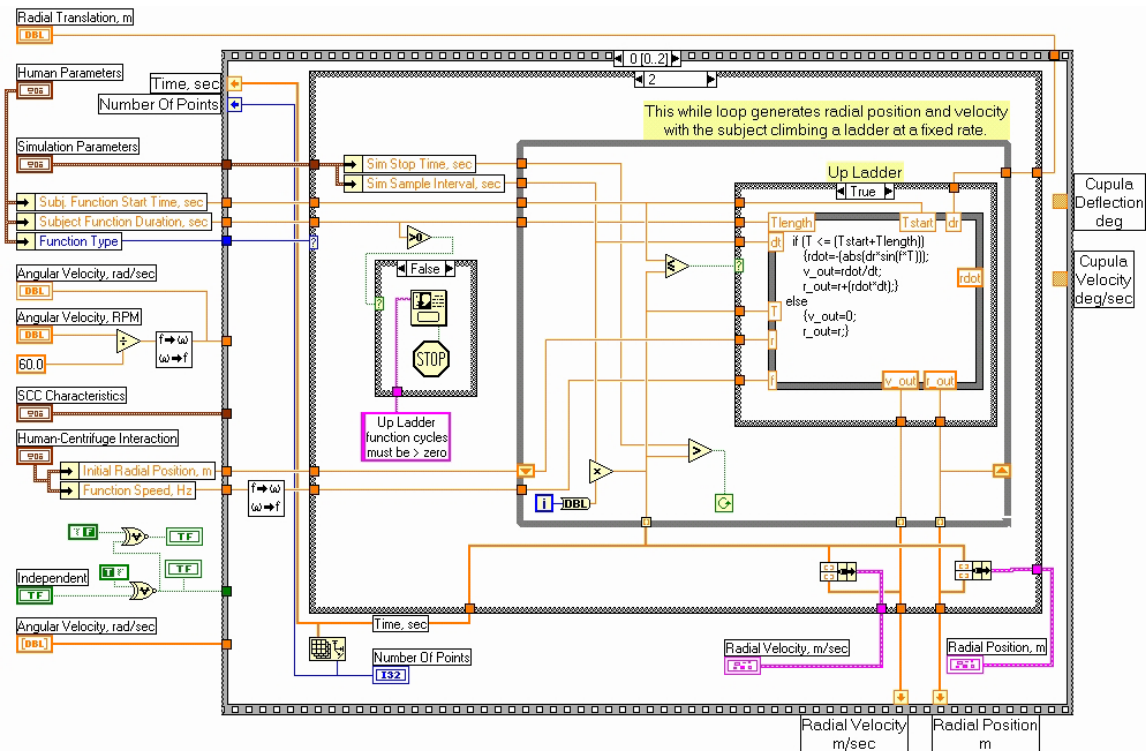
Figure 32: Determination of Subject Radial Velocity when Climbing Up a Ladder

44

c.   Radial Velocity of a Subject Climbing Up a Ladder

The third case, pictured in Figure 32, uses the negative absolute value of a sine function to generate the motion of a person climbing up a ladder. The user input, Radial Translation, becomes the amplitude of that sine function. The following sine function was utilized:

$$\dot{r} = -\left|\Delta r \sin\left(f\Delta t\right)\right|$$

$$v = \frac{\dot{r}}{\Delta t}; r_{t+\Delta t} = r_t + \dot{r}\Delta t$$

d.   Radial Velocity of a Subject Climbing Down a Ladder
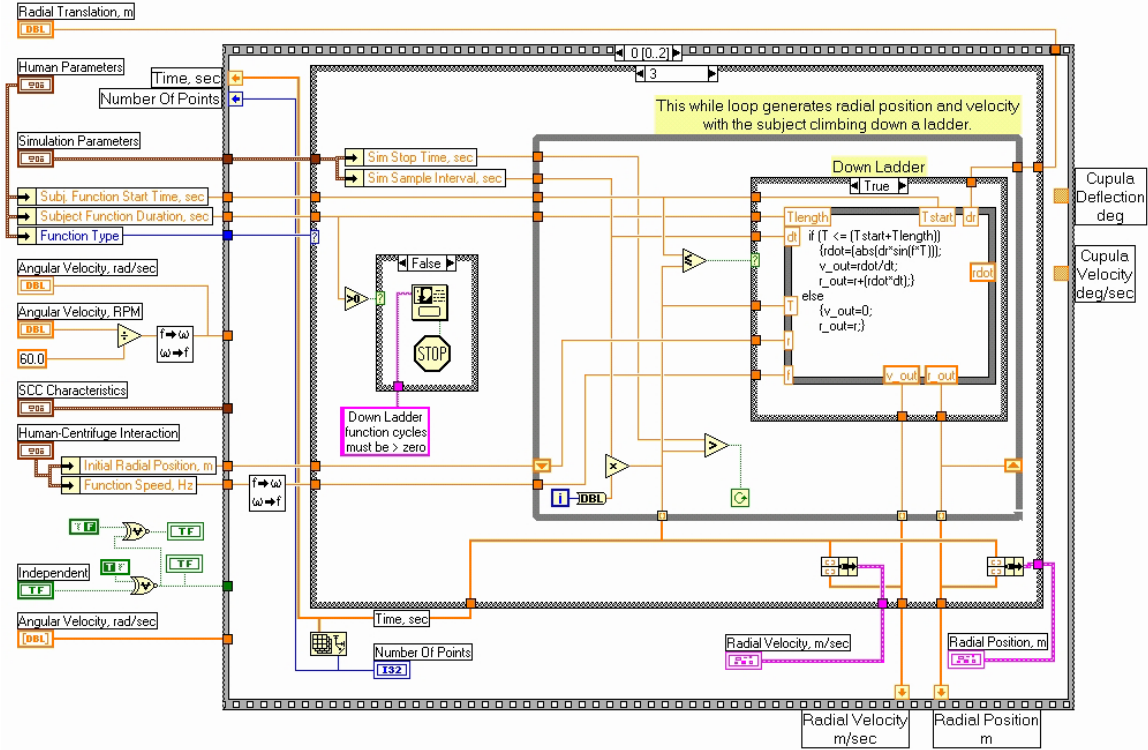
Figure 33: Determination of Subject Radial Velocity when Climbing Down a Ladder

The fourth case, pictured in Figure 33, uses the absolute value of a sine function to generate the motion of a person climbing down a ladder. The user input,

Radial Translation, becomes the amplitude of that sine function. The following sine function was utilized:

$$\dot{r} = \left| \Delta r \sin\left(f \Delta t \right) \right|$$

$$v = \frac{\dot{r}}{\Delta t}; r_{t+\Delta t} = r_t + \dot{r}\Delta t$$

e.   *Semi-Circular Canal Response*

As with the Centrifuge Steady State Response in the Centrifuge Dynamic Model, the Semi-Circular Canal Response in the Human Disorientation Model is computed within a subordinate VI, SCC Hand Math. The various parameters of the Semi-Circular Canal Model: Angular Velocity, Cupula Deflection, Cupula Velocity, Friction Losses, Radial Velocity, Radial Position, and Restoring Force are linked to the subordinate VI with the outputs, Cupula Deflection and Cupula Velocity, linked to Sequence Locals for use in a later frame.
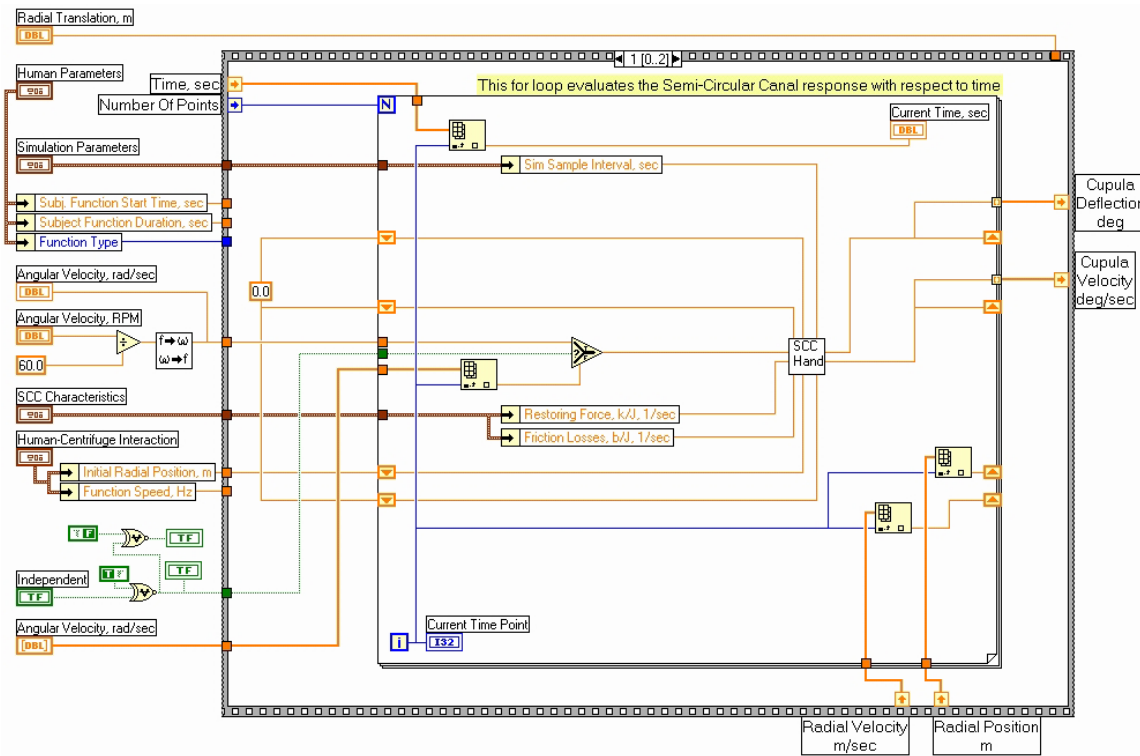
Figure 34: Semi-Circular Canal Response

46

The use of a subordinate VI for the computation of the Semi-Circular Canal Response reduced program complexity, enhanced troubleshooting, and easy substitution of the analytical check case for comparison purposes.

f.   Display of Human Disorientation Model Results

In the final frame of the Human Disorientation Model, the results of the State Space Analysis, Cupula Deflection and Cupula Velocity, together with Coriolis and G-Level Experienced are bundled with a one-dimensional Time array and plotted on the Front Panel.   Auto-indexing was not used with the controls in this VI because when running independently the empty one-dimensional Angular Velocity array would conflict with the auto-indexing capability of *LabVIEW*.
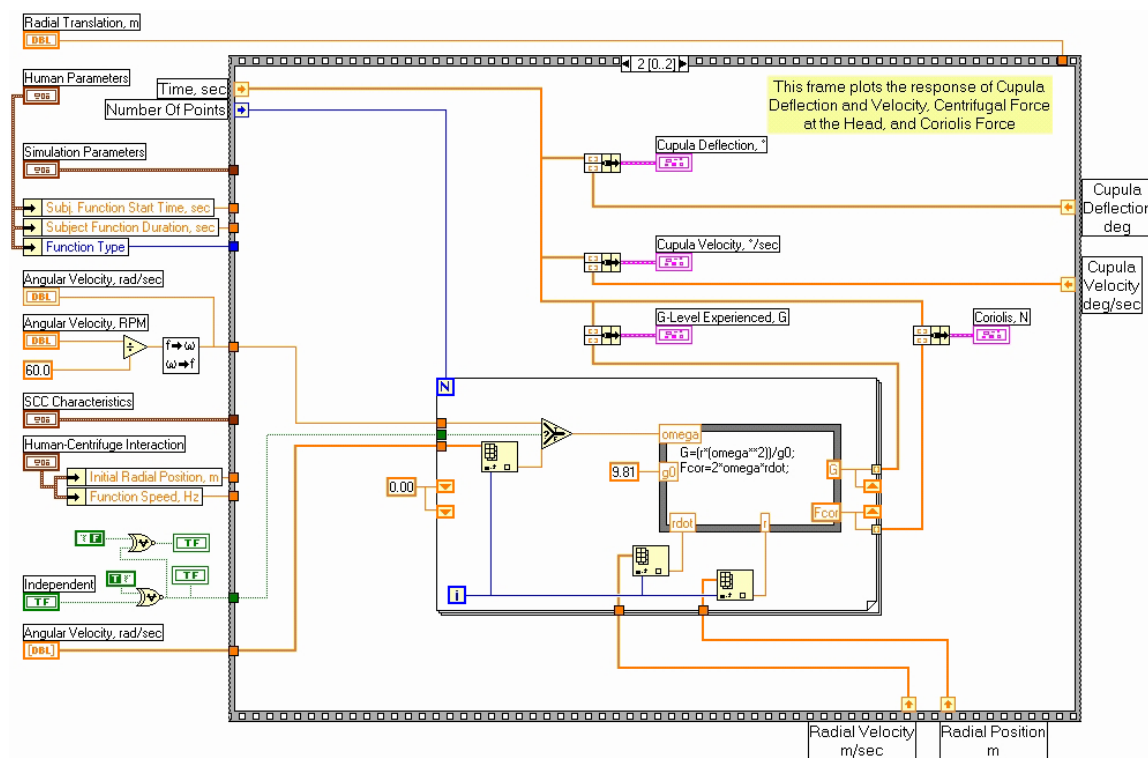
Figure 35: Display of Human Disorientation Model Results

E.   SEMI-CIRCULAR CANAL DYNAMIC MODEL

1.   Front Panel

The front panel of the Semi-Circular Canal Response, shown in Figure 36, is not designed for direct user manipulation.   Rather, this VI is designed to be a subordinate VI nested within the Human Disorientation State Space VI. The input Controls on the Front Panel, which are linked from the Human Disorientation Model, populate the variables of the equations that compute the Semi-Circular Canal Response of a person within a rotating centrifuge.   The output Indicators on the Front Panel, Cupula Deflection and Cupula Velocity, link the results of this VI to the Human Disorientation Model.   The major components of this VI are listed in Table 10.

SCC Hand	SCC Hand Math.vi
$\theta^\circ \rightarrow \theta^r$ $\theta^r \rightarrow \theta^\circ$	Degrees and Radians 2 way Converter.vi

Table 10: Major Components of the Human Disorientation Model
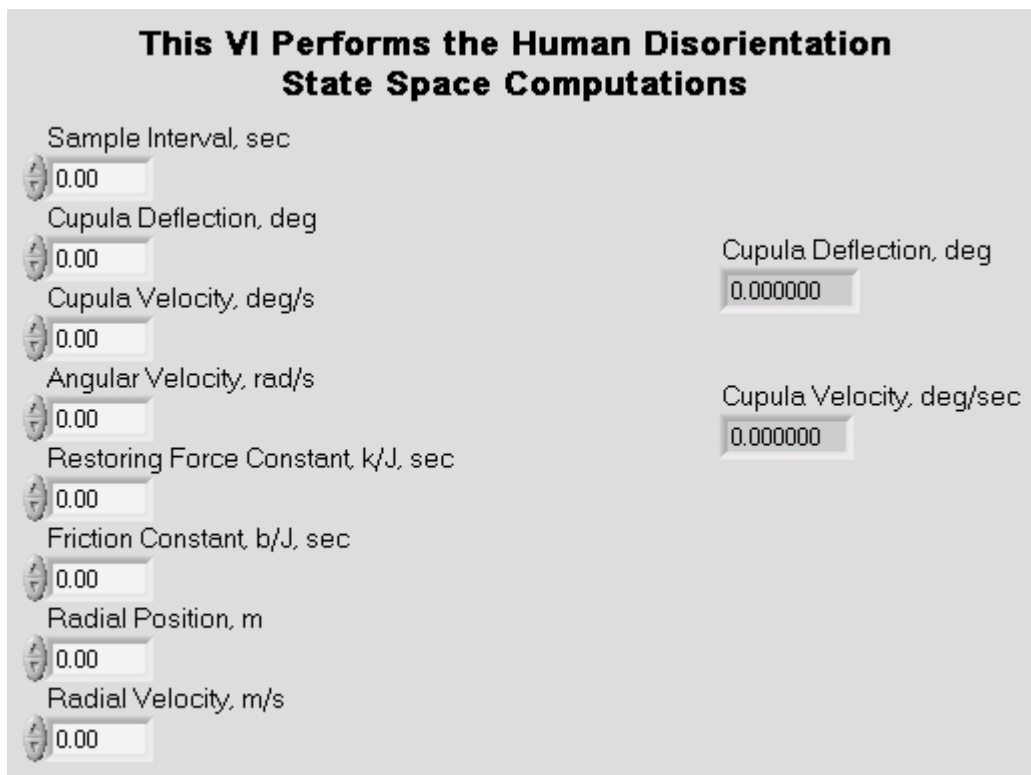
Figure 36: Semi-Circular Canal Dynamic Model User Interface

2.   Diagram

a.   *Cupula Deflection*

The diagram of the Semi-Circular Canal Response contains a Sequence Structure that consists of three frames. The first frame, pictured in Figure 37, collects the linked inputs and calculates Cupula Deflection. Cupula Deflection, computed in radians, is converted to and from degrees when linked outside of this VI for easier human interpretation. The third frame, not pictured, shows the system of equations used in this VI. The formula used in this frame is based on Equation (C.45) in Appendix C:

$$\phi_{t+\Delta t} = \frac{\left(1 + \frac{b\Delta t}{2J}\right)\left(\phi_t + \frac{\dot{\phi}_t \Delta t}{2}\right) + \left(-\frac{k\phi_t \Delta t^2}{4J} + \frac{\dot{\phi}\Delta t}{2} - \frac{b\dot{\phi}_t \Delta t^2}{4J} + \frac{2\omega V_R \Delta t^2}{2R}\right)}{1 + \frac{b\Delta t}{2J} + \frac{k\Delta t^2}{4J^2}}$$
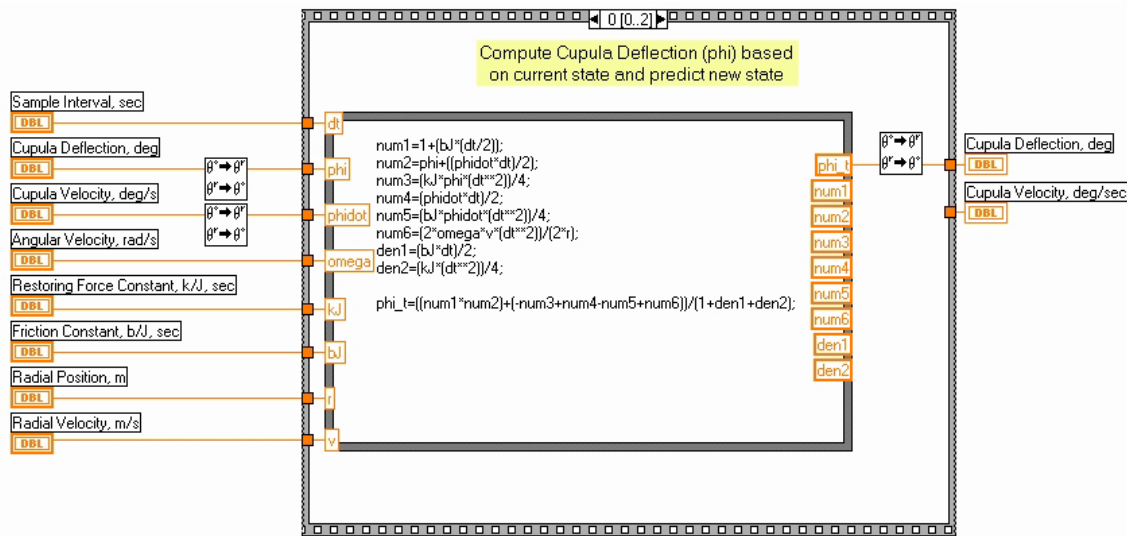
Figure 37: Determination of Cupula Deflection

b.   *Cupula Velocity*

The second frame, pictured in Figure 38, collects the linked inputs and calculates Cupula Velocity. Cupula Velocity, computed in radians per second, is converted to and from degrees/second when linked outside of this VI for easier human interpretation. The formula used in this frame is based on Equation (C.46) in Appendix C:

$$\dot{\phi}_{t+\Delta t} = \frac{\left(-\frac{k\Delta t}{2J}\right)\left(\phi_t + \frac{\dot{\phi}_t \Delta t}{2}\right) + \left(-\frac{k\phi_t \Delta t}{2J} + \dot{\phi} - \frac{b\dot{\phi}_t \Delta t}{2J} + \frac{2\omega V_R \Delta t}{R}\right)}{1 + \frac{b\Delta t}{2J} + \frac{k\Delta t^2}{4J^2}}$$
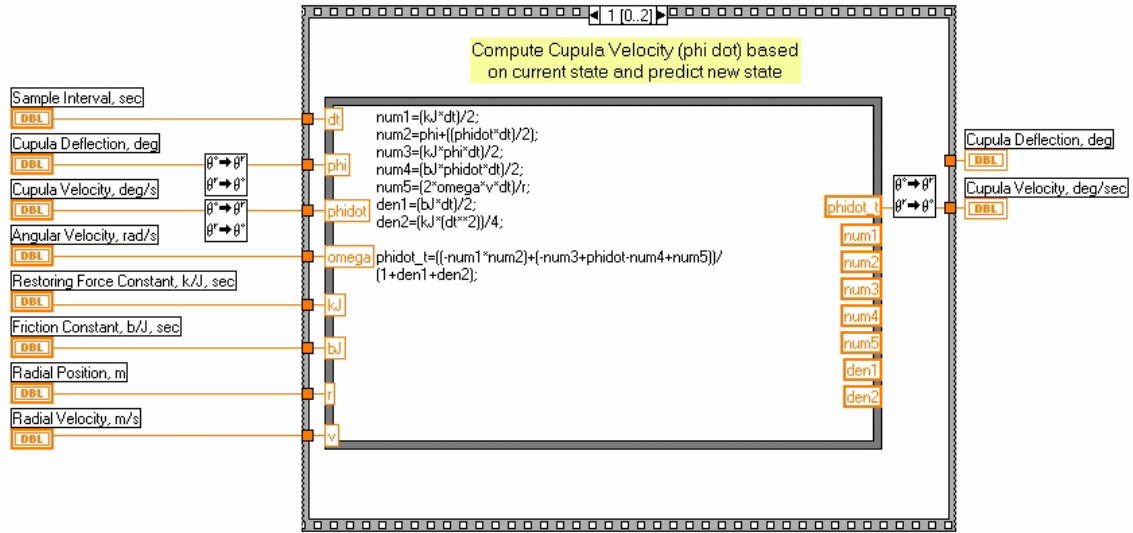
Figure 38: Determination of Cupula Velocity

IV.   RESULTS

A.   7.5 FOOT RADIUS CENTRIFUGE FOR VALIDATION EXPERIMENT

Figure 39: Experimental Apparatus and Volunteer Test Subjects

A 7ft. 6.5in. (1.15m) diameter Merry-Go-Round, pictured in Figure 39 was found on the Former Fort Ord in Marina, CA that enabled the conduct of a non-scientific validation experiment. This brief experiment, conducted between 9 and 10 AM on 10 September 2002, served to determine the relationship between the computer model's quantitative results and a person's qualitative experience. This experiment should be viewed as a rough guide for those conducting follow-on studies to establish the parameters to scientific experiments or the analysis of preexisting data.

1.   Test Subjects

A small number of test subjects were selected from Naval Postgraduate School students in the Space Systems Operations curriculum graduating in September 2002. They were selected due to their acquaintance with the author, their scheduling flexibility, and the variety of their military experience. The volunteers were briefed on how the

experiment would be conducted, and were instructed to report the discomfort they experienced during the three phases of each run. The small population of test subjects used in this experiment do not constitute a scientific sampling of results; however, these results provided anecdotal evidence of the level of discomfort experienced at particular cupula velocities.

Name	Background
LT Chris Howse, USNR	Naval Surface Warfare, Destroyers
CPT Mike York, USA	Army Air Defense Artillery, Patriot
LT Wes Sanders, USN	Naval Flight Officer, E-2C Hawkeye

Table 11: Test Subjects and Their Backgrounds

2.   0 Revolutions Per Minute

Cyclical movement of the head in a normal, non-rotating, environment did not produce disorientation in any of the test subjects.

3.   10 Revolutions Per Minute

a.   *Model Predictions*

The LabView computer model developed using the analysis contained in Appendix C predicted Cupula Deflections ranging from −5° to 1.75° and Cupula Velocities as great as ±9°/sec. The predicted Centrifugal Force was a maximum of about 0.13G.

b.   *Subject Experiences*

Utilizing the disorientation scale developed in Table 3, the test subjects were exposed (as closely as available equipment would permit) to the modeled conditions. During the first phase all subjects reported no feeling of disorientation or a Disorientation Level of 1 (Level 1). In the second phase all subjects reported a Level 2. In the third phase all subjects reported Level 1 to 1.5.
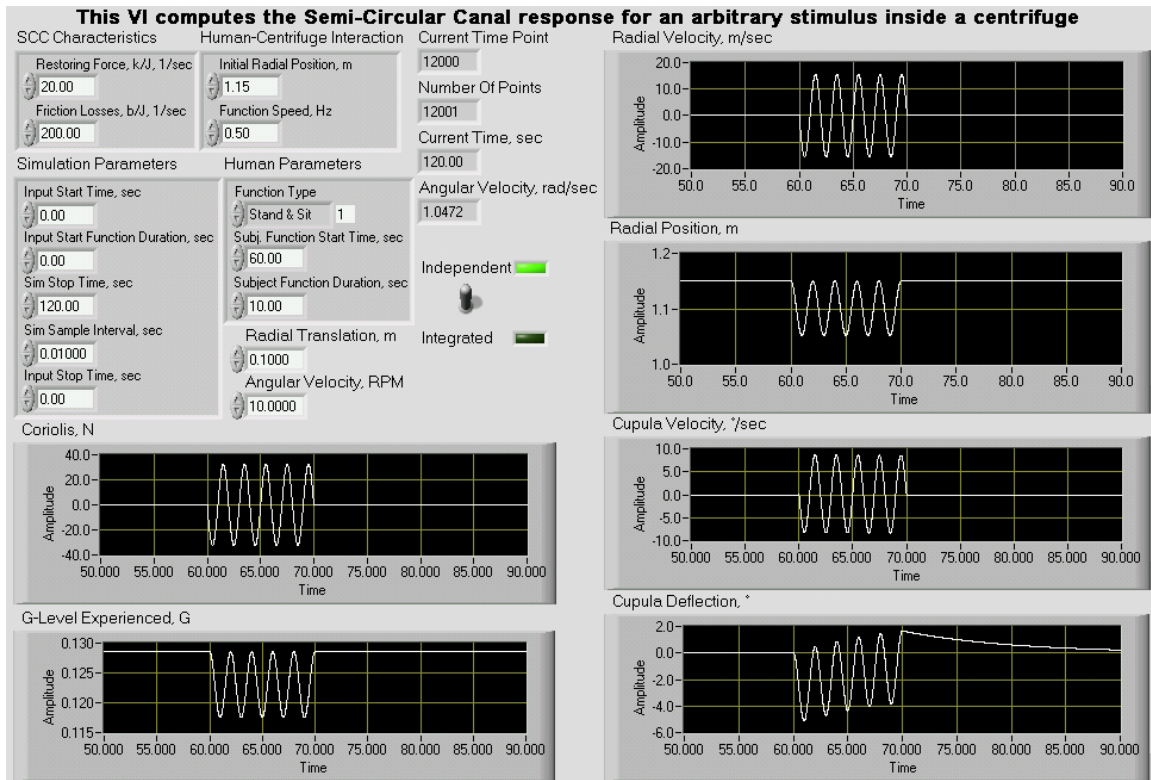
Figure 40: 10 RPM Validation Experiment Prediction

4. 20 Revolutions Per Minute

a. *Model Predictions*

The LabView computer model predicted Cupula Deflections ranging from −10° to 3°, Cupula Velocities as great as ±18°/sec, and Centrifugal Force at a maximum of about 0.51 G.

b. *Subject Experiences*

Once again using the scale developed in Table 3, the test subjects were exposed to the modeled conditions. During the first phase all subjects reported a Level 2 sensation largely resulting from Centrifugal Force. In the second phase, a Level 4 feeling was reported with the addition of an oculogyral illusion of the horizon rolling in phase with the head motion, a direct indication of the Coriolis induced torque in the axial plane shown in Equation (C.10). Finally, in the third phase a Level 3 feeling was reported.

Figure 41: LT Sanders Demonstrating the Test Subject's Perspective

Figure 42: LT Sanders Demonstrating Experiment Phases One and Three.

Figure 43: The Author Demonstrating Maximum Radial Position of the Head During Phase Two. Photograph by LT Wesley Sanders, USN

**Figure 44: The Author Demonstrating Minimum Radial Position of the Head.
Photograph by LT Wesley Sanders, USN**
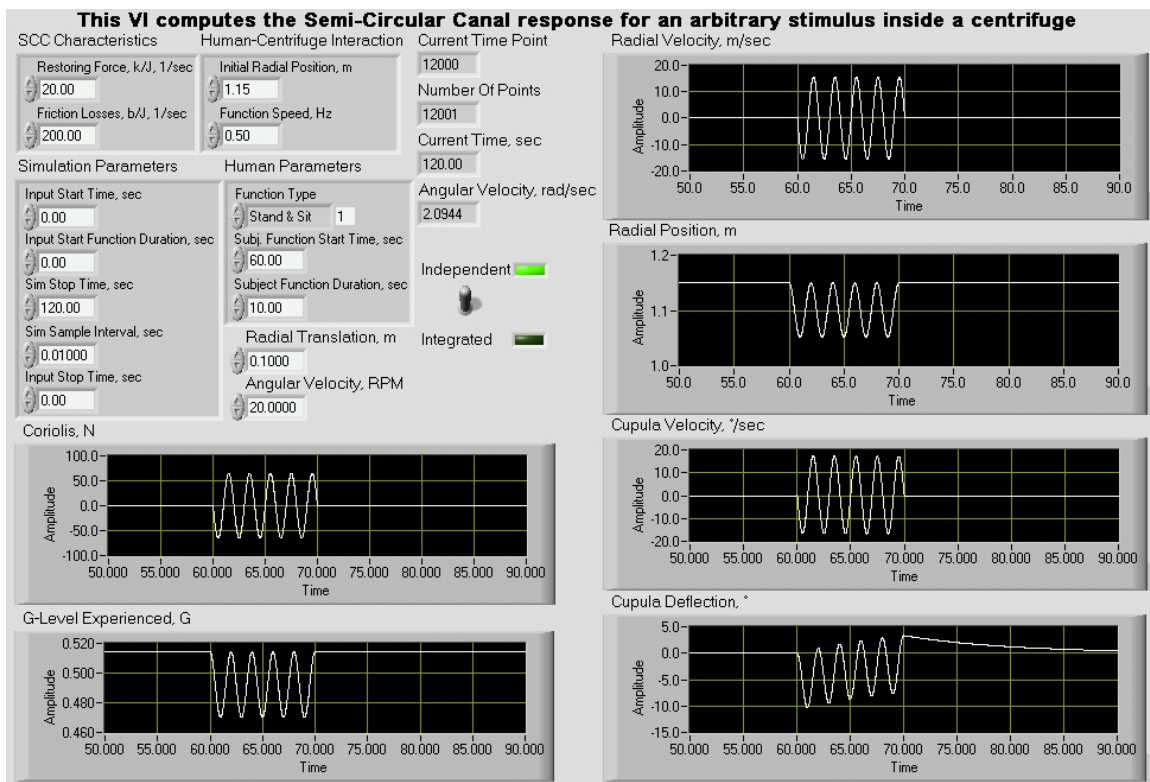
Figure 45: 20 RPM Validation Experiment Prediction

c. *Discussion of Validation Experiment Results*

Of particular note is the direct relationship between Angular Velocity, Coriolis, and Cupula Velocity shown in the computer model. This relationship was

55

repeated during the validation experiment as shown below in Table 12. It is also worth noting that Centrifugal Force quadrupled when Angular Velocity was doubled.

	10 RPM	20 RPM
Phase 1	1	2
Phase 2	2	4
Phase 3	1 to 1.5	3
Cupula Velocity	±9°/sec	±18°/sec
Centrifugal G	0.13	0.52

Table 12: Validation Experiment Results

Using the results in Table 12, larger centrifuges can be modeled by changing the parameters of the centrifuge. Noting that a minimal amount of discomfort was experienced at 10 RPM on a 1.15 m Centrifuge. The computer model shall evaluate 1.25 m (ISS CAM), 2.5 m, 5 m, and 10 m Centrifuges at no more than ±9°/sec of Cupula Velocity.

B.   1.25 METER RADIUS CENTRIFUGE

The ISS Centrifuge (not much larger than the Merry-Go-Round used in the validation experiment) is designed to accommodate small biological experiments within a gravitational environment that ranges from 0.01 G to 2 G[46]. The ISS Centrifuge is not designed to accommodate humans. However, should experiments be carried out to study the ability of a subject to tolerate Coriolis induced disorientation, the results in Figure 46 should serve to guide their development. The computer model, as shown in Figure 46, predicts Cupula Deflection results equivalent to those in the 10RPM Validation Experiment will be achieved at 11 RPM and 0.17 G when the same head motion is performed at the centrifuge's maximum radius. Note that 10 cm of increased centrifuge radius yields 0.04 G of increased Centrifugal Force at a level of disorientation that was deemed tolerable by the test subjects in the Validation Experiment.

---

[46] "Centrifuge"
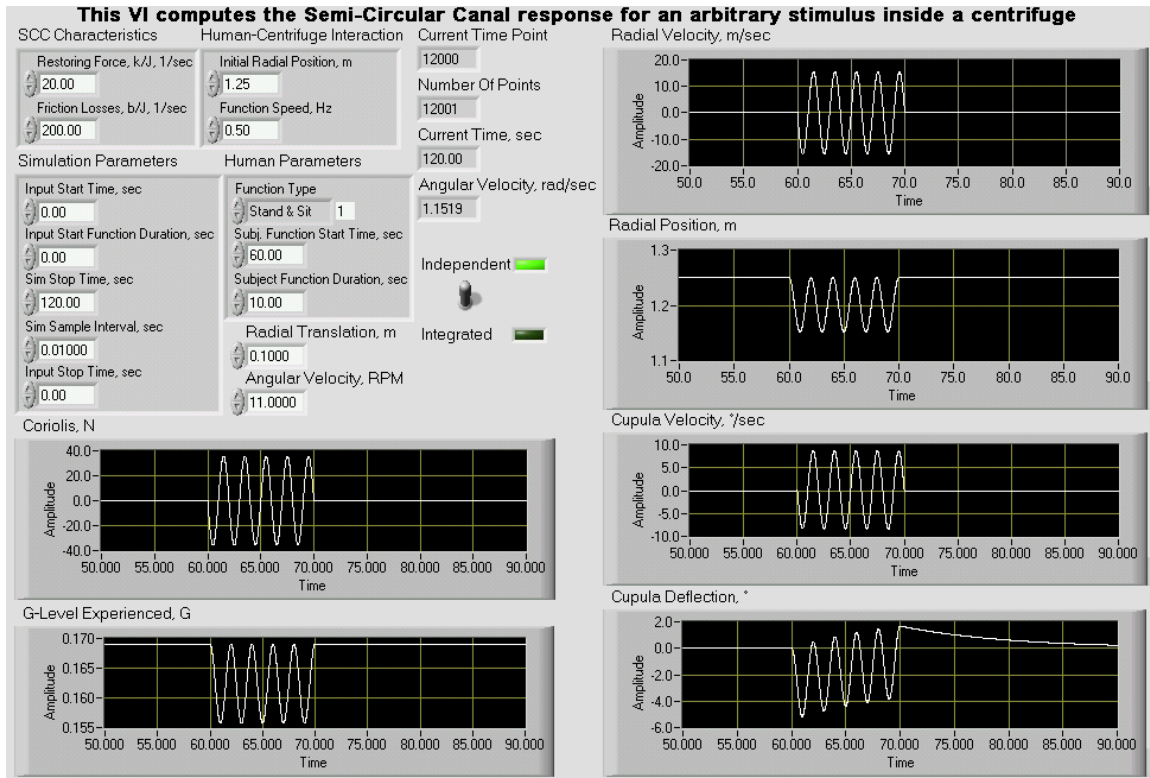
Figure 46: 1.25 m Centrifuge Human Disorientation Prediction

Additionally, the ISS Centrifuge Specifications shown in Table 1 allow for the development of a Centrifuge Dynamic Model for the purposes of scaling the properties of the ISS Centrifuge to fit larger centrifuges more suited for human occupation. Figure 47 details the results of the Centrifuge Dynamic Model when the ISS Centrifuge Specifications are used as the input parameters (2 G, 1.25 m throw arm/inner radius, and 300 sec. spin-up).

Increasing the EMF Proportionality Constant so that the Centrifugal Force is 1 G yields the results shown in Figure 48. By leaving the Electrical Parameters constant and changing the Inner and Outer Radius, the Centrifuge Dynamic Model can be scaled to approximate the effects of a similar, but larger, centrifuge on a spacecraft like the ISS.
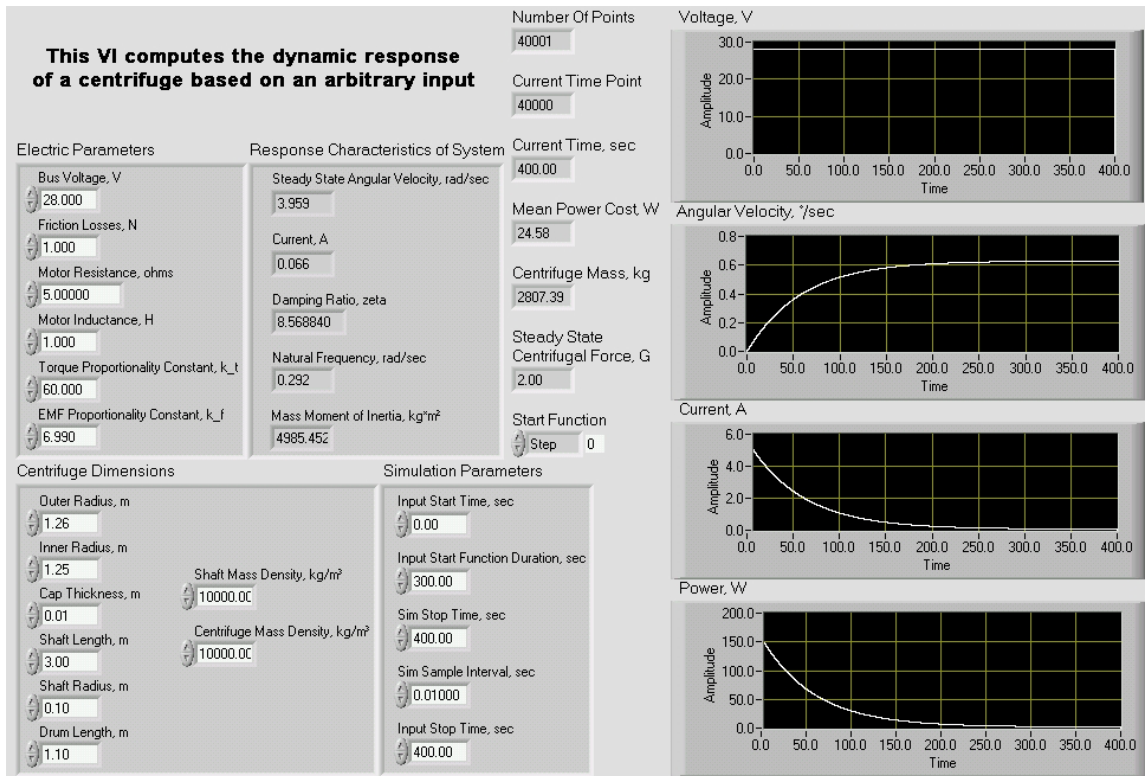
Figure 47: Centrifuge Dynamic Model of the ISS Centrifuge at 2 G
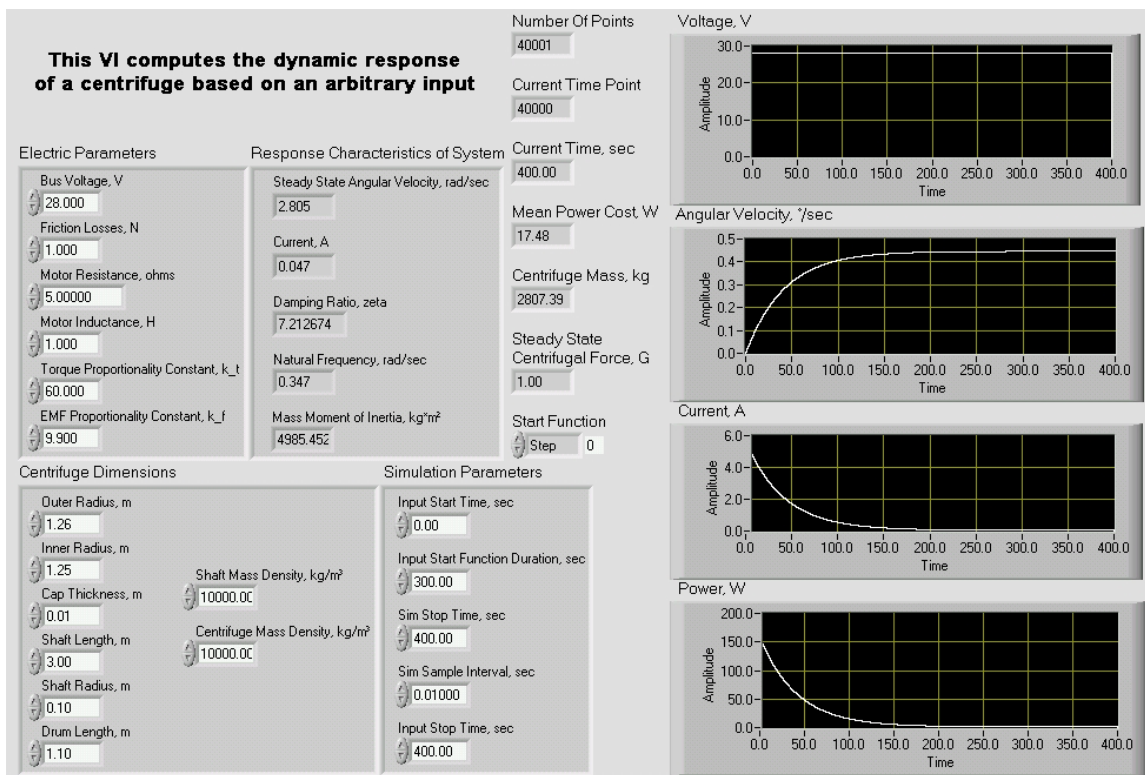
Figure 48: Centrifuge Dynamic Model Of The ISS Centrifuge At 1 G

58

C. 2.5 METER RADIUS CENTRIFUGE

A centrifuge with a 2.5 meter radius could contain a compartment large enough to accommodate a person and some limited exercise equipment. What would be the effect of Coriolis on a person exercising within such a rotating environment. Before modeling these conditions, the following assumptions must first be made: the astronaut is 1.83 m. (6 ft.) tall, when moving from a seated to a standing position the astronaut will translate radially through 0.3 m (1 ft.) to simulate a normal range of movement. The astronaut will start from a squatting position with his head at a radial position of 0.97 m (as if performing military presses on an exercise machine), the astronaut's feet will be at a radial position of 2.5 m, and the centrifuge will be spinning at 18.9 RPM to attain 1 G at the inner radius of the rotating drum.
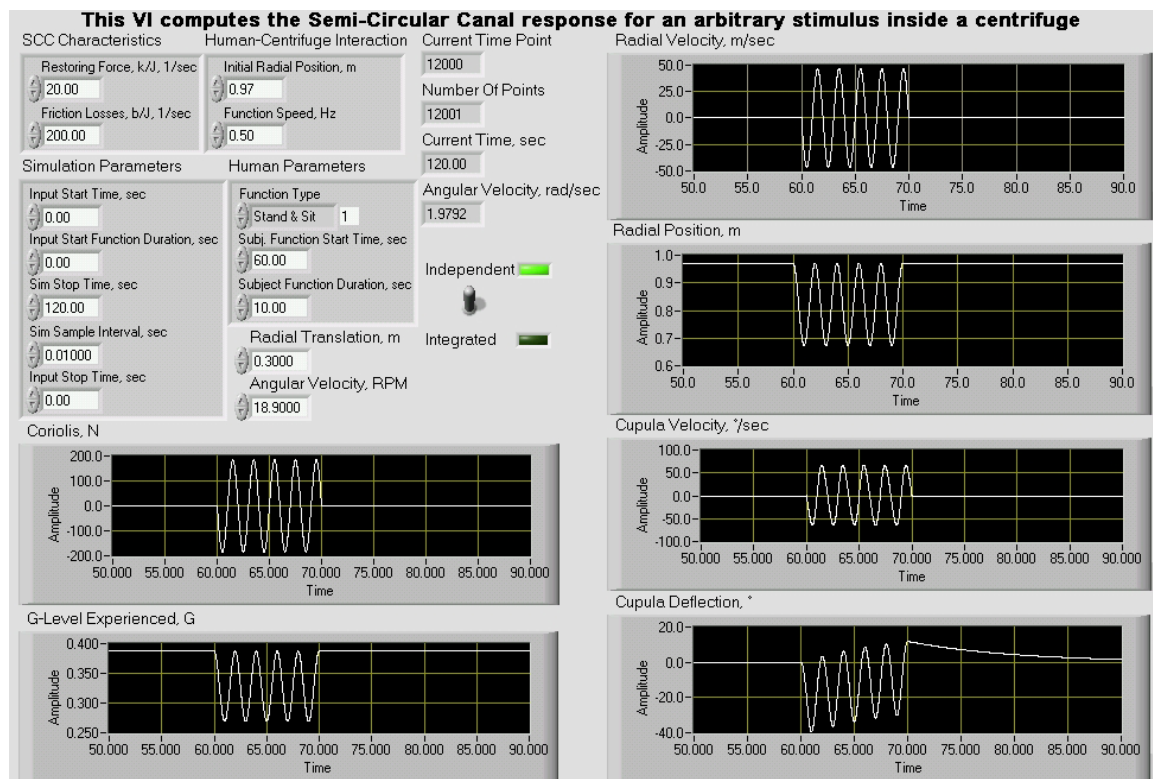
Figure 49: 2.5 Meter Centrifuge Human Disorientation Prediction at 1 G

A Human Disorientation Model of the 2.5 meter centrifuge at 1 G predicted a Cupula Velocity of ±70°/sec and Cupula Deflections between –20° and 10°. These

59

results are significantly greater than the Cupula Velocity and Deflection experienced during the 20 RPM Validation Experiment and would likely make the astronaut experiencing them very ill. The results are pictured in Figure 49.

Reducing the centrifuge angular velocity to 2.5 RPM yields results that more closely match the results from the validation experiment. As shown in Figure 50, Cupula Velocity was ±9°/sec and Cupula Deflection ranged between 1.75° to –5°. However, the Centrifugal Force at centrifuge's inner radius was less than 0.02 G. Based on these results, a 2.5 Meter Centrifuge would not provide a suitable environment for an astronaut to move about normally and exercise.
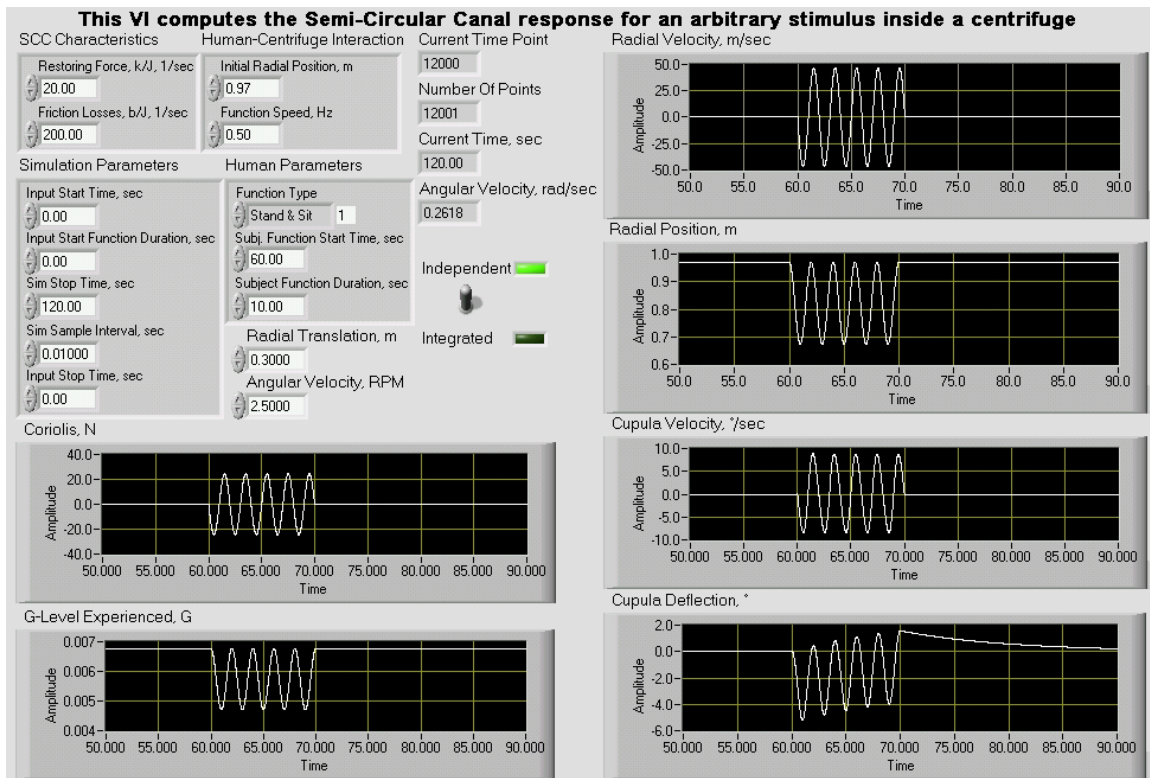
Figure 50: 2.5 Meter Centrifuge with Minimal Disorientation

D.   5 METER RADIUS CENTRIFUGE

1.   Human Disorientation

What would be the effect of Coriolis on a person moving about within a 5 meter radius centrifuge? Perhaps such a centrifuge could contain an exercise facility for

astronauts on a long term mission. Adapting the assumptions from the 2.5 m Centrifuge Analysis, the astronaut is 1.83 m (6 ft) tall. When moving from a seated to a standing position the astronaut will translate through 0.3 m in the radial plane, start from a squatting position with his head at a radial position of 3.47 m, and his feet will be at a radial position of 5 m. The centrifuge will be spinning at 13.38 RPM to attain 1 G at the inner radius of the rotating drum.

In the 5 m centrifuge, Cupula Velocity at 1 G was predicted to be ±12°/sec and the Cupula Deflection results ranged between −7° and 2.25°. These results are within the range of tolerance experienced during the Validation Experiment and an astronaut could possibly adapt to their effects. The results are pictured in Figure 51.
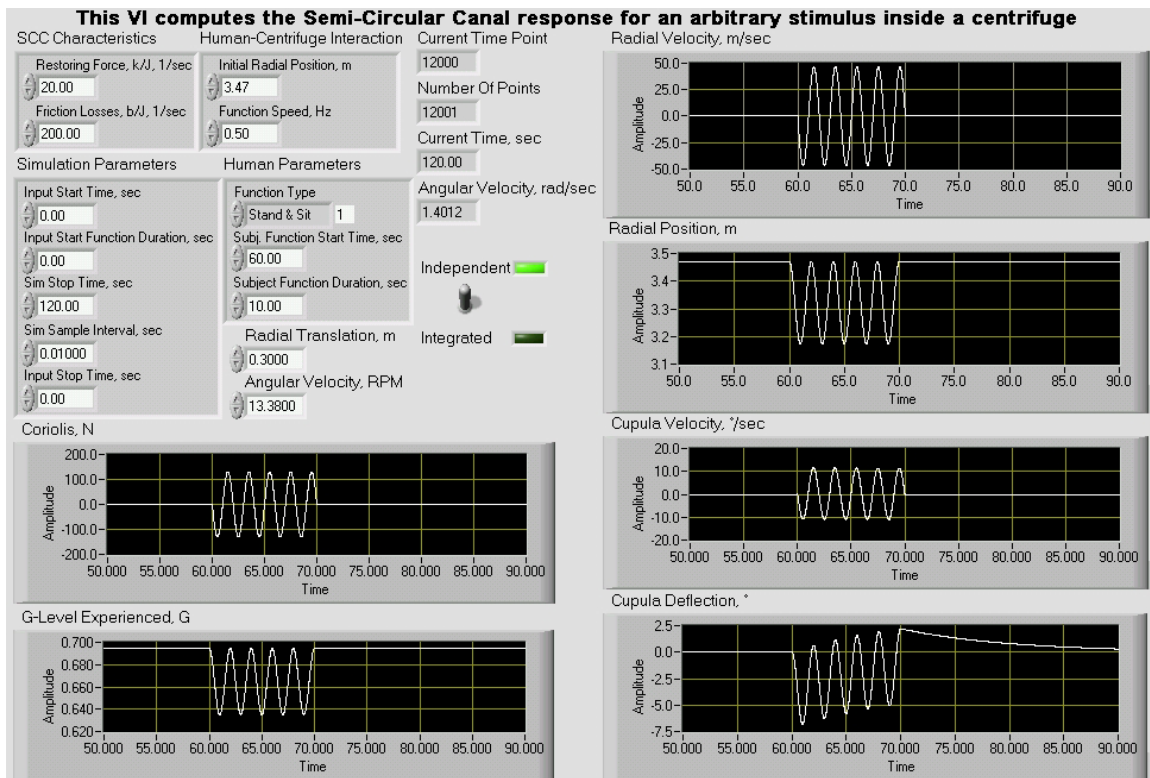
Figure 51: 5 Meter Centrifuge Human Disorientation Prediction at 1 G

Reducing the centrifuge angular velocity to 10 RPM yields results that more closely match the results from the 10 RPM validation experiment. As shown in Figure 52, Cupula Velocity was ±9°/sec and Cupula Deflection ranged between −5° to 1.5°.

However, the G-Level at the outer radius was reduced to 0.56 G. Based on these results, a 5 Meter Centrifuge would provide an astronaut the benefit of "Fractional G" to move about and exercise. However, at 1 G, there would be some disorientation and its usefulness would depend on the astronaut's ability to adapt.

2. Centrifuge Dynamic Model

Because of the possibility that a 5 m Centrifuge producing 1 G of Centrifugal Force might be useful; the Centrifuge Dynamic Model in Figure 48 was reconfigured to have an Outer Radius of 5.01 m, an Inner Radius of 5.00 m, and an EMF Proportionality Constant of 19.9. The results pictured in Figure 53 show that such a Centrifuge would require over 1 hour to spin-up and would weigh about 20200 kg.
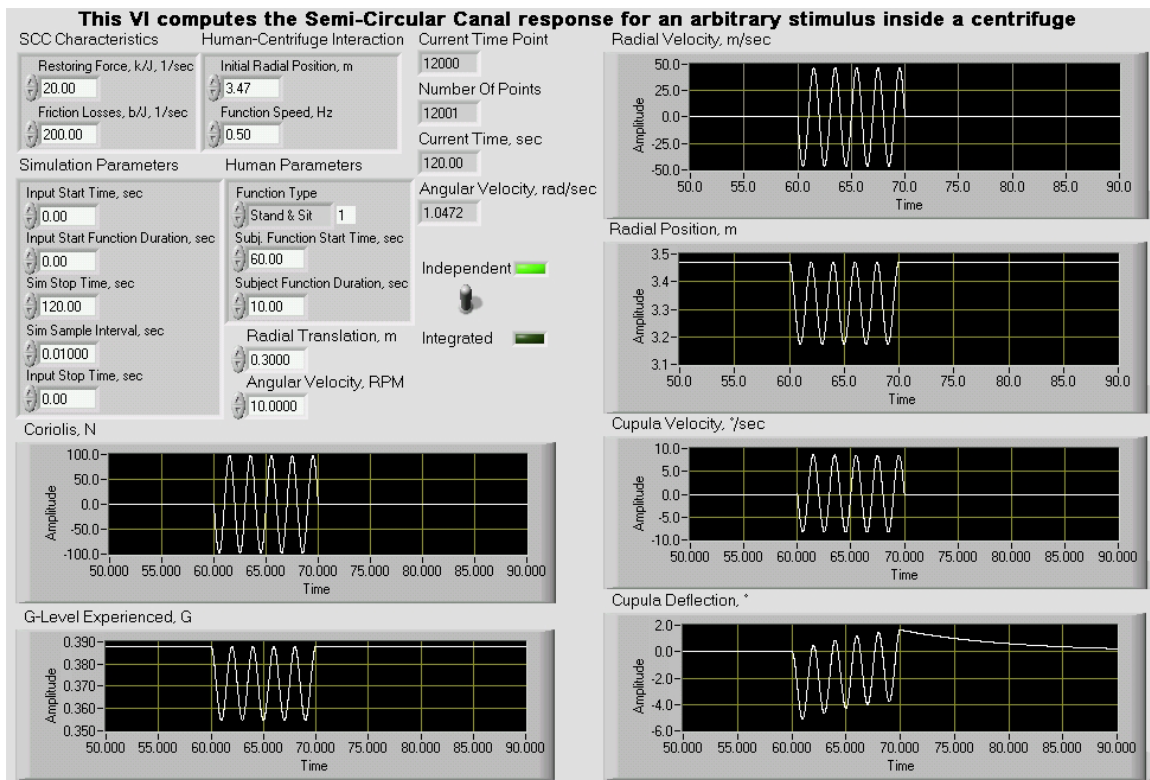
Figure 52: 5 Meter Centrifuge with Minimal Disorientation
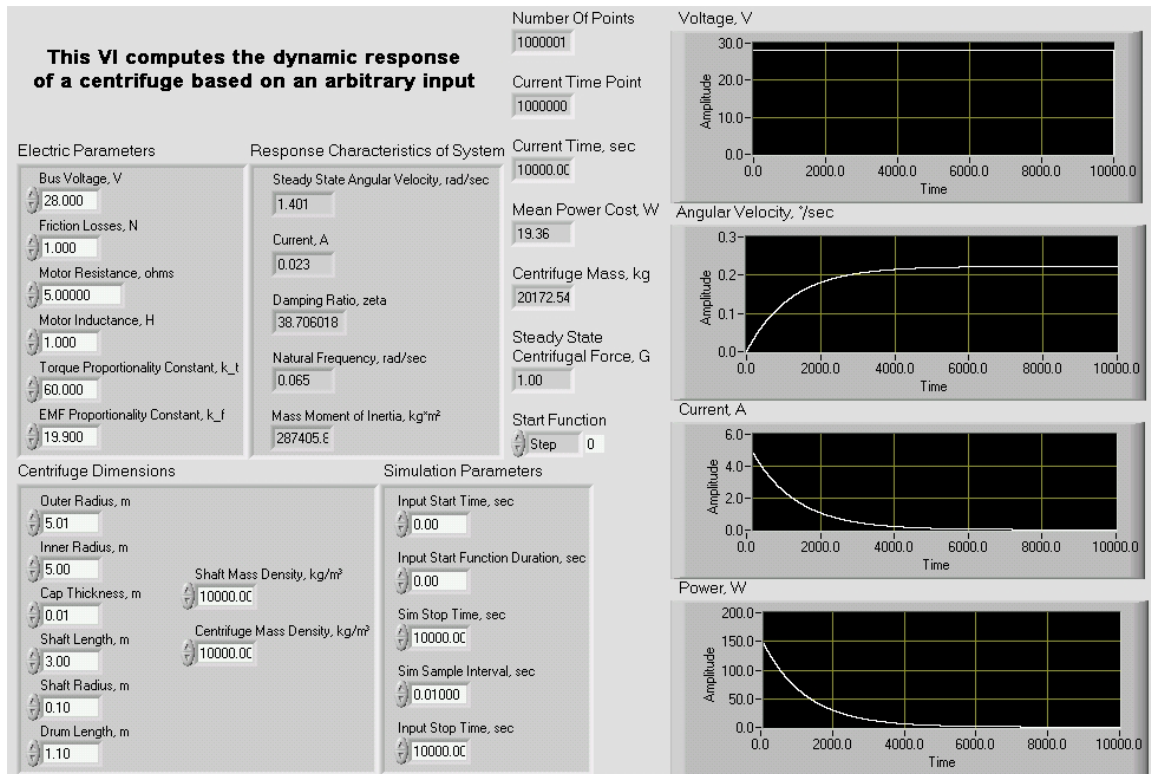
Figure 53: Centrifuge Dynamic Model of a 5 Meter Centrifuge at 1 G

E.   10 METER RADIUS CENTRIFUGE

1.   Human Disorientation

Again, what would be the effect of Coriolis on a person moving within a 10 meter radius centrifuge? Perhaps such a centrifuge could serve as a complete habitat containing berthing, exercise, and food preparation facilities. Adapting the assumptions from the 2.5 m Centrifuge Analysis, the astronaut is 1.83 m (6 ft) tall. When moving from a seated to a standing position the astronaut will translate through 0.3 m in the radial plane, start from a squatting position with his head at a radial position of 8.47 m, and his feet will be at a radial position of 10 m. The centrifuge will be spinning at 9.46 RPM to attain 1 G at the inner radius of the rotating drum.

In the 10 meter centrifuge at 1 G, Cupula Velocity was predicted to be ±2.75°/sec and Cupula Deflection ranged between −1.6° and 0.6°. These results, pictured in Figure 54, are less than those from the 10 RPM validation experiment and should be well tolerated by an astronaut. Based on these results, a 10 Meter Centrifuge would provide

an astronaut the benefit of a 1 G gravity field to move about and exercise without significant disorientation.
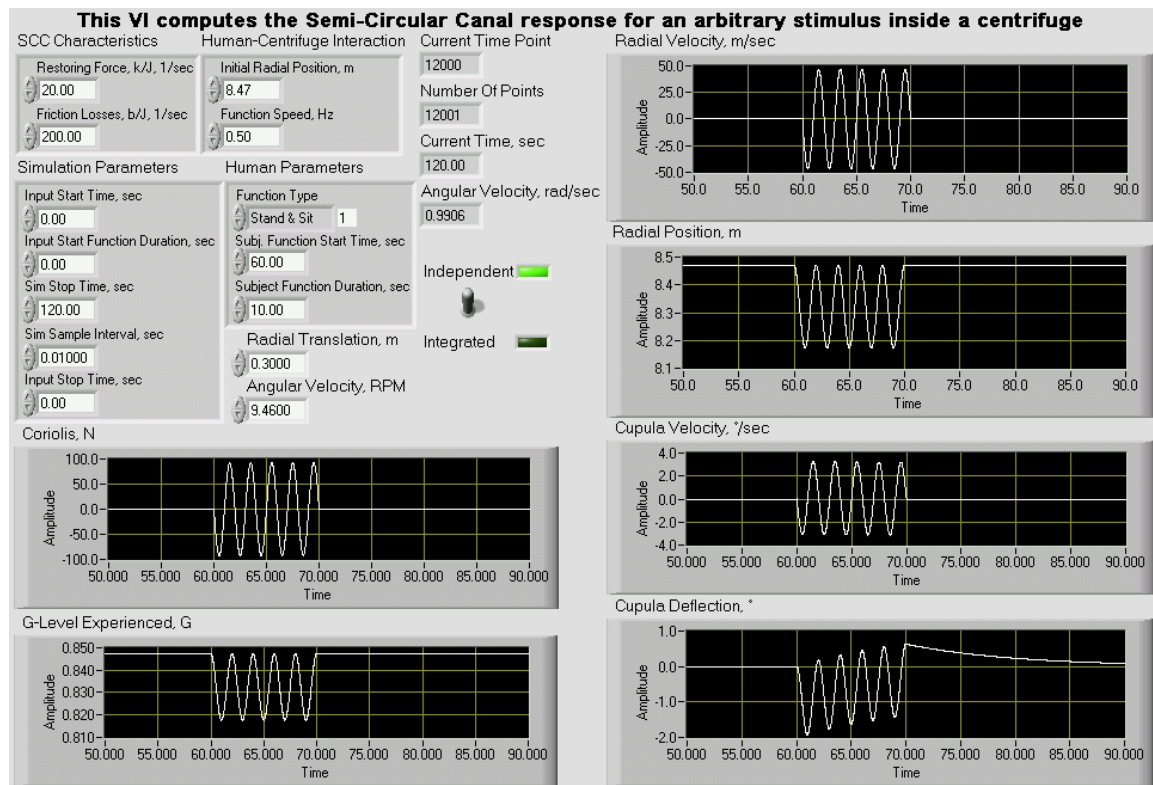
Figure 54: 10 Meter Centrifuge Human Disorientation Prediction at 1 G

2. Centrifuge Dynamic Model

Because of the possibility that a 5 m Centrifuge producing 1 G of Centrifugal Force might be useful; the Centrifuge Dynamic Model in Figure 48 was reconfigured to have an Outer Radius of 10.01 m, an Inner Radius of 10.00 m, and an EMF Proportionality Constant of 28.2. The results pictured in Figure 53 show that such a Centrifuge would require nearly 19.5 hours to spin-up and would weigh about 70800 kg.

F. COLLECTED RESULTS

The results of the model centrifuges, with respect to the human tolerance of Coriolis found during the Validation Experiment are listed in Table 13.
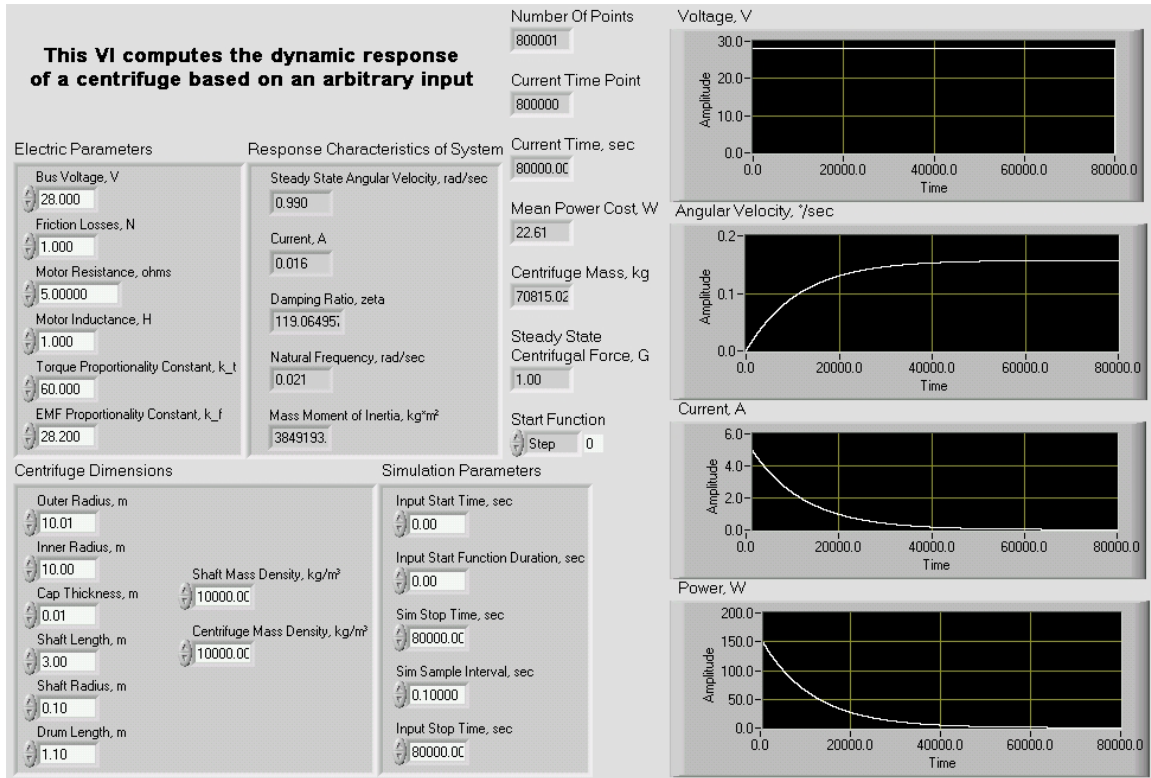
Figure 55: Centrifuge Dynamic Model of a 10 Meter Centrifuge at 1 G

Radius m	Radial Position m	Tolerable Speed RPM	Tolerable Centrifugal Force RPM	Spin Up Time min	Mass kg	Peak Power W	Steady State Current A	Power Required mW/s
2.5	0.97	2.5	0.02					
1.15	1.15	10	0.13					
1.25	1.25	11	0.17	5	2807	150	0.047	43.7
5	3.47	10	0.54	133	20173	150	0.023	1.936
10	8.47	9.46	1	1167	70815	150	0.016	0.282625

Table 13: Collected Results

The relationship between the radial position of the head and tolerable RPM is shown in Figure 56. Each point is labeled with the radial position associated with it. The relationship between the radial position of the head and tolerable RPM is shown in Figure 57. Each point is labeled with the radial position associated with it. The relationship between the centrifuge radius and spin-up time is shown in Figure 58. Each point is labeled with the centrifuge radius associated with it. The relationship between centrifuge

65

radius and centrifuge mass is shown in Figure 59. Each point is labeled with the centrifuge radius associated with it.
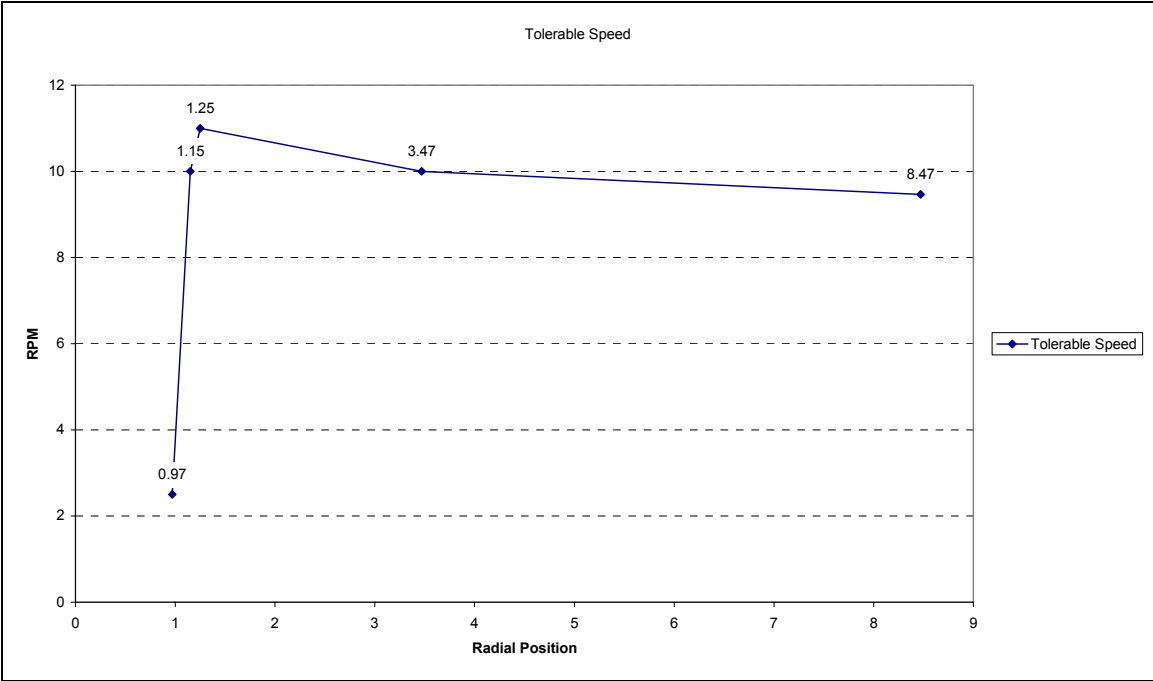
Figure 56: Tolerable Angular Velocity Versus Radial Position
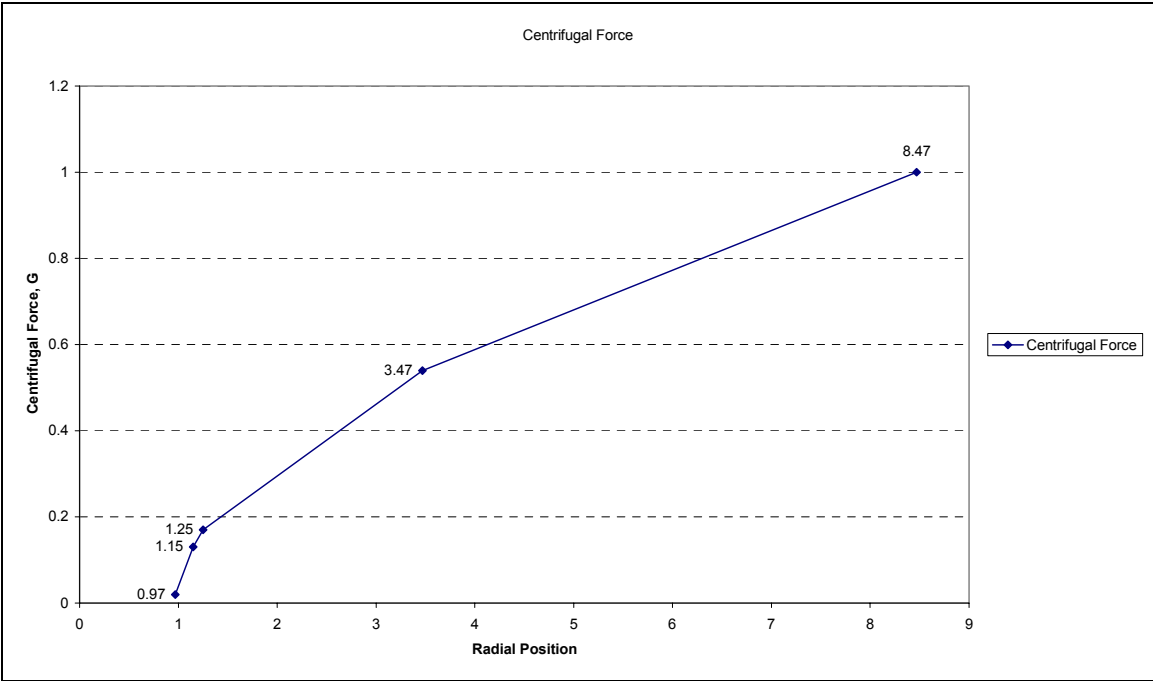
Figure 57: Tolerable Centrifugal Force Versus Radial Position
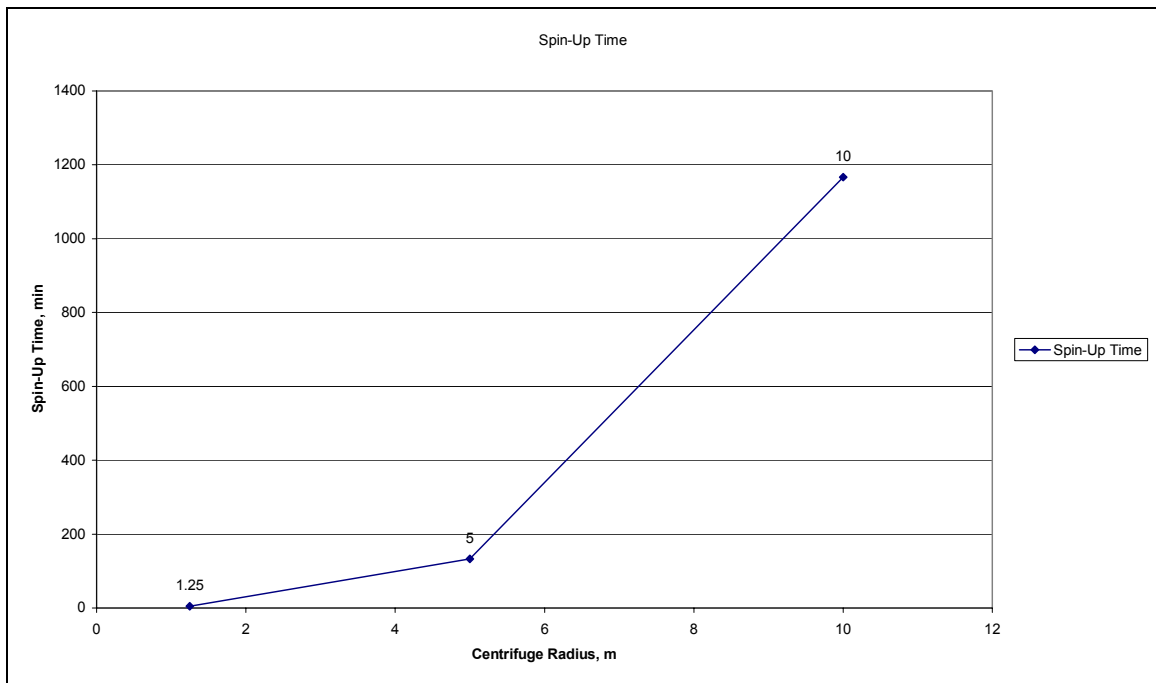
Figure 58: Spin-Up Time Versus Centrifuge Radius
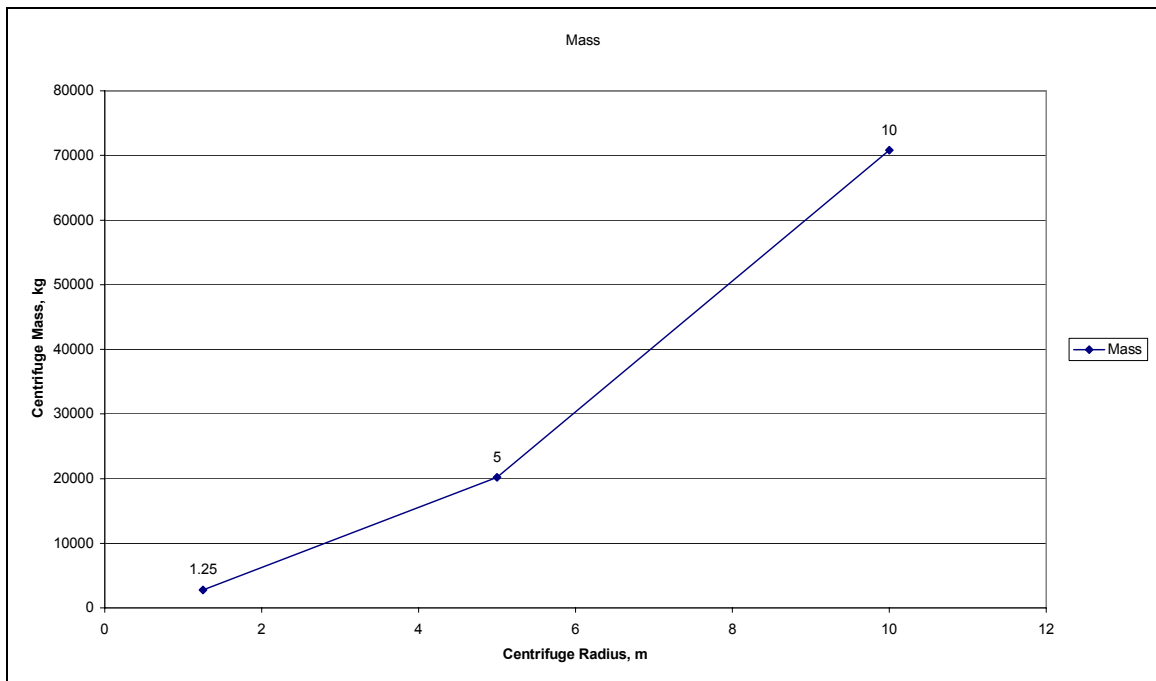
Figure 59: Centrifuge Mass Versus Centrifuge Radius

THIS PAGE INTENTIONALLY LEFT BLANK

V. CONCLUSION

A. VALIDATION EXPERIMENT

1. Effects of Coriolis on Human Disorientation

Movement of the head in the radial plane of a rotating environment generates a profound feeling of disorientation, an oculogyral illusion of the horizon twisting, and depending on the angular velocity could induce motion sickness. As demonstrated during the validation experiment, these feelings are directly proportional to the angular velocity of the centrifuge. The validation experiment showed that slower angular velocities generate less disorientation.

2. Validation Experiment

The validation experiment was designed to determine how the physical response of the Semi-Circular Canals, as reproduced by the Human Disorientation Model, corresponds to the various feelings associated with disorientation in a rotating environment. Utilizing a Merry-Go-Round to provide a 1.15 m Rotating Platform, three subjects were subjected to rotational motion at 10 and 20 RPM. At 10 RPM, a very mild sense of disorientation, akin to slight dizziness, was experienced when each subject moved their head back and forth, radially, through 10 cm for 10 sec. No disorientation was experienced at 10 RPM during spin up, spin down, and steady state rotation without head movement. At 20 RPM, a strong sense of disorientation, akin to nausea, was experienced accompanied by an illusion of the horizon tilting as each subject moved their head back and forth, radially, through 10 cm for 10 sec. The illusion moved in phase with the head movement. A mild sense of disorientation was experienced at 20 RPM during spin up, spin down, and steady state rotation that each subject related to their efforts to maintain their position against the strong, 0.52 G Centrifugal Force.

3. Human Tolerance of Coriolis

The Human Disorientation Model presented in this paper shows that the ability of a person to tolerate Coriolis is directly related to Cupula Velocity and not Cupula Deflection. Cupula Deflection other than zero stimulates the vestibular nerve the

magnitude of which is directly interpreted by the brain as rotational motion in the plane of the associated Semi-Circular Canal. Cupula Velocity is dependent on the torque produced during radial translation. This torque is the vector product of Coriolis Force and Radial Velocity. The Human Disorientation Model showed that Cupula Velocity for the same Radial Motion and Centrifugal Force was reduced when Centrifuge Radius was increased and Angular Velocity was decreased.

Assuming a 1 G Centrifugal Force, a centrifuge with a 5 m radius is the smallest that could be occupied by an astronaut where the astronaut could withstand the effects of disorientation. However, a 5 m centrifuge imparts enough disorientation that motion sickness would be experienced, impairing the mission. The problems associated with disorientation do not exist in the 10 m centrifuge.

4. Man Rated Centrifuge Characteristics Given Peak Electrical Power Load

This report calculated the dynamic characteristics of 5 and 10 m centrifuges based on a 150W Peak Load primer mover. The 5 and 10 m centrifuges simulated with the human dynamic model were input into the Centrifuge Dynamic Model of the ISS Centrifuge. Fixing the characteristics of Steady State Centrifugal Force and Peak Start-Up Power required only the EMF Proportionality Constant be changed together with the Inner and Outer Radius. The results were that a 10 m radius centrifuge would spin up in more than 19 hours and weigh 70815 kg, making it unfeasible in the near term. The 5 m radius centrifuge, on the other hand, weighing in at 20173 kg with a 133 min spin-up time is a feasible project that merits further consideration.

VI.   FOLLOW-ON RESEARCH

A.   GROUND-BASED RESEARCH OPPORTUNITIES

1.   Correlation with Existing Data

Existing data from previous human centrifuge studies can be utilized to further evaluate the model presented in this paper. Additionally, scientific research can be designed to further evaluate disorientation in a manner that best simulates the space environment.

2.   Manned Centrifuge Research

Existing centrifuges in the military and civilian sector can be utilized, together with these models, to conduct scientific research into the level of disorientation experienced compared to the physical response of the Semi-Circular Canals under differing conditions in a rotating environment.

3.   Dual-Use of a Manned Centrifuge as a Momentum Wheel

What are the benefits of a centrifuge when it is also used as a momentum wheel for the purpose of maintaining spacecraft stability? Would it be beneficial to use a centrifuge to replace control moment gyroscopes or standard momentum wheels?

4.   Dynamic Properties of Other Centrifuge Types Versus Disorientation

Given that Human Disorientation in a rotating environment is independent of the design of the centrifuge, would a radial-arm or tethered centrifuge be more feasible for deployment in the near-term? Could one be installed as an upgrade to the ISS or a future space station?

B.   POTENTIAL SPACE-BASED RESEARCH

1.   Use of The Disorientation Model to Design ISS Centrifuge Research

How will the animals proposed for use in ISS Centrifuge research respond to the rotating environment within that centrifuge? The Human Disorientation model allows for the Friction Constant and Restoring Force Constant of the cupula within any Semi-Circular Canal to be adjusted to fit those of any animal with vestibular organs similar to those in humans.

THIS PAGE INTENTIONALLY LEFT BLANK

VII.   APPENDICES

A.   APPENDIX A

1.   Modeling the External Dynamics of a Centrifuge

This section discusses the mathematical rigor behind the dynamics of a centrifuge.

Analytical Term	Meaning	Units
B	Friction Losses due to supports, bearings, and gears	N
i	Motor Current	A
J	Centrifuge Moment of Inertia	kg m²
k_f	EMF Coefficient	Unitless
k_τ	Torque Coefficient	Unitless
L	Motor Inductance	H
R	Motor Resistance	Ω
v	Drive Voltage	V
v_f	Load Induced Back EMF	V
ω	Centrifuge Angular Velocity	rad/s
θ	Centrifuge Angular Position	rad
τ	Motor Torque	N·m

Table 14: Centrifuge External Terms

2.   Analytical Model

The external analysis of the effects of a centrifuge (as illustrated in Figure 60) upon the spacecraft where it is installed is important in determining the size of centrifuge that optimizes human comfort and spacecraft bus impact.

$$J, \omega, \theta \qquad\qquad B, \tau, k_\tau, v, L, R, v_f, k_f, i$$
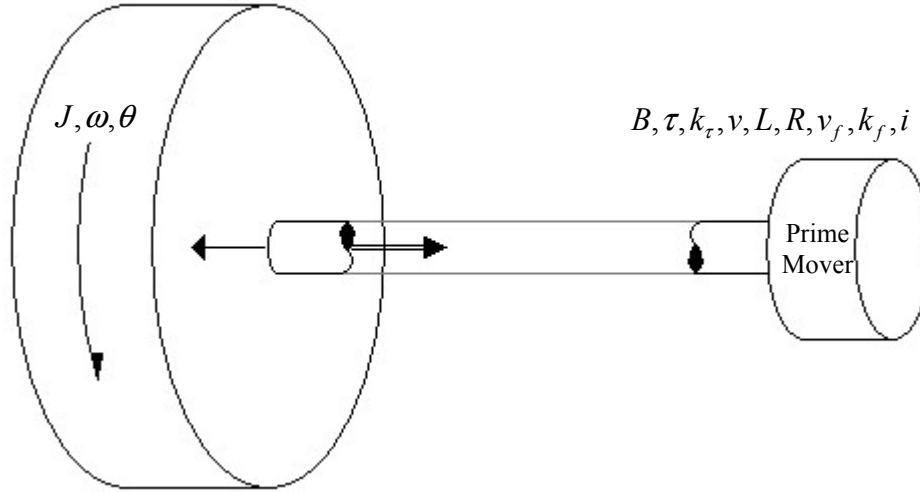
Prime Mover

Figure 60: Centrifuge External Terms

a.   Transfer Functions

The differential equations describing the instantaneous current flow within the Prime Mover and the Centrifuge are[47]:

$$Ri + L\frac{di}{dt} = v - k_f \frac{d\theta}{dt} \qquad (A.1)$$

$$k_\tau i = J\frac{d^2\theta}{dt^2} + B\frac{d\theta}{dt} \qquad (A.2)$$

The Laplace Transform of equations (A.1) and (A.2) are:

$$(R + sL)I = V - k_f s\Theta \qquad (A.3)$$

$$k_\tau I = (Js^2 + Bs)\Theta \qquad (A.4)$$

Solving both equations with respect to current in the Laplace Domain:

$$I = \frac{V - k_f(s\Theta)}{(R + sL)} = \frac{(Js + B)}{k_\tau}(s\Theta) \qquad (A.5)$$

Solving for angular velocity returns the transfer function that relates angular velocity to the drive voltage:

[47] John J. D'Azzo and Constantine H. Houpis, <u>Feedback Control System Analysis and Synthesis,</u> 2nd Ed., New York: McGraw Hill, 1966, pp. 44-47

$$\omega(s) = s\Theta = \frac{k_\tau}{\left[(R+sL)(Js+B)+k_\tau k_f\right]}V \tag{A.6}$$

Substituting equation (A.6) back into equation (A.5) returns the transfer function that relates motor armature current to the drive voltage:

$$\frac{I}{V} = \frac{(Js+B)}{\left[(R+sL)(Js+B)+k_\tau k_f\right]} \tag{A.7}$$

The instantaneous power consumed by the centrifuge and its prime mover is described by:

$$P = I \cdot V = V^2 \frac{(Js+B)}{\left[(R+sL)(Js+B)+k_\tau k_f\right]} \tag{A.8}$$

b.   Steady State Response

Letting:

$$\omega(s) = s\Theta \tag{A.9}$$

Equation (A.6) can be rewritten as:

$$\omega(s) = \frac{\left(\dfrac{k_\tau}{LJ}\right)}{\left[s^2 + \left(\dfrac{BL+RJ}{LJ}\right)s + \left(\dfrac{BR+k_\tau k_f}{LJ}\right)\right]}V(s) \tag{A.10}$$

If the input voltage is assumed to be a step input, then the Laplace Transform of that input voltage is (the subscript 'ss' represents steady state):

$$V(s) = \frac{V_{ss}}{s} \tag{A.11}$$

Substituting for the input voltage yields:

$$\omega(s) = \left(\frac{\left(\dfrac{k_\tau}{LJ}\right)}{\left[s^2 + \left(\dfrac{BL+RJ}{LJ}\right)s + \left(\dfrac{BR+k_\tau k_f}{LJ}\right)\right]}\right)\left(\frac{V_{ss}}{s}\right) \tag{A.12}$$

Utilizing the final value theorem to obtain the steady state angular velocity:

$$\omega_{ss} = \lim_{s \to 0}(s\omega(s)) \tag{A.13}$$

75

$$\omega_{ss} = \lim_{s \to 0} \left[\frac{k_\tau}{\left[(R + sL)(Js + B) + k_\tau k_f \right]} V_{ss} \right] \tag{A.14}$$

$$\omega_{ss} = \left[\frac{k_\tau}{(RB + k_\tau k_f)} V_{ss} \right] \tag{A.15}$$

Substituting the results from equation (A.15) into equation (A.5) yields the steady state current required to maintain a constant angular velocity:

$$i_{ss} = \frac{B}{k_\tau} \omega_{ss} \tag{A.16}$$

$$i_{ss} = \frac{B}{(RB + k_\tau k_f)} V_{ss} \tag{A.17}$$

Steady state power consumption is:

$$P_{ss} = V_{ss} i_{ss} \tag{A.18}$$

$$P_{ss} = \frac{B}{(RB + k_\tau k_f)} V_{ss}^2 \tag{A.19}$$

$$P_{ss} = \left(\frac{B}{(RB + k_\tau k_f)} \right) \left(\frac{(RB + k_\tau k_f)^2}{k_\tau^2} \right) \omega_{ss}^2 \tag{A.20}$$

$$P_{ss} = \frac{B}{k_\tau^2} (RB + k_\tau k_f) \omega_{ss}^2 \tag{A.21}$$

c.   *Transient Response*

Determining the centrifuge's response to transient events is necessary to determine it's Engineering Cost and effect on its human occupants. Once again, assuming a step input for the input voltage, the angular velocity transfer function can be written as:

$$\frac{\omega(s)}{V_{ss}} = \left(\frac{k_\tau}{BR + k_\tau k_f} \right) \left(\frac{\left[\frac{(BR + k_\tau k_f)}{LJ} \right]}{\left[s^2 + \left(\frac{BL + RJ}{LJ} \right) s + \left(\frac{BR + k_\tau k_f}{LJ} \right) \right]} \right) \left(\frac{1}{s} \right) \tag{A.22}$$

The dynamic response is contingent upon the roots of the following characteristic equation:

$$s^2 + \left(\frac{BL+RJ}{LJ}\right)s + \left(\frac{BR+k_\tau k_f}{LJ}\right) = 0 \tag{A.23}$$

The characteristic equation in equation (A.23) is in a form that shows the system has one or more complex conjugate roots. Therefore the damping ratio (ξ) and natural frequency (ω_n) can be determined using the following equation[48]:

$$s^2 + 2\xi\omega_n s + \omega_n^2 \tag{A.24}$$

$$2\xi\omega_n = \left(\frac{BL+RJ}{LJ}\right); \omega_n^2 = \left(\frac{BR+k_\tau k_f}{LJ}\right) \tag{A.25}$$

The complex roots of equation (A.24) are:

$$s_1 = -\xi\omega_n + \omega_n\sqrt{\xi^2-1}$$
$$s_2 = -\xi\omega_n - \omega_n\sqrt{\xi^2-1} \tag{A.26}$$

Defining a 'damped natural frequency (ω_d)' as:

$$\omega_d \equiv \omega_n\sqrt{\xi^2-1} \tag{A.27}$$

The roots in equation (A.26) may be simplified as:

$$s_1 = -\xi\omega_n + \omega_d$$
$$s_2 = -\xi\omega_n - \omega_d \tag{A.28}$$

Using equation (A.28), equation (A.22) may be rewritten in terms of damping ratio and natural frequency as follows:

$$\left(\frac{\omega(s)}{V_{ss}}\right) = \left(\frac{k_\tau}{(BR+k_\tau k_f)}\right)\left(\frac{\omega_n^2}{s(s^2+2\xi\omega_n s+\omega_n^2)}\right) \tag{A.29}$$

$$\left(\frac{\omega(s)}{V_{ss}}\right) = \left(\frac{k_\tau}{(BR+k_\tau k_f)}\right)\left(\frac{(BR+k_\tau k_f)}{JL}\right)\left(\frac{1}{s(s-s_1)(s-s_2)}\right) \tag{A.30}$$

$$\left(\frac{\omega(s)}{V_{ss}}\right) = \left(\frac{k_\tau}{JL}\right)\left(\frac{1}{s(s-s_1)(s-s_2)}\right) \tag{A.31}$$

---

[48] D'Azzo and Houpis, p. 246 and equation 7-110

$$\left(\frac{\omega(s)}{V_{ss}}\right) = \left(\frac{k_\tau}{JL}\right)\left(\frac{1}{s\left(s+(\xi\omega_n-\omega_d)\right)\left(s+(\xi\omega_n+\omega_d)\right)}\right) \qquad (A.32)$$

Utilizing Laplace Transform Tables[49], the inverse Laplace Transform of equation (A.32) is:

$$\left(\frac{\omega(t)}{V_{ss}}\right) = \left(\frac{k_\tau}{JL}\right)\mathcal{L}^{-1}\left(\frac{1}{s\left(s+(\xi\omega_n-\omega_d)\right)\left(s+(\xi\omega_n-\omega_d)\right)}\right) \qquad (A.33)$$

$$F(s) = \left(\frac{1}{(s+0)\left(s+(\xi\omega_n-\omega_d)\right)\left(s+(\xi\omega_n-\omega_d)\right)}\right) \qquad (A.34)$$

$$f(t) = \frac{e^{-at}}{(b-a)(c-a)} + \frac{e^{-bt}}{(c-b)(a-b)} + \frac{e^{-ct}}{(a-c)(b-c)} \qquad (A.35)$$

$$f(t) = \frac{\left(1-\left(\dfrac{(\xi\omega_n+\omega_d)e^{-(\xi\omega_n-\omega_d)t}}{(\xi\omega_n+\omega_d)-(\xi\omega_n-\omega_d)}\right)+\left(\dfrac{(\xi\omega_n-\omega_d)e^{-(\xi\omega_n+\omega_d)t}}{(\xi\omega_n+\omega_d)-(\xi\omega_n-\omega_d)}\right)\right)}{(\xi\omega_n-\omega_d)(\xi\omega_n+\omega_d)} \qquad (A.36)$$

Equation (A.36) reduces to:

$$f(t) = \frac{1-\left(\dfrac{e^{-\xi\omega_n t}}{\omega_d}\right)\left(\dfrac{(\xi\omega_n+\omega_d)e^{\omega_d t}-(\xi\omega_n-\omega_d)e^{-\omega_d t}}{2}\right)}{(\xi\omega_n)^2-\omega_d^2} \qquad (A.37)$$

By noting that:

$$\frac{1}{(\xi\omega_n)^2-\omega_d^2} = \frac{1}{\xi^2\omega_n^2-\omega_n^2(\xi^2-1)} = \frac{1}{\omega_n^2} \qquad (A.38)$$

And:

$$\frac{\omega_d}{\omega_n} = \frac{\omega_n\sqrt{\xi^2-1}}{\omega_n} = \sqrt{\xi^2-1} \qquad (A.39)$$

Equation (A.37) may be further reduced by applying Equations (A.38) and (A.39):

[49] D'Azzo and Houpis, p. 698 and Laplace Transform 15

$$f(t) = \frac{1 - \left(\dfrac{e^{-\xi\omega_n t}}{\omega_d}\right)\xi\omega_n\left(\dfrac{e^{\omega_d t} - e^{-\omega_d t}}{2}\right) - \left(\dfrac{e^{-\xi\omega_n t}}{\omega_d}\right)\omega_d\left(\dfrac{e^{\omega_d t} + e^{-\omega_d t}}{2}\right)}{\omega_n^2} \qquad (A.40)$$

$$f(t) = \left[\frac{1}{\omega_n^2} - \xi\left(\frac{e^{-\xi\omega_n t}}{\omega_n\omega_d}\right)\left(\frac{e^{\omega_d t} - e^{-\omega_d t}}{2}\right) - \frac{\omega_d}{\omega_n}\left(\frac{e^{-\xi\omega_n t}}{\omega_n\omega_d}\right)\left(\frac{e^{\omega_d t} + e^{-\omega_d t}}{2}\right)\right] \qquad (A.41)$$

$$f(t) = \left[\frac{1}{\omega_n^2} - \xi\left(\frac{e^{-\xi\omega_n t}}{\omega_n\omega_d}\right)\left(\frac{e^{\omega_d t} - e^{-\omega_d t}}{2}\right) - \sqrt{\xi^2 - 1}\left(\frac{e^{-\xi\omega_n t}}{\omega_n\omega_d}\right)\left(\frac{e^{\omega_d t} + e^{-\omega_d t}}{2}\right)\right] \qquad (A.42)$$

Noting the identities of the hyperbolic sine and cosine are[50]:

$$\cosh(\omega_d t) = \frac{\left[e^{\omega_d t} + e^{-\omega_d t}\right]}{2} \qquad (A.43)$$

$$\sinh(\omega_d t) = \frac{\left(e^{\omega_d t} - e^{-\omega_d t}\right)}{2} \qquad (A.44)$$

Equation (A.42) may be simplified by appropriately substituting equations (A.43) and (A.44):

$$f(t) = \left[\frac{1}{\omega_n^2} - \left[\left(\frac{e^{-\xi\omega_n t}}{\omega_n\omega_d}\right)\left(\xi\sinh(\omega_d t) + \left(\sqrt{\xi^2 - 1}\right)\cosh(\omega_d t)\right)\right]\right] \qquad (A.45)$$

Recalling from equation (A.33):

$$\left(\frac{\omega(t)}{V_{ss}}\right) = \left(\frac{k_\tau}{JL}\right)\mathcal{L}^{-1}F(s)$$

The general solution for angular velocity can be expressed by substituting equation (A.45) for the Inverse Laplace Transform in equation (A.33):

$$\omega(t) = \left(\frac{V_{ss}k_\tau}{JL}\right)\left[\frac{1}{\omega_n^2} - \left[\left(\frac{e^{-\xi\omega_n t}}{\omega_n\omega_d}\right)\left(\xi\sinh(\omega_d t) + \left(\sqrt{\xi^2 - 1}\right)\cosh(\omega_d t)\right)\right]\right] \qquad (A.46)$$

To develop analytical expressions for ξ and ω_d, the earlier definitions of equation (A.46) must be revisited. From equations (A.25) and (A.27) we know that:

$$2\xi\omega_n = \left(\frac{BL + RJ}{LJ}\right); \omega_n^2 = \left(\frac{BR + k_\tau k_f}{LJ}\right); \omega_d \equiv \omega_n\sqrt{\xi^2 - 1}$$

---

[50] Douglas F. Riddle, <u>Calculus and Analytic Geometry</u>, Alternate Ed., Belmont: Wadsworth, 1984, p. 406

Solving for ξ results in:

$$\frac{\xi^2 \omega_n^2}{\omega_n^2} = \frac{\left(\dfrac{BL + RJ}{2JL}\right)^2}{\left(\dfrac{BR + k_\tau k_f}{JL}\right)} \tag{A.47}$$

$$\xi = \left(\frac{BL + RJ}{2JL}\right)\sqrt{\left(\frac{JL}{BR + k_\tau k_f}\right)} \tag{A.48}$$

Solving for ω_d results in:

$$\omega_d^2 \equiv \left(\frac{BR + k_\tau k_f}{JL}\right)\left[\left(\frac{BL + RJ}{2JL}\right)^2\left(\frac{JL}{BR + k_\tau k_f}\right) - 1\right] \tag{A.49}$$

$$\omega_d^2 = \left(\frac{BL + RJ}{2JL}\right)^2 - \left(\frac{BR + k_\tau k_f}{JL}\right) \tag{A.50}$$

$$\omega_d^2 = \frac{\left((BL)^2 + 2BRJL + (RJ)^2\right) - 4JL\left(BR + k_\tau k_f\right)}{4(JL)^2} \tag{A.51}$$

$$\omega_d = \sqrt{\left(\frac{BL - RJ}{2JL}\right)^2 - \left(\frac{k_\tau k_f}{JL}\right)} \tag{A.52}$$

d.   Over-Damped Angular Velocity Response

The angular velocity response of the centrifuge and its prime mover are greatly dependent upon the magnitude of ξ. If $\xi > 1$ then ω_d, as shown by equation (A.27) will be a real number. The system's response, as governed by equation (A.46), will be asymptotic in character, or 'over-damped'. The over-damped result is:

$$\omega_{\xi > 1}(t) = \frac{V_{ss} k_\tau}{JL}\left[\frac{1}{\omega_n^2} - \frac{e^{-\xi \omega_n t}}{\omega_n \omega_d}\left[\xi \sinh(\omega_d t) + \sqrt{\xi^2 - 1}\cosh(\omega_d t)\right]\right] \tag{A.53}$$

$$\omega_{\xi > 1}(t) = \frac{V_{ss} k_\tau}{JL}\frac{1}{\omega_n^2}\left[1 - \frac{\omega_n}{\omega_d}e^{-\xi \omega_n t}\left[\xi \sinh(\omega_d t) + \sqrt{\xi^2 - 1}\cosh(\omega_d t)\right]\right] \tag{A.54}$$

Recall from equation (A.25) that:

$$\omega_n^2 = \left(\frac{BR + k_\tau k_f}{LJ}\right)$$

Substituting for ω_n^{-2} yields:

$$\omega_{\xi>1}(t) = \frac{V_{ss}k_\tau}{JL} \frac{JL}{\left(BR+k_\tau k_f\right)}\left[1-\frac{\omega_n}{\omega_d}e^{-\xi\omega_n t}\left[\xi\sinh\left(\omega_d t\right)+\sqrt{\xi^2-1}\cosh\left(\omega_d t\right)\right]\right] \quad (A.55)$$

$$\omega_{\xi>1}(t) = \frac{V_{ss}k_\tau}{\left(BR+k_\tau k_f\right)}\left[1-\frac{\omega_n}{\omega_d}e^{-\xi\omega_n t}\left[\xi\sinh\left(\omega_d t\right)+\sqrt{\xi^2-1}\cosh\left(\omega_d t\right)\right]\right] \quad (A.56)$$

Recall from equation (A.15) that:

$$\omega_{ss} = \frac{V_{ss}k_\tau}{\left(RB+k_\tau k_f\right)}$$

Therefore, the final form of the over-damped response equation is:

$$\omega_{\xi>1}(t) = \omega_{ss}\left[1-\frac{\omega_n}{\omega_d}e^{-\xi\omega_n t}\left[\xi\sinh\left(\omega_d t\right)+\sqrt{\xi^2-1}\cosh\left(\omega_d t\right)\right]\right] \quad (A.57)$$

e.   *Critically-Damped Angular Velocity Response*

If $\xi=1$, then:

$$\omega_d = \omega_n\sqrt{\xi^2-1} = 0 \quad (A.58)$$

Thus, the system's angular velocity response will be:

$$\omega_{\xi=1}(t) = \frac{V_{ss}k_\tau}{JL}\lim_{\xi\to 1}\left[\frac{1}{\omega_n^2}-\frac{e^{-\xi\omega_n t}}{\omega_n\omega_d}\left[\xi\sinh\left(\omega_d t\right)+\sqrt{\xi^2-1}\cosh\left(\omega_d t\right)\right]\right] \quad (A.59)$$

$$\omega_{\xi=1}(t) = \frac{V_{ss}k_\tau}{JL}\lim_{\xi\to 1}\left[\frac{1}{\omega_n^2}-\frac{e^{-\xi\omega_n t}}{\omega_n}\left[\frac{\xi\sinh\left(\omega_d t\right)}{\omega_d}+\frac{\sqrt{\xi^2-1}\cosh\left(\omega_d t\right)}{\omega_d}\right]\right] \quad (A.60)$$

$$\omega_{\xi=1}(t) = \frac{V_{ss}k_\tau}{JL}\lim_{\xi\to 1}\left[\frac{1}{\omega_n^2}-\frac{e^{-\xi\omega_n t}}{\omega_n}\left[\frac{\xi\sinh\left(\omega_n t\sqrt{\xi^2-1}\right)}{\omega_n\sqrt{\xi^2-1}}+\frac{\sqrt{\xi^2-1}\cosh\left(\omega_n t\sqrt{\xi^2-1}\right)}{\omega_n\sqrt{\xi^2-1}}\right]\right] \quad (A.61)$$

$$\omega_{\xi=1}(t) = \frac{V_{ss}k_\tau}{JL}\left[\frac{1}{\omega_n^2}-\frac{e^{-\xi\omega_n t}}{\omega_n}\left[\lim_{\xi\to 1}\left(\frac{\sinh\left(\omega_n t\sqrt{\xi^2-1}\right)}{\omega_n\sqrt{\xi^2-1}}\right)+\frac{1}{\omega_n}\right]\right] \quad (A.62)$$

81

Using substitution, the limit of the hyperbolic sine term was found to be indeterminate (the value found was zero over zero). L'Hopital's Rule[51,52] was applied to evaluate the limit's result:

$$\lim_{\xi \to 1} \frac{\sinh\left(\omega_n t \sqrt{\xi^2 - 1}\right)}{\omega_n \sqrt{\xi^2 - 1}} = \lim_{\xi \to 1} \frac{\dfrac{d}{d\xi}\left[\sinh\left(\omega_n t \sqrt{\xi^2 - 1}\right)\right]}{\dfrac{d}{d\xi}\left[\omega_n \sqrt{\xi^2 - 1}\right]} \tag{A.63}$$

$$\lim_{\xi \to 1} \frac{\xi \sinh\left(\omega_n t \sqrt{\xi^2 - 1}\right)}{\omega_n \sqrt{\xi^2 - 1}} = \lim_{\xi \to 1} \frac{\left[\left(\cosh\left(\omega_n t \sqrt{\xi^2 - 1}\right)\right)\omega_n t \dfrac{d}{d\xi}\sqrt{\xi^2 - 1}\right]}{\omega_n \dfrac{d}{d\xi}\sqrt{\xi^2 - 1}} \tag{A.64}$$

$$\lim_{\xi \to 1} \frac{\xi \sinh\left(\omega_n t \sqrt{\xi^2 - 1}\right)}{\omega_n \sqrt{\xi^2 - 1}} = \cosh(0)t = t \tag{A.65}$$

Substituting the evaluated result of the hyperbolic sine term from equation (A.65), equation (A.62) reduces to:

$$\omega_{\xi=1}(t) = \frac{V_{ss}k_\tau}{JL}\left[\frac{1}{\omega_n^2} - \frac{e^{-\xi\omega_n t}}{\omega_n}\left[t + \frac{1}{\omega_n}\right]\right] \tag{A.66}$$

Equation (A.66) may be further reduced as follows:

$$\omega_{\xi=1}(t) = \frac{V_{ss}k_\tau}{JL}\frac{1}{\omega_n^2}\left[1 - e^{-\xi\omega_n t}\left[\omega_n t + 1\right]\right] \tag{A.67}$$

Recalling the value of ω_n^{-2} from equation (A.25):

$$\omega_{\xi=1}(t) = \frac{V_{ss}k_\tau}{JL}\frac{JL}{\left(BR + k_\tau k_f\right)}\left[1 - e^{-\xi\omega_n t}\left[\omega_n t + 1\right]\right] \tag{A.68}$$

$$\omega_{\xi=1}(t) = \frac{V_{ss}k_\tau}{\left(BR + k_\tau k_f\right)}\left[1 - e^{-\xi\omega_n t}\left[\omega_n t + 1\right]\right] \tag{A.69}$$

Recalling the value of ω_{ss} from equation (A.15) results in the final form of the Critically-damped Angular Velocity Response Equation:

---

[51] D'Azzo and Houpis, p. 130

[52] Riddle, pp. 667-674

$$\omega_{\xi=1}(t) = \omega_{ss}\left[1 - e^{-\xi\omega_n t}\left[\omega_n t + 1\right]\right] \tag{A.70}$$

f.   Under-Damped Angular Velocity Response

When $\xi < 1$, then ω_d becomes imaginary:

$$\omega_d = \omega_n\sqrt{\xi^2 - 1} = \omega_n\sqrt{-1}\sqrt{1-\xi^2} = j\omega_n\sqrt{1-\xi^2} \tag{A.71}$$

Substituting equation (A.71) into the general form for angular velocity yields:

$$\omega_{\xi<1}(t) = \omega_{ss}\left[1 - \left[\left(\frac{\omega_n e^{-\xi\omega_n t}}{j\omega_n\sqrt{1-\xi^2}}\right)\left(\xi\sinh\left(j\omega_n t\sqrt{1-\xi^2}\right) + \left(j\sqrt{1-\xi^2}\right)\cosh\left(j\omega_n t\sqrt{1-\xi^2}\right)\right)\right]\right] \tag{A.72}$$

$$\omega_{\xi<1}(t) = \omega_{ss}\left[1 - e^{-\xi\omega_n t}\left(\left(\frac{\xi}{j\sqrt{1-\xi^2}}\right)\left(\frac{\sinh\left(j\omega_n t\sqrt{1-\xi^2}\right)}{j}\right) + \cosh\left(j\omega_n t\sqrt{1-\xi^2}\right)\right)\right] \tag{A.73}$$

The imaginary component may be eliminated from equation (A.73) by substitution using the following identities[53]:

$$\sinh(ju) = j\sin(u) \Rightarrow \frac{\sinh(ju)}{j} = \sin(u) \tag{A.74}$$

$$\cosh(ju) = \cos(u) \tag{A.75}$$

$$u = \omega_n t\sqrt{1-\xi^2} \tag{A.76}$$

The result is:

$$\omega_{\xi<1}(t) = \omega_{ss}\left[1 - \frac{e^{-\xi\omega_n t}}{\sqrt{1-\xi^2}}\left(\xi\sin\left(\omega_n t\sqrt{1-\xi^2}\right) + \sqrt{1-\xi^2}\cos\left(\omega_n t\sqrt{1-\xi^2}\right)\right)\right] \tag{A.77}$$

Taking advantage of the Angle-Sum Relation of Sine[54]:

$$\sin(u + \phi) = \sin u \cos\phi + \cos u \sin\phi \tag{A.78}$$

And the Quotient Relation of Tangent[55]:

---

[53] William H. Beyer, <u>CRC Standard Mathematical Tables</u>, 28th Ed., Boca Raton: CRC Press, p. 172

[54] Beyer, p. 139

[55] Beyer, p. 138

83

83

$$\tan\phi = \frac{\sin\phi}{\cos\phi} \tag{A.79}$$

Then the like terms in sine and cosine may be equated as follows:

$$\sin\phi = \sqrt{1-\xi^2} \tag{A.80}$$

$$\cos\phi = \xi \tag{A.81}$$

$$\phi = \tan^{-1}\left(\frac{\sqrt{1-\xi^2}}{\xi}\right) \tag{A.82}$$

And the sine and cosine terms within equation (A.77) may be reduced as follows:

$$\sin\left(\omega_n\left(\sqrt{1-\xi^2}\right)t+\phi\right) = \xi\sin\left(\omega_n t\sqrt{1-\xi^2}\right)+\left(\sqrt{1-\xi^2}\right)\cos\left(\omega_n t\sqrt{1-\xi^2}\right) \tag{A.83}$$

Recalling equations A.83, A.84, and A.85:

$$\sin\left(\omega_n\left(\sqrt{1-\xi^2}\right)t+\phi\right) = \cos(\phi)\sin\left(\omega_n t\sqrt{1-\xi^2}\right)+\sin(\phi)\cos\left(\omega_n t\sqrt{1-\xi^2}\right) \tag{A.84}$$

The result being a pair of equations that further reduces equation A.80 and is the final result for the Under-damped Angular Velocity Response:

$$\omega_{\xi<1}(t) = \omega_{ss}\left[1-e^{-\xi\omega_n t}\left(\frac{\sin\left(\omega_n\left(\sqrt{1-\xi^2}\right)t+\phi\right)}{\sqrt{1-\xi^2}}\right)\right] \tag{A.85}$$

$$\phi = \tan^{-1}\left(\frac{\sqrt{1-\xi^2}}{\xi}\right) \tag{A.86}$$

g. Over-Damped Current Response

Knowing the prime mover's instantaneous current requirements is important to understanding the overall power requirements. The current to voltage transfer function can be obtained through the substitution of equation (A.7) into equation (A.10):

$$\frac{I(s)}{V(s)} = \left(\frac{I(s)}{\omega(s)}\right)\left(\frac{\omega(s)}{V(s)}\right) \tag{A.87}$$

$$\frac{I(s)}{V(s)} = \left(\frac{Js+B}{k_\tau}\right)\left(\frac{\left(\dfrac{k_\tau}{JL}\right)}{s^2 + \left(\dfrac{BL+RJ}{JL}\right)s + \left(\dfrac{BR+k_\tau k_f}{JL}\right)}\right) \tag{A.88}$$

$$\frac{I(s)}{V(s)} = \left(\frac{\left(\dfrac{Js+B}{JL}\right)}{s^2 + \left(\dfrac{BL+RJ}{JL}\right)s + \left(\dfrac{BR+k_\tau k_f}{JL}\right)}\right) \tag{A.89}$$

$$\frac{I(s)}{V(s)} = \left(\frac{1}{L}\right)\left(\frac{\left(s+\dfrac{B}{J}\right)}{s^2 + \left(\dfrac{BL+RJ}{JL}\right)s + \left(\dfrac{BR+k_\tau k_f}{JL}\right)}\right) \tag{A.90}$$

Noting the same characteristic equation as found in equation (A.23), the ξ and ω_n terms found in equation (A.25) may again be substituted:

$$\frac{I(s)}{V(s)} = \left(\frac{1}{L}\right)\left(\frac{\left(s+\dfrac{B}{J}\right)}{s^2 + \left(2\xi\omega_n\right)s + \left(\omega_n^2\right)}\right) \tag{A.91}$$

Recalling the definition for ω_d found in equation (A.27):

$$\frac{I(s)}{V(s)} = \left(\frac{1}{L}\right)\left(\frac{\left(s+\dfrac{B}{J}\right)}{\left(s+\left(\xi\omega_n-\omega_d\right)\right)\left(s+\left(\xi\omega_n+\omega_d\right)\right)}\right) \tag{A.92}$$

Once again, we assume a step input for the system voltage as found in equation (A.11). This results in a step-response transfer function for the current drawn by the system's prime mover:

$$\frac{I(s)}{V_{ss}} = \left(\frac{1}{L}\right)\left(\frac{\left(s+\dfrac{B}{J}\right)}{\left(s+\left(\xi\omega_n-\omega_d\right)\right)\left(s+\left(\xi\omega_n+\omega_d\right)\right)}\right) \tag{A.93}$$

Taking the Inverse Laplace Transform of equation (A.93) yields:

$$\mathcal{L}^{-1}\left(\frac{I(s)}{V_{ss}}\right) = \mathcal{L}^{-1}\left(\frac{1}{L}\left(\frac{\left(s+\dfrac{B}{J}\right)}{s\left(s+\left(\xi\omega_n-\omega_d\right)\right)\left(s+\left(\xi\omega_n+\omega_d\right)\right)}\right)\right) \quad \text{(A.94)}$$

$$\frac{i(t)}{V_{ss}} = \frac{1}{L}\mathcal{L}^{-1}\left(\frac{\left(s+\dfrac{B}{J}\right)}{s\left(s+\left(\xi\omega_n-\omega_d\right)\right)\left(s+\left(\xi\omega_n+\omega_d\right)\right)}\right) \quad \text{(A.95)}$$

Referring to the Inverse Laplace Transform Tables[56] yields the following expressions:

$$F(s) = \frac{s+\alpha}{(s+a)(s+b)(s+c)} \quad \text{(A.96)}$$

$$f(t) = \frac{(\alpha-a)e^{-at}}{(b-a)(c-a)} + \frac{(\alpha-b)e^{-bt}}{(c-b)(a-b)} + \frac{(\alpha-c)e^{-ct}}{(a-c)(b-c)} \quad \text{(A.97)}$$

The subtle difference between equation (A.97) and equation (A.35) should be noted. The effects of friction and moment of inertia are much more profound when predicting current than angular velocity.

Finding the simplest solution of the Laplace Domain Component of the general current response solution follows:

$$f(t) = \mathcal{L}^{-1}\left(\frac{\left(s+\dfrac{B}{J}\right)}{s\left(s+\left(\xi\omega_n-\omega_d\right)\right)\left(s+\left(\xi\omega_n+\omega_d\right)\right)}\right) \quad \text{(A.98)}$$

$$f(t) = \frac{\dfrac{B}{J} - \dfrac{\left(\xi\omega_n+\omega_d\right)\left(B/J-\left(\xi\omega_n-\omega_d\right)\right)e^{-\left(\xi\omega_n-\omega_d\right)t}}{\left(\xi\omega_n+\omega_d\right)-\left(\xi\omega_n-\omega_d\right)} + \dfrac{\left(\xi\omega_n-\omega_d\right)\left(B/J-\left(\xi\omega_n+\omega_d\right)\right)e^{-\left(\xi\omega_n+\omega_d\right)t}}{\left(\xi\omega_n+\omega_d\right)-\left(\xi\omega_n-\omega_d\right)}}{\left(\xi\omega_n-\omega_d\right)\left(\xi\omega_n+\omega_d\right)} \quad \text{(A.99)}$$

$$f(t) = \frac{\dfrac{B}{J} - \dfrac{\left(\xi\omega_n+\omega_d\right)\left(B/J-\left(\xi\omega_n-\omega_d\right)\right)e^{-\left(\xi\omega_n-\omega_d\right)t}}{2\omega_d} + \dfrac{\left(\xi\omega_n-\omega_d\right)\left(B/J-\left(\xi\omega_n+\omega_d\right)\right)e^{-\left(\xi\omega_n+\omega_d\right)t}}{2\omega_d}}{\left(\left(\xi\omega_n\right)^2-\omega_d^2\right)} \quad \text{(A.100)}$$

---

[56] D'Azzo and Houpis, p. 698, Laplace Transform 16

$$f(t) = \frac{\dfrac{B}{J} - \dfrac{\omega_n^2\left(\xi+\dfrac{\omega_d}{\omega_n}\right)\left(\dfrac{B/J}{\omega_n}-\left(\xi-\dfrac{\omega_d}{\omega_n}\right)\right)e^{-(\xi\omega_n-\omega_d)t}}{2\omega_d} + \dfrac{\omega_n^2\left(\xi-\dfrac{\omega_d}{\omega_n}\right)\left(\dfrac{B/J}{\omega_n}-\left(\xi+\dfrac{\omega_d}{\omega_n}\right)\right)e^{-(\xi\omega_n+\omega_d)t}}{2\omega_d}}{\left((\xi\omega_n)^2-\omega_d^2\right)} \quad (A.101)$$

Noting that:

$$\frac{1}{(\xi\omega_n)^2-\omega_d^2} = \frac{1}{\xi^2\omega_n^2-\omega_n^2(\xi^2-1)} = \frac{1}{\omega_n^2} \quad (A.102)$$

$$\frac{\omega_d}{\omega_n} = \frac{\omega_n\sqrt{\xi^2-1}}{\omega_n} = \sqrt{\xi^2-1} \quad (A.103)$$

Equation (A.101) may be reduced by applying the substitutions noted in equations (A.102) and (A.103):

$$f(t) = \frac{\dfrac{B}{J} - \dfrac{\omega_n\left(\xi+\sqrt{\xi^2-1}\right)\left(\dfrac{B/J}{\omega_n}-\left(\xi-\sqrt{\xi^2-1}\right)\right)e^{-(\xi\omega_n-\omega_d)t}}{2\sqrt{\xi^2-1}} + \dfrac{\omega_n\left(\xi-\sqrt{\xi^2-1}\right)\left(\dfrac{B/J}{\omega_n}-\left(\xi+\sqrt{\xi^2-1}\right)\right)e^{-(\xi\omega_n+\omega_d)t}}{2\sqrt{\xi^2-1}}}{\omega_n^2} \quad (A.104)$$

$$f(t) = \frac{\dfrac{B/J}{\omega_n} - \left(\dfrac{e^{-\xi\omega_n t}}{\sqrt{\xi^2-1}}\right)\dfrac{\left(\xi+\sqrt{\xi^2-1}\right)\left(\dfrac{B/J}{\omega_n}-\left(\xi-\sqrt{\xi^2-1}\right)\right)e^{\omega_d t}}{2} + \left(\dfrac{e^{-\xi\omega_n t}}{\sqrt{\xi^2-1}}\right)\dfrac{\left(\xi-\sqrt{\xi^2-1}\right)\left(\dfrac{B/J}{\omega_n}-\left(\xi+\sqrt{\xi^2-1}\right)\right)e^{-\omega_d t}}{2}}{\omega_n} \quad (A.105)$$

$$f(t) = \frac{\dfrac{B}{J\omega_n} - \left(\dfrac{e^{-\xi\omega_n t}}{\sqrt{\xi^2-1}}\right)\left(\dfrac{\left(\xi+\sqrt{\xi^2-1}\right)\left(\dfrac{B}{J\omega_n}-\left(\xi-\sqrt{\xi^2-1}\right)\right)e^{\omega_d t}}{2} - \dfrac{\left(\xi-\sqrt{\xi^2-1}\right)\left(\dfrac{B}{J\omega_n}-\left(\xi+\sqrt{\xi^2-1}\right)\right)e^{-\omega_d t}}{2}\right)}{\omega_n} \quad (A.106)$$

$$f(t) = \frac{\dfrac{B}{J\omega_n} - \left(\dfrac{e^{-\xi\omega_n t}}{\sqrt{\xi^2-1}}\right)\left(\dfrac{\left(\xi\dfrac{B}{J\omega_n}+\sqrt{\xi^2-1}\dfrac{B}{J\omega_n}+1\right)e^{\omega_d t}}{2} - \dfrac{\left(\xi\dfrac{B}{J\omega_n}-\sqrt{\xi^2-1}\dfrac{B}{J\omega_n}+1\right)e^{-\omega_d t}}{2}\right)}{\omega_n} \quad (A.107)$$

$$f(t) = \frac{\dfrac{B}{J\omega_n} - e^{-\xi\omega_n t}\left(\dfrac{B}{J\omega_n}\cosh(\omega_d t)+\dfrac{\dfrac{B}{J\omega_n}}{\sqrt{\xi^2-1}}\sinh(\omega_d t)\right)}{\omega_n} \quad (A.108)$$

Substituting the reduced Inverse Laplace Transform back into equation (A.95):

$$\frac{i(t)}{V_{ss}} = \frac{\dfrac{B}{J\omega_n} - e^{-\xi\omega_n t}\left(\dfrac{B}{J\omega_n}\cosh\left(\omega_d t\right) + \dfrac{\dfrac{B}{J\omega_n}}{\sqrt{\xi^2-1}}\sinh\left(\omega_d t\right)\right)}{L\omega_n} \tag{A.109}$$

Factoring out the common coefficient yields:

$$\frac{i(t)}{V_{ss}} = \frac{B}{JL\omega_n^2}\left[1 - e^{-\xi\omega_n t}\left(\cosh\left(\omega_d t\right) + \frac{\left(\xi - \dfrac{J\omega_n}{B}\right)}{\sqrt{\xi^2-1}}\sinh\left(\omega_d t\right)\right)\right] \tag{A.110}$$

The leading coefficient can be reduced by using values previously defined in equations (A.17) and (A.25):

$$\frac{B}{JL\omega_n^2} = \left(\frac{B}{JL}\right)\left(\frac{JL}{BR+k_\tau k_f}\right) = \frac{B}{BR+k_\tau k_f} = \frac{i_{ss}}{V_{ss}} \tag{A.111}$$

Further reducing equation (A.110) to the following:

$$\frac{i(t)}{V_{ss}} = \frac{i_{ss}}{V_{ss}}\left[1 - e^{-\xi\omega_n t}\left(\cosh\left(\omega_d t\right) + \frac{\left(\xi - \dfrac{J\omega_n}{B}\right)}{\sqrt{\xi^2-1}}\sinh\left(\omega_d t\right)\right)\right] \tag{A.112}$$

Therefore, the general and over-damped solution for current is:

$$i(t) = i_{ss}\left[1 - e^{-\xi\omega_n t}\left(\cosh\left(\omega_d t\right) + \frac{\left(\xi - \dfrac{J\omega_n}{B}\right)}{\sqrt{\xi^2-1}}\sinh\left(\omega_d t\right)\right)\right] \tag{A.113}$$

In comparison, the general form of the current response (equation (A.113)) contrasts with the general form of the angular velocity response (equation (A.46)) only in the coefficient of the hyperbolic sine term.

Equation (A.46) is repeated here for the purpose of comparison:

$$\omega(t) = \left(\frac{V_{ss}k_\tau}{JL}\right)\left[\frac{1}{\omega_n^2} - \left[\left(\frac{e^{-\xi\omega_n t}}{\omega_n\omega_d}\right)\left(\xi\sinh(\omega_d t) + \left(\sqrt{\xi^2-1}\right)\cosh(\omega_d t)\right)\right]\right]$$

h. Critically-Damped Current Response

Noting the similarities between the general form of the current response (equation (A.113)) and the general form of the angular velocity response (equation (A.46)), the critically-damped current response can be deduced from the critically-damped angular velocity response. Recalling from equation (A.70):

$$\omega_{\xi=1}(t) = \omega_{ss}\left[1 - e^{-\xi\omega_n t}\left[\omega_n t + 1\right]\right]$$

Therefore:

$$i_{\xi=1}(t) = i_{ss}\left[1 - e^{-\omega_n t}\left(\left(1 - \frac{J\omega_n}{B}\right)\omega_n t + 1\right)\right] \tag{A.114}$$

i. Under-Damped Current Response

As with the general, over-damped, and critically damped cases; the under-damped current response can be deduced from the under damped angular velocity response. Recalling from equation (A.77):

$$\omega_{\xi<1}(t) = \omega_{ss}\left[1 - \frac{e^{-\xi\omega_n t}}{\sqrt{1-\xi^2}}\left(\xi\sin\left(\omega_n t\sqrt{1-\xi^2}\right) + \sqrt{1-\xi^2}\cos\left(\omega_n t\sqrt{1-\xi^2}\right)\right)\right]$$

Realigning the coefficients in order to provide easier deduction yields:

$$\omega_{\xi<1}(t) = \omega_{ss}\left[1 - e^{-\xi\omega_n t}\left(\cos\left(\omega_n t\sqrt{1-\xi^2}\right) + \frac{\xi}{\sqrt{1-\xi^2}}\sin\left(\omega_n t\sqrt{1-\xi^2}\right)\right)\right] \tag{A.115}$$

Note the coefficient of the sine term in equation (A.115) is the inverse of the phase angle terms in equation (A.86).

$$\phi = \tan^{-1}\left(\frac{\sqrt{1-\xi^2}}{\xi}\right)$$

Through deduction, the under-damped current response is:

$$i_{\xi<1}(t) = i_{ss}\left[1 - e^{-\xi\omega_n t}\left(\cos\left(\omega_n t\sqrt{1-\xi^2}\right) + \frac{\left(\xi - \dfrac{J\omega_n}{B}\right)}{\sqrt{1-\xi^2}}\sin\left(\omega_n t\sqrt{1-\xi^2}\right)\right)\right] \quad \text{(A.116)}$$

Expressed in terms of phase angle:

$$i_{\xi<1}(t) = i_{ss}\left(1 - \frac{e^{-\xi\omega_n t}}{\sqrt{1-\xi^2}}\sin\left(\omega_n\sqrt{1-\xi^2}\,t + \phi\right)\right) \quad \text{(A.117)}$$

$$\phi = \tan^{-1}\frac{\sqrt{1-\xi^2}}{\left(\xi - \dfrac{J\omega_n}{B}\right)} \quad \text{(A.118)}$$

j. *Collected Results*

Angular Velocity Transfer Function, equation (A.22):

$$\frac{\omega(s)}{V_{ss}} = \left(\frac{k_\tau}{BR + k_\tau k_f}\right)\left(\frac{\left[\dfrac{(BR + k_\tau k_f)}{LJ}\right]}{\left[s^2 + \left(\dfrac{BL + RJ}{LJ}\right)s + \left(\dfrac{BR + k_\tau k_f}{LJ}\right)\right]}\right)\left(\frac{1}{s}\right)$$

Steady State Angular Velocity Response, equation (A.15):

$$\omega_{ss} = \left[\frac{k_\tau}{(RB + k_\tau k_f)}V_{ss}\right]$$

Natural Frequency, equation (A.25):

$$\omega_n^2 = \left(\frac{BR + k_\tau k_f}{LJ}\right)$$

Damped Natural Frequency, equation (A.27):

$$\omega_d \equiv \omega_n\sqrt{\xi^2 - 1}$$

Damping Ratio, equation (A.48):

$$\xi = \left(\frac{BL + RJ}{2JL}\right)\sqrt{\left(\frac{JL}{BR + k_\tau k_f}\right)}$$

Over-Damped Angular Velocity Response, equation (A.57):

$$\omega_{\xi>1}(t) = \omega_{ss}\left[1 - \frac{\omega_n}{\omega_d}e^{-\xi\omega_n t}\left[\xi\sinh(\omega_d t) + \sqrt{\xi^2 - 1}\cosh(\omega_d t)\right]\right]$$

Critically-Damped Angular Velocity Response, equation (A.70):

$$\omega_{\xi=1}(t) = \omega_{ss}\left[1 - e^{-\xi\omega_n t}\left[\omega_n t + 1\right]\right]$$

Under-Damped Angular Velocity Response, equations (A.85) and (A.86):

$$\omega_{\xi<1}(t) = \omega_{ss}\left[1 - e^{-\xi\omega_n t}\left(\frac{\sin\left(\omega_n\left(\sqrt{1-\xi^2}\right)t + \phi\right)}{\sqrt{1-\xi^2}}\right)\right]$$

$$\phi = \tan^{-1}\left(\frac{\sqrt{1-\xi^2}}{\xi}\right)$$

Current Transfer Function, equation (A.90):

$$\frac{I(s)}{V(s)} = \left(\frac{1}{L}\right)\left(\frac{\left(s + \frac{B}{J}\right)}{s^2 + \left(\frac{BL + RJ}{JL}\right)s + \left(\frac{BR + k_\tau k_f}{JL}\right)}\right)$$

Current Steady State Response, equation (A.111):

$$i_{ss} = V_{ss}\frac{B}{BR + k_\tau k_f}$$

Over-Damped Current Response, equation (A.113):

$$i_{\xi>1}(t) = i_{ss}\left[1 - e^{-\xi\omega_n t}\left(\cosh(\omega_d t) + \frac{\left(\xi - \frac{J\omega_n}{B}\right)}{\sqrt{\xi^2 - 1}}\sinh(\omega_d t)\right)\right]$$

Critically-Damped Current Response, equation (A.114):

$$i_{\xi=1}(t) = i_{ss}\left[1 - e^{-\omega_n t}\left(\left(1 - \frac{J\omega_n}{B}\right)\omega_n t + 1\right)\right]$$

91

Under-Damped Current Response, equation (A.117) and (A.118):

$$i_{\xi<1}(t) = i_{ss}\left(1 - \frac{e^{-\xi\omega_n t}}{\sqrt{1-\xi^2}}\sin\left(\omega_n\sqrt{1-\xi^2}\,t + \phi\right)\right)$$

$$\phi = \tan^{-1}\frac{\sqrt{1-\xi^2}}{\left(\xi - \dfrac{J\omega_n}{B}\right)}$$

3. State-Space Formulation of the Centrifuge External Dynamics Problem

A second means of solving the relationship for current and angular velocity was needed in order to ascertain the validity of the Analytical Model. Recalling from equations (A.1) and (A.2):

$$Ri + L\frac{di}{dt} = v - k_f\frac{d\theta}{dt}$$

$$k_\tau i = J\frac{d^2\theta}{dt^2} + B\frac{d\theta}{dt}$$

Rewriting in terms of ω:

$$Ri + L\frac{di}{dt} = V - k_f\omega \tag{A.119}$$

$$J\frac{d\omega}{dt} + B\omega = k_\tau i \tag{A.120}$$

Solving for the derivatives yields:

$$\frac{di}{dt} = -\left(\frac{R}{L}i + \frac{k_f}{L}\omega\right) + \frac{V}{L} \tag{A.121}$$

$$\frac{d\omega}{dt} = \frac{k_\tau}{J}i - \frac{B}{J}\omega \tag{A.122}$$

Rewriting equations (A.121) and (A.122) in matrix form for simultaneous resolution:

$$\frac{d}{dt}\begin{vmatrix} i \\ \omega \end{vmatrix} = \begin{vmatrix} (R/L) & -(k_f/L) \\ (k_\tau/J) & -(B/J) \end{vmatrix}\begin{vmatrix} i \\ \omega \end{vmatrix} + \begin{vmatrix} (1/L) \\ 0 \end{vmatrix}V \tag{A.123}$$

Equation (A.123) may be represented by the state-space formulation:

$$\dot{\overline{\mathbf{X}}} = \mathbf{A}\overline{\mathbf{X}} + \mathbf{BU} \qquad \text{(A.124)}$$

Where:

$$\overline{\mathbf{X}} = \begin{vmatrix} i \\ \omega \end{vmatrix} \qquad \text{(A.125)}$$

$$\mathbf{A} = \begin{vmatrix} \left(\dfrac{R}{L}\right) & \left(-\dfrac{k_f}{L}\right) \\ \left(\dfrac{k_\tau}{J}\right) & \left(-\dfrac{B}{J}\right) \end{vmatrix} \qquad \text{(A.126)}$$

$$\mathbf{B} = \begin{vmatrix} L^{-1} \\ 0 \end{vmatrix} \qquad \text{(A.127)}$$

$$\mathbf{U} = V \qquad \text{(A.128)}$$

And:

$$\dot{\overline{\mathbf{X}}} = \frac{\overline{\mathbf{X}}_{t+\Delta t} - \overline{\mathbf{X}}_t}{\Delta t} \qquad \text{(A.129)}$$

Substituting equation (A.129) into equation (A.124) yields:

$$\frac{\overline{\mathbf{X}}_{t+\Delta t} - \overline{\mathbf{X}}_t}{\Delta t} \approx \mathbf{A}\left(\frac{\overline{\mathbf{X}}_{t+\Delta t} + \overline{\mathbf{X}}_t}{2}\right) + \mathbf{BU} \qquad \text{(A.130)}$$

Simplifying equation (A.130):

$$\overline{\mathbf{X}}_{t+\Delta t} - \overline{\mathbf{X}}_t = \mathbf{A}\Delta t\left(\frac{\overline{\mathbf{X}}_{t+\Delta t} + \overline{\mathbf{X}}_t}{2}\right) + \mathbf{BU}\Delta t \qquad \text{(A.131)}$$

$$\overline{\mathbf{X}}_{t+\Delta t} = \mathbf{A}\Delta t\left(\frac{\overline{\mathbf{X}}_{t+\Delta t} + \overline{\mathbf{X}}_t}{2}\right) + \mathbf{BU}\Delta t + \overline{\mathbf{X}}_t \qquad \text{(A.132)}$$

$$\overline{\mathbf{X}}_{t+\Delta t} - \mathbf{A}\Delta t\left(\frac{\overline{\mathbf{X}}_{t+\Delta t}}{2}\right) = \mathbf{A}\Delta t\left(\frac{\overline{\mathbf{X}}_t}{2}\right) + \mathbf{BU}\Delta t + \overline{\mathbf{X}}_t \qquad \text{(A.133)}$$

$$\left(\mathbf{I} - \frac{\mathbf{A}\Delta t}{2}\right)\overline{\mathbf{X}}_{t+\Delta t} = \left(\mathbf{I} + \frac{\mathbf{A}\Delta t}{2}\right)\overline{\mathbf{X}}_t + \mathbf{BU}\Delta t \qquad \text{(A.134)}$$

$$\overline{\mathbf{X}}_{t+\Delta t} = \left(\mathbf{I} - \frac{\mathbf{A}\Delta t}{2}\right)^{-1}\left[\left(\mathbf{I} + \frac{\mathbf{A}\Delta t}{2}\right)\overline{\mathbf{X}}_t + \mathbf{BU}\Delta t\right] \qquad \text{(A.135)}$$

The two terms in equation (A.135) containing the identity matrix must be resolved before the determinant can be found. First:

$$\left[\mathbf{I} + \frac{\mathbf{A}\Delta t}{2} \right] = \begin{vmatrix} 1 & 0 \\ 0 & 1 \end{vmatrix} + \frac{\Delta t}{2} \begin{vmatrix} \left(R/L \right) & -\left(k_f/L \right) \\ \left(k_\tau/J \right) & -\left(B/J \right) \end{vmatrix} \tag{A.136}$$

$$\left[\mathbf{I} + \frac{\mathbf{A}\Delta t}{2} \right] = \begin{vmatrix} 1 & 0 \\ 0 & 1 \end{vmatrix} + \begin{vmatrix} \left(R\Delta t/2L \right) & -\left(k_f\Delta t/2L \right) \\ \left(k_\tau\Delta t/2J \right) & -\left(B\Delta t/2J \right) \end{vmatrix} \tag{A.137}$$

$$\left[\mathbf{I} + \frac{\mathbf{A}\Delta t}{2} \right] = \begin{vmatrix} 1 + \left(R\Delta t/2L \right) & -\left(k_f\Delta t/2L \right) \\ \left(k_\tau\Delta t/2J \right) & 1 - \left(B\Delta t/2J \right) \end{vmatrix} \tag{A.138}$$

Second, the inverted term:

$$\left[\mathbf{I} - \frac{\mathbf{A}\Delta t}{2} \right] = \begin{vmatrix} 1 & 0 \\ 0 & 1 \end{vmatrix} - \frac{\Delta t}{2} \begin{vmatrix} \left(R/L \right) & -\left(k_f/L \right) \\ \left(k_\tau/J \right) & -\left(B/J \right) \end{vmatrix} \tag{A.139}$$

$$\left[\mathbf{I} - \frac{\mathbf{A}\Delta t}{2} \right] = \begin{vmatrix} 1 & 0 \\ 0 & 1 \end{vmatrix} - \begin{vmatrix} \left(R\Delta t/2L \right) & -\left(k_f\Delta t/2L \right) \\ \left(k_\tau\Delta t/2J \right) & -\left(B\Delta t/2J \right) \end{vmatrix} \tag{A.140}$$

$$\left[\mathbf{I} - \frac{\mathbf{A}\Delta t}{2} \right] = \begin{vmatrix} 1 - \left(R\Delta t/2L \right) & \left(k_f\Delta t/2L \right) \\ -\left(k_\tau\Delta t/2J \right) & 1 + \left(B\Delta t/2J \right) \end{vmatrix} \tag{A.141}$$

The inverse of a matrix can be found using the following rule[57]:

$$\mathbf{M}_{2\times 2} = \begin{vmatrix} a & b \\ c & d \end{vmatrix}$$

---

[57] Dennis G. Zill, <u>A First Course in Differential Equations with Applications</u>, 4th Ed., Boston: PWS-Kent, 1989, p. 384

$$\mathbf{M}_{2\times2}^{-1} = \frac{\begin{vmatrix} d & -b \\ -c & a \end{vmatrix}}{(ad)-(bc)}$$

Therefore, the second term is:

$$\left[\mathbf{I}-\frac{\mathbf{A}\Delta t}{2}\right] = \frac{\begin{vmatrix} \left(1+\dfrac{B\Delta t}{2J}\right) & \left(-\dfrac{k_f\Delta t}{2L}\right) \\ \left(\dfrac{k_\tau\Delta t}{2J}\right) & \left(1-\dfrac{R\Delta t}{2L}\right) \end{vmatrix}}{\left(1-\dfrac{R\Delta t}{2L}\right)\left(1+\dfrac{B\Delta t}{2J}\right)-\left(\dfrac{k_f\Delta t}{2L}\right)\left(-\dfrac{k_\tau\Delta t}{2J}\right)} \tag{A.142}$$

$$\left[\mathbf{I}-\frac{\mathbf{A}\Delta t}{2}\right] = \frac{\begin{vmatrix} \left(1+\dfrac{B\Delta t}{2J}\right) & \left(-\dfrac{k_f\Delta t}{2L}\right) \\ \left(\dfrac{k_\tau\Delta t}{2J}\right) & \left(1-\dfrac{R\Delta t}{2L}\right) \end{vmatrix}}{\left(1-\dfrac{R\Delta t}{2L}+\dfrac{B\Delta t}{2J}-\dfrac{BR\Delta t^2}{4JL}-\dfrac{k_f k_\tau \Delta t^2}{4JL}\right)} \tag{A.143}$$

Recalling the terms defined in equations (A.125), (A.126), (A.127), (A.128), (A.138), and (A.143) yields the following when substituted into equation (A.135):

$$\overline{\mathbf{X}}_{t+\Delta t} = \frac{\left[\begin{vmatrix} \left(1+\dfrac{B\Delta t}{2J}\right) & \left(-\dfrac{k_f\Delta t}{2L}\right) \\ \left(\dfrac{k_\tau\Delta t}{2J}\right) & \left(1-\dfrac{R\Delta t}{2L}\right) \end{vmatrix}\begin{vmatrix} \left(1+\dfrac{R\Delta t}{2L}\right) & \left(-\dfrac{k_f\Delta t}{2L}\right) \\ \left(\dfrac{k_\tau\Delta t}{2J}\right) & \left(1-\dfrac{B\Delta t}{2J}\right) \end{vmatrix}\begin{vmatrix} i \\ \omega \end{vmatrix}_t + \begin{vmatrix} \dfrac{1}{L} \\ 0 \end{vmatrix}V\Delta t\right]}{\left(1-\dfrac{R\Delta t}{2L}+\dfrac{B\Delta t}{2J}-\dfrac{BR\Delta t^2}{4JL}-\dfrac{k_f k_\tau \Delta t^2}{4JL}\right)} \tag{A.144}$$

$$\overline{\mathbf{X}}_{t+\Delta t} = \frac{\begin{vmatrix} \left(1+\dfrac{B\Delta t}{2J}\right) & \left(-\dfrac{k_f\Delta t}{2L}\right) \\ \left(\dfrac{k_\tau\Delta t}{2J}\right) & \left(1-\dfrac{R\Delta t}{2L}\right) \end{vmatrix}\left[\begin{vmatrix} i+\dfrac{iR\Delta t}{2L}-\dfrac{k_f\omega\Delta t}{2L} \\ \dfrac{ik_\tau\Delta t}{2J}+\omega-\dfrac{B\omega\Delta t}{2J} \end{vmatrix}_t + \begin{vmatrix} \left(\dfrac{V\Delta t}{L}\right) \\ 0 \end{vmatrix}\right]}{\left(1-\dfrac{R\Delta t}{2L}+\dfrac{B\Delta t}{2J}-\dfrac{BR\Delta t^2}{4JL}-\dfrac{k_f k_\tau \Delta t^2}{4JL}\right)} \tag{A.145}$$

$$\overline{\mathbf{X}}_{t+\Delta t} = \frac{\begin{vmatrix} \left(1+\dfrac{B\Delta t}{2J}\right) & \left(-\dfrac{k_f\Delta t}{2L}\right) \\ \left(\dfrac{k_\tau\Delta t}{2J}\right) & \left(1-\dfrac{R\Delta t}{2L}\right) \end{vmatrix} \begin{vmatrix} i_t+\dfrac{i_tR\Delta t}{2L}-\dfrac{k_f\omega_t\Delta t}{2L}+\dfrac{V\Delta t}{L} \\ \dfrac{i_tk_\tau\Delta t}{2J}+\omega_t-\dfrac{B\omega_t\Delta t}{2J} \end{vmatrix}}{\left(1-\dfrac{R\Delta t}{2L}+\dfrac{B\Delta t}{2J}-\dfrac{BR\Delta t^2}{4JL}-\dfrac{k_fk_\tau\Delta t^2}{4JL}\right)} \quad \text{(A.146)}$$

$$\overline{\mathbf{X}}_{t+\Delta t} = \frac{\begin{vmatrix} \left(1+\dfrac{B\Delta t}{2J}\right)\left(i_t+\dfrac{i_tR\Delta t}{2L}-\dfrac{k_f\omega_t\Delta t}{2L}+\dfrac{V\Delta t}{L}\right)+\left(-\dfrac{k_f\Delta t}{2L}\right)\left(\dfrac{i_tk_\tau\Delta t}{2J}+\omega_t-\dfrac{B\omega_t\Delta t}{2J}\right) \\ \left(\dfrac{k_\tau\Delta t}{2J}\right)\left(i_t+\dfrac{i_tR\Delta t}{2L}-\dfrac{k_f\omega_t\Delta t}{2L}+\dfrac{V\Delta t}{L}\right)+\left(1-\dfrac{R\Delta t}{2L}\right)\left(\dfrac{i_tk_\tau\Delta t}{2J}+\omega_t-\dfrac{B\omega_t\Delta t}{2J}\right) \end{vmatrix}}{\left(1-\dfrac{R\Delta t}{2L}+\dfrac{B\Delta t}{2J}-\dfrac{BR\Delta t^2}{4JL}-\dfrac{k_fk_\tau\Delta t^2}{4JL}\right)} \quad \text{(A.147)}$$

$$\begin{vmatrix} i \\ \omega \end{vmatrix}_{t+\Delta t} = \frac{\begin{vmatrix} \left(1+\dfrac{B\Delta t}{2J}\right)\left(i_t+\dfrac{i_tR\Delta t}{2L}-\dfrac{k_f\omega_t\Delta t}{2L}+\dfrac{V\Delta t}{L}\right)-\left(\dfrac{i_tk_fk_\tau\Delta t^2}{4JL}+\dfrac{k_f\omega_t\Delta t}{2L}-\dfrac{Bk_f\omega_t\Delta t^2}{4JL}\right) \\ \left(\dfrac{i_tk_\tau\Delta t}{2J}+\dfrac{i_tk_\tau R\Delta t^2}{4JL}-\dfrac{k_fk_\tau\omega_t\Delta t^2}{4JL}+\dfrac{k_\tau V\Delta t^2}{2JL}\right)+\left(1-\dfrac{R\Delta t}{2L}\right)\left(\dfrac{i_tk_\tau\Delta t}{2J}+\omega_t-\dfrac{B\omega_t\Delta t}{2J}\right) \end{vmatrix}}{\left(1-\dfrac{R\Delta t}{2L}+\dfrac{B\Delta t}{2J}-\dfrac{BR\Delta t^2}{4JL}-\dfrac{k_fk_\tau\Delta t^2}{4JL}\right)} \quad \text{(A.148)}$$

The simultaneous solution of $i_{t+\Delta t}$ and $\omega_{t+\Delta t}$ yields the final form of each equation.

$$i_{t+\Delta t} = \frac{\left(1+\dfrac{B\Delta t}{2J}\right)\left(i_t+\dfrac{i_tR\Delta t}{2L}-\dfrac{k_f\omega_t\Delta t}{2L}+\dfrac{V\Delta t}{L}\right)-\left(\dfrac{i_tk_fk_\tau\Delta t^2}{4JL}+\dfrac{k_f\omega_t\Delta t}{2L}-\dfrac{Bk_f\omega_t\Delta t^2}{4JL}\right)}{\left(1-\dfrac{R\Delta t}{2L}+\dfrac{B\Delta t}{2J}-\dfrac{BR\Delta t^2}{4JL}-\dfrac{k_fk_\tau\Delta t^2}{4JL}\right)} \quad \text{(A.149)}$$

$$\omega_{t+\Delta t} = \frac{\left(\dfrac{i_tk_\tau\Delta t}{2J}+\dfrac{i_tk_\tau R\Delta t^2}{4JL}-\dfrac{k_fk_\tau\omega_t\Delta t^2}{4JL}+\dfrac{k_\tau V\Delta t^2}{2JL}\right)+\left(1-\dfrac{R\Delta t}{2L}\right)\left(\dfrac{i_tk_\tau\Delta t}{2J}+\omega_t-\dfrac{B\omega_t\Delta t}{2J}\right)}{\left(1-\dfrac{R\Delta t}{2L}+\dfrac{B\Delta t}{2J}-\dfrac{BR\Delta t^2}{4JL}-\dfrac{k_fk_\tau\Delta t^2}{4JL}\right)} \quad \text{(A.150)}$$

The numerical results of the analytical model (Equations (A.15), (A.17), (A.25), (A.27), (A.48), (A.57), (A.70), (A.85), (A.90), (A.111), (A.113), (A.114), (A.117), and (A.118)) and the state space model (Equations (A.15), (A.17), and (A.123)) have been compared and are equivalent.

THIS PAGE INTENTIONALLY LEFT BLANK

B.   APPENDIX B

1.   Modeling the Internal Dynamics of a Centrifuge

This section discusses the mathematical rigor behind the dynamics of a rotational environment.

Equation Section (Next)

Analytical Term	Meaning	Units
$\bar{i}_R$	Centrifuge Radial Axis	Unitless
$\bar{i}_v$	Centrifuge Angular Axis	Unitless
$\bar{i}_k$	Centrifuge Axial Axis	Unitless
R	Linear Position	m
V	Linear Velocity	m/s
θ	Angular Position	rad
ω	Angular Velocity	rad/s
g_0	Average Earth Gravity at Sea Level, 9.81 m/s²	m/s²
g_C	Centrifugal Acceleration	m/s²
G	"G" Level	Unitless
F	Force	N

Table 15: Centrifgue Internal Terms

2.   Velocity

The velocity of a subject (as shown in Figure 61) within a centrifuge may be expressed in terms relative to the external world as follows:

$$V_{ext} = \frac{d\overline{\mathbf{R}}}{dt} + \left(\overrightarrow{\omega} \times \overline{\mathbf{R}} \right) \tag{B.1}$$

3.   Acceleration

Similarly, the acceleration of a subject within a centrifuge may be expressed in terms relative to the external world as follows:

$$\frac{\sum F_{ext}}{m} = \frac{d\overline{\mathbf{V}}_{ext}}{dt} + \left(\overrightarrow{\omega} \times \overline{\mathbf{V}}_{ext} \right) \tag{B.2}$$

99

Substituting the equation (B.1) into equation (B.2) yields:

$$\frac{\sum F_{ext}}{m} = \frac{d\left(\frac{d\overline{\mathbf{R}}}{dt} + (\overline{\omega} \times \overline{\mathbf{R}})\right)}{dt} + \left(\overline{\omega} \times \left(\frac{d\overline{\mathbf{R}}}{dt} + (\overline{\omega} \times \overline{\mathbf{R}})\right)\right) \quad (B.3)$$

Expanding equation (B.3) and collecting terms results in the following:

$$\frac{\sum F_{ext}}{m} = \left(\frac{d^2\overline{\mathbf{R}}}{dt^2} + \left(\frac{d\overline{\omega}}{dt} \times \overline{\mathbf{R}}\right)\right) + \left(2\overline{\omega} \times \frac{d\overline{\mathbf{R}}}{dt}\right) + \left(\overline{\omega} \times (\overline{\omega} \times \overline{\mathbf{R}})\right) \quad (B.4)$$
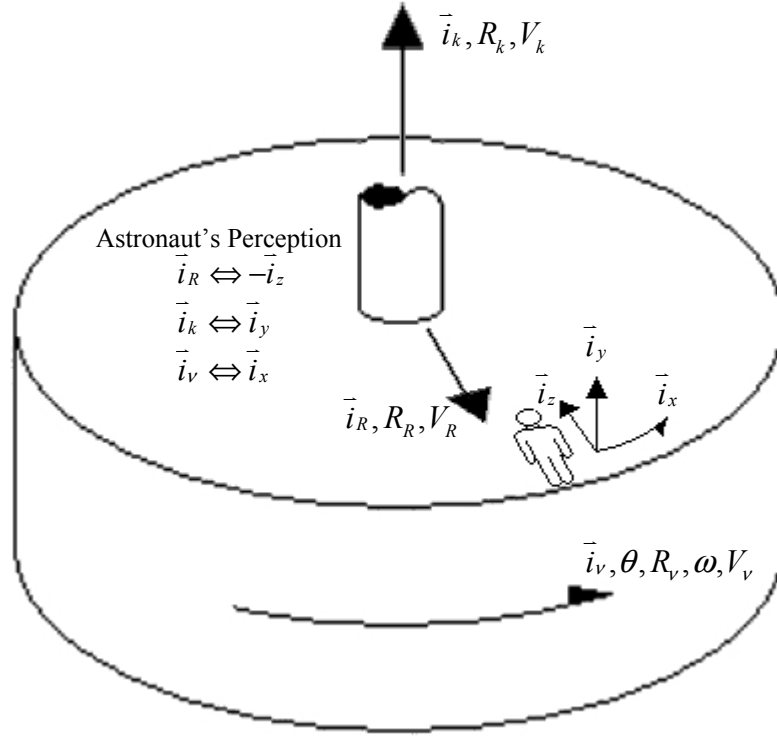

Figure 61: Centrifuge Internal Terms

a.   *Special Condition: Micro-Gravity, No Thrust*

In a micro-gravity environment, there will normally be no external forces acting on the centrifuge. Therefore:

$$\frac{\sum F_{ext}}{m} = 0 \quad (B.5)$$

100

b.   *Special Condition: Centrifuge Steady State*

Once the centrifuge is "up to speed" angular velocity will remain constant. Therefore:

$$\frac{d\overline{\omega}}{dt} = 0 \tag{B.6}$$

c.   *Application of Special Conditions*

Under the special conditions detailed in equations (B.5) and (B.6), equation (B.4) may be reduced as follows:

$$0 = \left(\frac{d^2\overline{R}}{dt^2} + \left(0 \times \overline{R}\right)\right) + \left(2\overline{\omega} \times \frac{d\overline{R}}{dt}\right) + \left(\overline{\omega} \times \left(\overline{\omega} \times \overline{R}\right)\right) \tag{B.7}$$

$$0 = \frac{d^2\overline{R}}{dt^2} + \left(2\overline{\omega} \times \frac{d\overline{R}}{dt}\right) + \left(\overline{\omega} \times \left(\overline{\omega} \times \overline{R}\right)\right) \tag{B.8}$$

$$\frac{d^2\overline{R}}{dt^2} = \left(\overline{\omega} \times \left(\overline{R} \times \overline{\omega}\right)\right) - \left(2\overline{\omega} \times \frac{d\overline{R}}{dt}\right) \tag{B.9}$$

4.   Apparent Forces

Equation (B.9) shows three groups of terms. The first of which is Apparent Acceleration:

$$\frac{d^2\overline{R}}{dt^2}$$

The second term is Centrifugal Force:

$$\overline{\omega} \times \left(\overline{R} \times \overline{\omega}\right)$$

The third term is Coriolis Force:

$$-\left(2\overline{\omega} \times \frac{d\overline{R}}{dt}\right)$$

a.   *Centrifugal Force*

The axial components of centrifugal force may be developed by utilizing Vector Analysis:

$$\mathbf{R} \times \vec{\omega} = \begin{vmatrix} \vec{i}_R & \vec{i}_v & \vec{i}_k \\ R & 0 & 0 \\ 0 & 0 & \omega \end{vmatrix} = -R\omega \vec{i}_v \qquad (\text{B.10})$$

$$\vec{\omega} \times \left(\mathbf{R} \times \vec{\omega}\right) = \begin{vmatrix} \vec{i}_R & \vec{i}_v & \vec{i}_k \\ 0 & 0 & \omega \\ 0 & -R\omega & 0 \end{vmatrix} = R\omega^2 \vec{i}_R \qquad (\text{B.11})$$

The results of equation (B.11) may be validated through comparison with two references[58,59] and by recalling equation (B.5):

$$\frac{F_{centrifugal}}{m} = R\omega^2 \vec{i}_R \qquad (\text{B.12})$$

b.   Coriolis Force

As with centrifugal force, the axial components of Coriolis Force may be developed by utilizing Vector Analysis:

$$-\left(2\vec{\omega} \times \frac{d\mathbf{R}}{dt}\right) = -2 \begin{vmatrix} \vec{i}_R & \vec{i}_v & \vec{i}_k \\ 0 & 0 & \omega \\ \left(\frac{dR_R}{dt}\right) & \left(\frac{dR_v}{dt}\right) & \left(\frac{dR_k}{dt}\right) \end{vmatrix} = 2\left(\omega\left(\frac{dR_v}{dt}\right)\vec{i}_R - \omega\left(\frac{dR_R}{dt}\right)\vec{i}_v\right) \quad (\text{B.13})$$

The results of equation (B.13) may be validated through the use of two references[60,61] and by recalling equations (B.5) and (B.6):

$$\frac{F_{coriolis}}{m} = 2\left(\omega\frac{dR_v}{dt}\vec{i}_R - \omega\frac{dR_R}{dt}\vec{i}_v\right) \qquad (\text{B.14})$$

Note that equation (B.14) shows that there are two components of Coriolis Force in a centrifuge. The first is the result of a linear change in angular position (for example, walking a distance across the floor into or away from the rotation of the

---

[58] J.L. Meriam and L.G. Kraige, Engineering Mechanics Vol. 2: Dynamics, 2nd Edition, New York: John Wiley and Sons, 1986, pp. 223-224 and 350

[59] Dare A. Wells and Harold S. Slusher, Schaum's Outline of Theory and Problems of Physics for Engineering and Science, New York: McGraw-Hill, 1983, p. 39

[60] Meriam and Kraige, Dynamics, p. 350

[61] Wells and Slusher, p. 64

centrifuge). This force appears as either an increase or decrease in apparent gravity, as follows:

$$\frac{F_{coriolis,horizontal}}{m} = 2\omega\frac{dR_v}{dt}\vec{i}_R \tag{B.15}$$

The second component of Coriolis Force is the result of a linear change in radial position (examples include: sitting, standing, or climbing a ladder). This force appears as a shear force that occurs with or against the rotation of the centrifuge, as follows:

$$\frac{F_{coriolis,vertical}}{m} = -2\omega\frac{dR_R}{dt}\vec{i}_v \tag{B.16}$$

5. Vertical Coriolis Versus Centrifgue Radius

Focusing on the disorienting effects of vertical Coriolis on human equilibrium, a relationship between vertical Coriolis and centrifuge radius should be developed.

Redefining centrifugal acceleration in terms of G-Level yields:

$$\frac{F_{centrifugal}}{m} = a_{centrifugal}\vec{i}_R = R\omega^2\vec{i}_R \tag{B.17}$$

$$g_{centrifugal} = \frac{a_{centrifgual}}{g_0} = \frac{R\omega^2}{g_0} \tag{B.18}$$

Therefore, to find the proportionality of vertical Coriolis to centrifugal radius, the following expression must be developed:

$$\frac{\left(\dfrac{F_{coriolis,vertical}}{m}\right)}{g_{centrifugal}} = \frac{\left(-2\omega\dfrac{dR_R}{dt}\right)}{\left(\dfrac{R\omega^2}{g_0}\right)}\vec{i}_v = \frac{2g_0\left(\dfrac{dR_R}{dt}\right)}{R\omega}\vec{i}_v \tag{B.19}$$

Redefining centrifugal acceleration in terms of angular velocity yields:

$$\omega = \sqrt{\frac{g_{centrifugal}g_0}{R}} \tag{B.20}$$

Thus, equation (B.19) may be redefined as:

$$\frac{\left(\dfrac{F_{coriolis,vertical}}{m}\right)}{g_{centrifugal}} = \frac{2g_0\left(\dfrac{dR_R}{dt}\right)}{R\sqrt{\dfrac{g_{centrifugal}g_0}{R}}}\vec{i}_v \qquad (B.21)$$

$$\frac{\left(\dfrac{F_{coriolis,vertical}}{m}\right)}{g_{centrifugal}} = 2\left(\frac{dR_R}{dt}\right)\sqrt{\left(\frac{g_0}{R}\right)^2 \frac{R}{g_{centrifugal}g_0}} \qquad (B.22)$$

$$\frac{\left(\dfrac{F_{coriolis,vertical}}{m}\right)}{g_{centrifugal}} = 2\left(\frac{dR_R}{dt}\right)\sqrt{\frac{g_0}{Rg_{centrifugal}}} \qquad (B.23)$$

Therefore, for a given "G-Level," the vertical Coriolis is inversely proportional to the square root of the centrifuge radius.

6.   Gravity Gradient

Developing a relationship that defines gravity gradient is useful in scaling experiments so that their applicability to a human's experience of a centrifugal environment is best reproduced. Recalling from equation (B.18):

$$g_{centrifugal} = \frac{R\omega^2}{g_0}$$

The radial change in apparent gravity, gravity gradient is the derivative of equation (B.18) with relation to radial position:

$$\frac{d}{dR}\left(g_{centrifugal}\right) = \frac{\omega^2}{g_0}\frac{d}{dR}(R) \qquad (B.24)$$

$$\frac{dg_{centrifugal}}{dR} = \frac{\omega^2}{g_0}(1) = \frac{\omega^2}{g_0} \qquad (B.25)$$

To find the proportion of gravity gradient to centrifugal radius, the following expression must be developed:

$$\frac{\dot{g}_{centrifugal}}{g_{centrifugal}} = \frac{\left(\dfrac{\omega^2}{g_0}\right)}{\left(\dfrac{R\omega^2}{g_0}\right)} = \frac{1}{R} \qquad (B.26)$$

Therefore, for a given "G-Level," the gravity gradient is inversely proportional to the centrifuge radius.

THIS PAGE INTENTIONALLY LEFT BLANK

C.   APPENDIX C

1.   Modeling the Human Ability to Sense Rotation

This section discusses the mathematical rigor behind the human disorientation model.

Equation Section (Next)

Analytical Term	Meaning	Units
b	Torque per unit of relative angular velocity[62]	1/s
F_h	Force on the head	N
$\vec{i}_{R,v,k}$	Centrifuge Radial, Angular, and Axial Axes	Unitless
J_h	Mass Moment of Inertia of the head	kg·m²
k	Torque per unit of relative angular displacement	1/s
R	Linear Position	M
V	Linear Velocity	m/s
θ	Angular Position	rad
τ_h	Torque on the head	N·m
ϕ	Cupula Angular Position	rad
$\dot{\phi}$	Cupula Angular Velocity	rad/s
$\ddot{\psi}$	Head Angular Acceleration	rad
ω	Centrifuge Angular Velocity	rad/s

Table 16: Human Perception Terms

2.   Coriolis in a Centrifuge

The somatogravic illusion (shown in Figure 62) of level ground generated by the centrifuge is disrupted whenever an Astronaut moves as shown in Appendix B, equation (B.9):

$$\frac{d^2\overline{R}}{dt^2} = \left(\overline{\omega}\times\left(\overline{R}\times\overline{\omega}\right)\right) - \left(2\overline{\omega}\times\frac{d\overline{R}}{dt}\right)$$
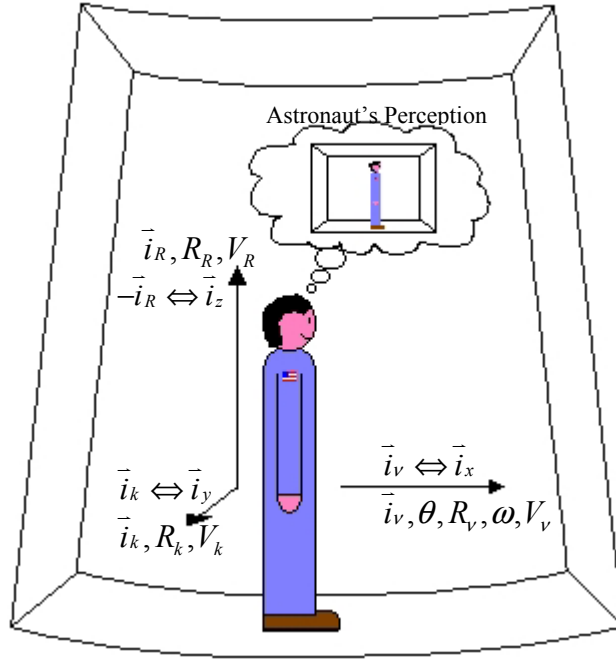
---

[62] Milsum, p. 187

Figure 62: Human Perception of the Centrifugal Environment

As the Astronaut Moves, a new Somatogravic Illusion is generated due to the application of new force vectors. The added force vectors result from the Coriolis Term in equation (B.9) and are detailed in equation (B.14):

$$\frac{F_{coriolis}}{m} = 2\left(\omega \frac{dR_v}{dt} \vec{i}_R - \omega \frac{dR_R}{dt} \vec{i}_v \right)$$

Solving equation (B.14) in terms of Force and expressing position change in terms of velocity yields:

$$-F_{coriolis} = 2m\omega V_v \vec{i}_R - 2m\omega V_R \vec{i}_v \qquad \text{(C.1)}$$

3.   Describing the Semi-Circular Canals in Terms of Head Rotation

The relationship between the orientation of the head in space and the semi-circular canals is given by the following second order equation based on Newton's Second Law[63]:

$$b\left(\dot{\psi} - \dot{\theta}\right) + k\left(\psi - \theta\right) = J\ddot{\theta} \qquad \text{(C.2)}$$

---

[63] Milsum, p. 187

Cupula Deflection (ϕ) per unit relative angular displacement between the skull and endolymph fluid is defined as[64]:

$$\phi = a(\psi - \theta) \tag{C.3}$$

The coefficient, a, is the area ratio between the canal and ampulla, however this model is based on a general case and thus:

$$a = 1 \tag{C.4}$$

$$\phi = \psi - \theta \tag{C.5}$$

Rewriting equation (C.2) as a consequence of equation (C.5) yields:

$$J\ddot{\phi} + b\dot{\phi} + k\phi = J\ddot{\psi} \tag{C.6}$$

4.   Torque Imposed on the Endolymph by Coriolis

The endolymph in the semi-circular canal resides in what is essentially a thin tube. It's Mass Moment of Inertia (J_h)[65] is best described as:

$$J_h = m_h R_R^2 \tag{C.7}$$

Substituting equation (C.7) into the right side of equation (C.6) yields:

$$J\ddot{\psi} = m_h R^2 \ddot{\psi} = \tau_h \tag{C.8}$$

Noting the definition of torque (τ)[66]:

$$\tau = F \times R \tag{C.9}$$

Determining the value of τ requires that the vector product of Coriolis and distance from the center of rotation be found:

$$\tau_h = \begin{vmatrix} \vec{i}_R & \vec{i}_v & \vec{i}_k \\ 2m_h\omega V_v & -2m_h\omega V_R & 0 \\ R & 0 & 0 \end{vmatrix} = 2m_h\omega V_R R\vec{i}_k \tag{C.10}$$

It is worth noting that τ_h due to Coriolis is only felt in the axial plane.

$$\tau_h \vec{i}_k = \tau_k \tag{C.11}$$

---

[64] Milsum, p. 187

[65] Meriam and Kraige, <u>Dynamics</u>, p. 630

[66] Meriam and Kraige, <u>Engineering Mechanics Vol. 1: Statics</u>, 2nd Edition, New York: John Wiley and Sons, 1986, p. 30

5. Quantitative Analysis of Angular Acceleration Inputs Resulting from Coriolis

To determine, through quantitative analysis, the angular acceleration input from the semi-circular canals as a result of Coriolis, the solution to ϕ and Cupula Veloctiy ($\dot{\phi}$) must be found. Recalling equation (C.8) and substituting the determinant of equation (C.10) yields the following:

$$m_h R^2 \ddot{\psi} = \tau_k = 2 m_h \omega V_R R \tag{C.12}$$

Solving equation (C.12) in terms of $\ddot{\psi}$:

$$\ddot{\psi} = \frac{2 m_h \omega V_R R}{m_h R^2} = \frac{2 \omega V_R}{R} \tag{C.13}$$

Substituting the result of equation (C.13) into the right side of equation (C.6):

$$J\ddot{\phi} + b\dot{\phi} + k\phi = J \frac{2 \omega V_R}{R} \tag{C.14}$$

$$\ddot{\phi} + \frac{b}{J}\dot{\phi} + \frac{k}{J}\phi = \frac{2 \omega V_R}{R} \tag{C.15}$$

Allowing:

$$\begin{vmatrix} \phi \\ \dot{\phi} \end{vmatrix} = \begin{vmatrix} x_1 \\ x_2 \end{vmatrix} \tag{C.16}$$

By substitution:

$$\dot{x}_2 + \frac{b}{J}x_2 + \frac{k}{J}x_1 = \frac{2 \omega V_R}{R} \tag{C.17}$$

Noting that:

$$\dot{x}_1 = x_2 \tag{C.18}$$

$$\dot{x}_2 = \frac{2 \omega V_R}{R} - \frac{b}{J}x_2 - \frac{k}{J}x_1 \tag{C.19}$$

Equations (C.18) and (C.19) may be solved simultaneously using matrix algebra:

$$\frac{d}{dt}\begin{vmatrix} x_1 \\ x_2 \end{vmatrix} = \begin{vmatrix} 0 & 1 \\ \left(-\dfrac{k}{J}\right) & \left(-\dfrac{b}{J}\right) \end{vmatrix} \begin{vmatrix} x_1 \\ x_2 \end{vmatrix} + \begin{vmatrix} 0 \\ \left(\dfrac{2 \omega V_R}{R}\right) \end{vmatrix} \tag{C.20}$$

By letting:

$$\mathbf{X} = \begin{vmatrix} x_1 \\ x_2 \end{vmatrix} \tag{C.21}$$

$$\mathbf{A} = \begin{vmatrix} 0 & 1 \\ \left(-\dfrac{k}{J}\right) & \left(-\dfrac{b}{J}\right) \end{vmatrix} \tag{C.22}$$

$$\mathbf{U} = \begin{vmatrix} 0 \\ \left(\dfrac{2\omega V_R}{R}\right) \end{vmatrix} \tag{C.23}$$

Equation (C.20) can be simplified as follows:

$$\dot{\mathbf{X}} = \mathbf{A}\overline{\mathbf{X}} + \mathbf{U} \tag{C.24}$$

Noting that:

$$\dot{\mathbf{X}} = \frac{\mathbf{X}_{t+\Delta t} - \mathbf{X}_t}{\Delta t} \tag{C.25}$$

Equation (C.24) can be expanded as follows:

$$\frac{\mathbf{X}_{t+\Delta t} - \mathbf{X}_t}{\Delta t} \approx \mathbf{A}\left(\frac{\mathbf{X}_{t+\Delta t} + \mathbf{X}_t}{2}\right) + \mathbf{U} \tag{C.26}$$

Solving for $\mathbf{X}_{t+\Delta t}$ yields:

$$\mathbf{X}_{t+\Delta t} - \mathbf{X}_t = \mathbf{A}\Delta t\left(\frac{\mathbf{X}_{t+\Delta t} + \mathbf{X}_t}{2}\right) + \mathbf{U} \tag{C.27}$$

$$\mathbf{X}_{t+\Delta t} = \mathbf{A}\Delta t\left(\frac{\mathbf{X}_{t+\Delta t} + \mathbf{X}_t}{2}\right) + \mathbf{U} + \mathbf{X}_t \tag{C.28}$$

Removing the $\mathbf{X}_{t+\Delta t}$ from the right side of equation (C.28):

$$\mathbf{X}_{t+\Delta t} = \left(\frac{\mathbf{A}\Delta t\mathbf{X}_{t+\Delta t} + \mathbf{A}\Delta t\mathbf{X}_t}{2}\right) + \mathbf{U} + \mathbf{X}_t \tag{C.29}$$

$$\mathbf{X}_{t+\Delta t} - \mathbf{A}\Delta t\left(\frac{\mathbf{X}_{t+\Delta t}}{2}\right) = \mathbf{A}\Delta t\left(\frac{\mathbf{X}_t}{2}\right) + \mathbf{U} + \mathbf{X}_t \tag{C.30}$$

$$\left[\mathbf{I} - \frac{\mathbf{A}\Delta t}{2}\right]\mathbf{X}_{t+\Delta t} = \left[\mathbf{I} + \frac{\mathbf{A}\Delta t}{2}\right]\mathbf{X}_t + \mathbf{U}\Delta t \tag{C.31}$$

$$\mathbf{X}_{t+\Delta t} = \left[\mathbf{I} - \frac{\mathbf{A}\Delta t}{2}\right]^{-1}\left(\left[\mathbf{I} + \frac{\mathbf{A}\Delta t}{2}\right]\mathbf{X}_t + \mathbf{U}\Delta t\right) \tag{C.32}$$

111

The two terms in equation (C.32) containing the identity matrix must be resolved before the determinant can be found. First:

$$\left[\mathbf{I}+\frac{\mathbf{A}\Delta t}{2}\right]=\begin{vmatrix}1 & 0\\0 & 1\end{vmatrix}+\frac{\Delta t}{2}\begin{vmatrix}0 & 1\\-\left(k/J\right) & -\left(b/J\right)\end{vmatrix} \tag{C.33}$$

$$\left[\mathbf{I}+\frac{\mathbf{A}\Delta t}{2}\right]=\begin{vmatrix}1 & 0\\0 & 1\end{vmatrix}+\begin{vmatrix}0 & \Delta t/2\\-\left(k\Delta t/2J\right) & -\left(b\Delta t/2J\right)\end{vmatrix} \tag{C.34}$$

$$\left[\mathbf{I}+\frac{\mathbf{A}\Delta t}{2}\right]=\begin{vmatrix}1 & \Delta t/2\\-\left(k\Delta t/2J\right) & 1-\left(b\Delta t/2J\right)\end{vmatrix} \tag{C.35}$$

Second, the inverted term:

$$\left[\mathbf{I}-\frac{\mathbf{A}\Delta t}{2}\right]=\begin{vmatrix}1 & 0\\0 & 1\end{vmatrix}-\frac{\Delta t}{2}\begin{vmatrix}0 & 1\\-\left(k/J\right) & -\left(b/J\right)\end{vmatrix} \tag{C.36}$$

$$\left[\mathbf{I}-\frac{\mathbf{A}\Delta t}{2}\right]=\begin{vmatrix}1 & 0\\0 & 1\end{vmatrix}-\begin{vmatrix}0 & \Delta t/2\\-\left(k\Delta t/2J\right) & -\left(b\Delta t/2J\right)\end{vmatrix} \tag{C.37}$$

$$\left[\mathbf{I}-\frac{\mathbf{A}\Delta t}{2}\right]=\begin{vmatrix}1 & -\Delta t/2\\\left(k\Delta t/2J\right) & 1+\left(b\Delta t/2J\right)\end{vmatrix} \tag{C.38}$$

The inverse of a matrix can be found using the following rule[67]:

$$\mathbf{M}_{2\times2}=\begin{vmatrix}a & b\\c & d\end{vmatrix}$$

$$\mathbf{M}_{2\times2}^{-1}=\frac{\begin{vmatrix}d & -b\\-c & a\end{vmatrix}}{\left(ad\right)-\left(bc\right)}$$

[67] Zill, p. 384

Therefore, the second term is:

$$\left[\mathbf{I} - \frac{\mathbf{A}\Delta t}{2}\right] = \frac{\begin{vmatrix} \left(1 + \dfrac{b\Delta t}{2J}\right) & \left(\dfrac{\Delta t}{2}\right) \\ \left(-\dfrac{k\Delta t}{2J}\right) & 1 \end{vmatrix}}{\left[\left(1 + \dfrac{b\Delta t}{2J}\right) - \left(-\dfrac{\Delta t}{2J}\right)\left(\dfrac{k\Delta t}{2J}\right)\right]} \tag{C.39}$$

$$\left[\mathbf{I} - \frac{\mathbf{A}\Delta t}{2}\right] = \frac{\begin{vmatrix} \left(1 + \dfrac{b\Delta t}{2J}\right) & \left(\dfrac{\Delta t}{2}\right) \\ \left(-\dfrac{k\Delta t}{2J}\right) & 1 \end{vmatrix}}{\left[1 + \dfrac{b\Delta t}{2J} + \dfrac{k\Delta t^2}{4J^2}\right]} \tag{C.40}$$

Recalling the terms defined in equations (C.16), (C.21), (C.23), (C.32), (C.35), and (C.40) yields the following:

$$\mathbf{X}_{t+\Delta t} = \frac{\begin{vmatrix} \left(1 + \dfrac{b\Delta t}{2J}\right) & \left(\dfrac{\Delta t}{2}\right) \\ \left(-\dfrac{k\Delta t}{2J}\right) & 1 \end{vmatrix}}{\left[1 + \dfrac{b\Delta t}{2J} + \dfrac{k\Delta t^2}{4J^2}\right]} \left(\begin{vmatrix} 1 & {\Delta t}/{2} \\ -\left({k\Delta t}/{2J}\right) & 1 - \left({b\Delta t}/{2J}\right) \end{vmatrix} \begin{vmatrix} \phi \\ \dot{\phi} \end{vmatrix}_t + \Delta t \begin{vmatrix} 0 \\ \dfrac{2\omega V_R}{R} \end{vmatrix}\right) \tag{C.41}$$

$$\mathbf{X}_{t+\Delta t} = \frac{\begin{vmatrix} \left(1 + \dfrac{b\Delta t}{2J}\right) & \left(\dfrac{\Delta t}{2}\right) \\ \left(-\dfrac{k\Delta t}{2J}\right) & 1 \end{vmatrix} \left(\begin{vmatrix} \phi_t + {\dot{\phi}_t \Delta t}/{2} \\ -\left({k\phi_t \Delta t}/{2J}\right) + \dot{\phi} - \left({b\dot{\phi}_t \Delta t}/{2J}\right) \end{vmatrix} + \begin{vmatrix} 0 \\ \dfrac{2\omega V_R \Delta t}{R} \end{vmatrix}\right)}{\left[1 + \dfrac{b\Delta t}{2J} + \dfrac{k\Delta t^2}{4J^2}\right]} \tag{C.42}$$

$$\mathbf{X}_{t+\Delta t} = \frac{\begin{vmatrix} \left(1 + \dfrac{b\Delta t}{2J}\right) & \left(\dfrac{\Delta t}{2}\right) \\ \left(-\dfrac{k\Delta t}{2J}\right) & 1 \end{vmatrix} \begin{vmatrix} \phi_t + \dfrac{\dot{\phi}_t \Delta t}{2} \\ -\left(\dfrac{k\phi_t \Delta t}{2J}\right) + \dot{\phi} - \left(\dfrac{b\dot{\phi}_t \Delta t}{2J}\right) + \left(\dfrac{2\omega V_R \Delta t}{R}\right) \end{vmatrix}}{\left[1 + \dfrac{b\Delta t}{2J} + \dfrac{k\Delta t^2}{4J^2}\right]} \tag{C.43}$$

113

$$\left.\begin{vmatrix}\phi\\\dot{\phi}\end{vmatrix}\right|_{t+\Delta t} = \frac{\begin{vmatrix}\left(1+\dfrac{b\Delta t}{2J}\right)\left(\phi_t+\dfrac{\dot{\phi}_t\Delta t}{2}\right)+\left(-\dfrac{k\phi_t\Delta t^2}{4J}+\dfrac{\dot{\phi}\Delta t}{2}-\dfrac{b\dot{\phi}_t\Delta t^2}{4J}+\dfrac{2\omega V_R\Delta t^2}{2R}\right)\\[4mm]\left(-\dfrac{k\Delta t}{2J}\right)\left(\phi_t+\dfrac{\dot{\phi}_t\Delta t}{2}\right)+\left(-\dfrac{k\phi_t\Delta t}{2J}+\dot{\phi}-\dfrac{b\dot{\phi}_t\Delta t}{2J}+\dfrac{2\omega V_R\Delta t}{R}\right)\end{vmatrix}}{\left[1+\dfrac{b\Delta t}{2J}+\dfrac{k\Delta t^2}{4J^2}\right]} \quad \text{(C.44)}$$

The simultaneous solution of $\phi_{t+\Delta t}$ and $\dot{\phi}_{t+\Delta t}$ yields the final form of each equation.

$$\phi_{t+\Delta t}=\frac{\left(1+\dfrac{b\Delta t}{2J}\right)\left(\phi_t+\dfrac{\dot{\phi}_t\Delta t}{2}\right)+\left(-\dfrac{k\phi_t\Delta t^2}{4J}+\dfrac{\dot{\phi}\Delta t}{2}-\dfrac{b\dot{\phi}_t\Delta t^2}{4J}+\dfrac{2\omega V_R\Delta t^2}{2R}\right)}{1+\dfrac{b\Delta t}{2J}+\dfrac{k\Delta t^2}{4J^2}} \quad \text{(C.45)}$$

$$\dot{\phi}_{t+\Delta t}=\frac{\left(-\dfrac{k\Delta t}{2J}\right)\left(\phi_t+\dfrac{\dot{\phi}_t\Delta t}{2}\right)+\left(-\dfrac{k\phi_t\Delta t}{2J}+\dot{\phi}-\dfrac{b\dot{\phi}_t\Delta t}{2J}+\dfrac{2\omega V_R\Delta t}{R}\right)}{1+\dfrac{b\Delta t}{2J}+\dfrac{k\Delta t^2}{4J^2}} \quad \text{(C.46)}$$

6.   Analytical Check Case

An analytical check case was performed using *Mathematica* version 4.[68]   The numerical results of the *Mathematica* model and the state-space model (Equations (C.45) and (C.46)) were compared and found to be equivalent.

---

[68] Stephen Wolfram, Mathematica, CD-ROM Ver. 4, Champaign IL: Wolfram Media Inc., 1999

D. APPENDIX D

1. Supporting Subroutines

Equation Section (Next)Several LabView Programs were written to simplify the code used in the main computer models. The details behind each supporting sub-routine are listed in the following sections.

2. Unit Conversion Subroutines

The natural unit for angular position is radians. It is difficult to visualize the 6.283 radians that make up a complete circle. Degrees, Hertz, and RPMs however, are much easier for the user to conceptualize and communicate to a target audience. Therefore, an automated means of performing the repetitious conversion process from a human measure (degrees) to a natural measure (radians) is needed.

Analytical Term	Meaning	Units
b	Torque per unit of relative angular velocity[69]	1/s
F_h	Force on the head	N
$\vec{i}_{R,v,k}$	Centrifuge Radial, Angular, and Axial Axes	Unitless
J_h	Mass Moment of Inertia of the head	kg·m²
k	Torque per unit of relative angular displacement	1/s
R	Linear Position	M
V	Linear Velocity	m/s
θ	Angular Position	rad
τ_h	Torque on the head	N·m
ϕ	Cupula Angular Position	rad
$\dot{\phi}$	Cupula Angular Velocity	rad/s
$\ddot{\psi}$	Head Angular Acceleration	rad
ω	Centrifuge Angular Velocity	rad/s

Table 17: Terms Used in the Unit Conversion Subroutines

---

[69] Milsum, p. 187
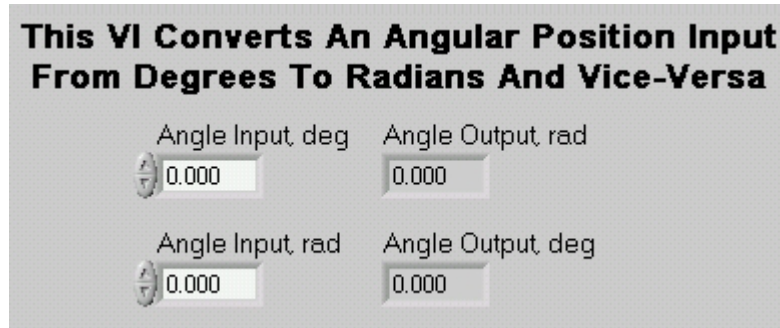
a.   *Degrees to Radians Converter*

Figure 63: Degrees to Radians Converter Front Panel

The front panel of the Degrees to Radians Converter, shown in Figure 24, is not designed for direct user manipulation.   Rather, this VI is designed to be a subordinate VI invoked whenever a routine conversion between degrees and radians is required. The Angle Input Controls, are linked from an outside source. The necessary conversion computations are performed with the results passed to the Angle Output Indicators.
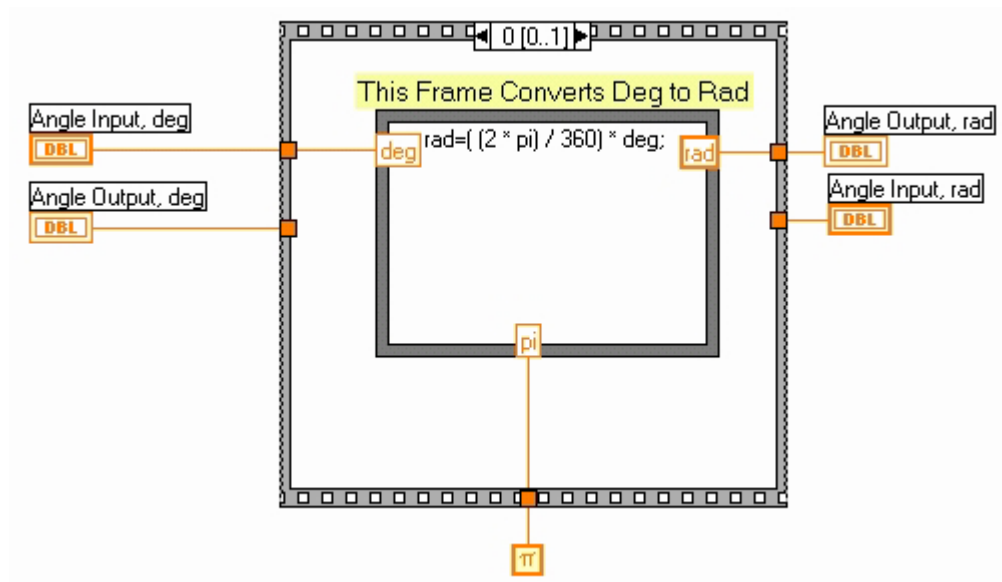
Figure 64: Line Diagram of the Process to Convert Degrees to Radians

Equation (D.1) was used to perform the calculation shown in Figure 64.[70]

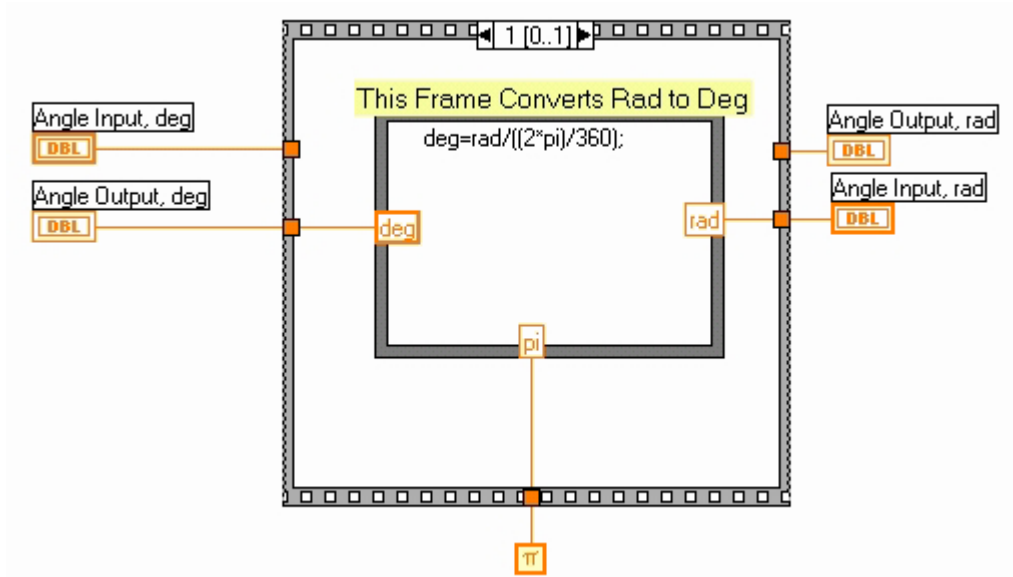$$\theta_{radians} = 2\pi \frac{\theta_{degrees}}{360} \qquad (D.1)$$

Figure 65: Line Diagram of the Process to Convert Radians to Degrees

Equation (D.1) was solved for degrees resulting in equation   which was used to perform the calculation shown in Figure 65.[71]

$$\frac{360}{2\pi}\theta_{radians} = \theta_{degrees} \qquad (D.2)$$

b.   *Frequency to Omega 2-Way Converter*

The front panel of the Frequency to Omega Converter, shown in Figure 66, is not designed for direct user manipulation. Rather, this VI is designed to be a subordinate VI invoked whenever a routine conversion between hertz and radians per second is required. The Angular Velocity Input Controls, are linked from an outside source. The necessary conversion computations are performed with the results passed to the Angular Velocity Output Indicators.
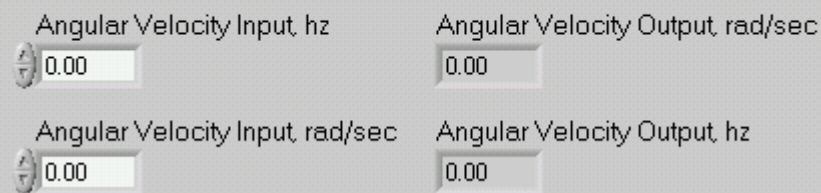
---

[70] Beyer, p. 152

[71] Beyer, p. 152

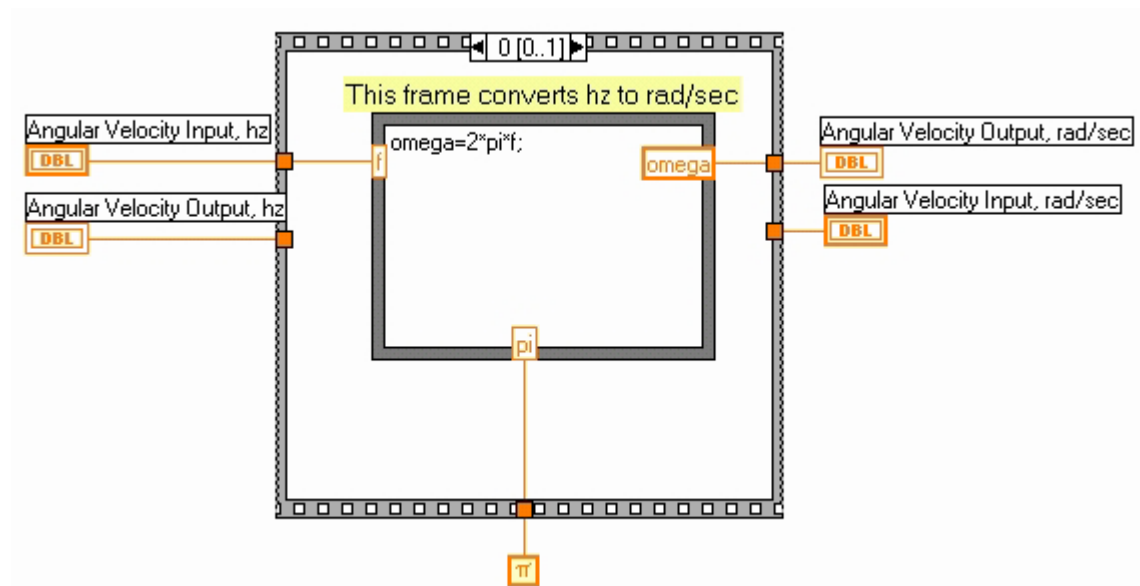**Figure 66: Frequency to Omega Converter Front Panel**

Figure 67: Line Diagram of Process to Convert Hertz to Radians Per Second

The formula used in Figure 67, Equation (D.3), is derived from the fact that there are 2π radians in a complete circle[72], and one hertz represents one revolution per second.

$$\omega = 2\pi f \qquad\qquad (D.3)$$

---

[72] Beyer, p. 152

Solving equation (D.3) for *f* yields equation   which was used in the computation shown in Figure 68.
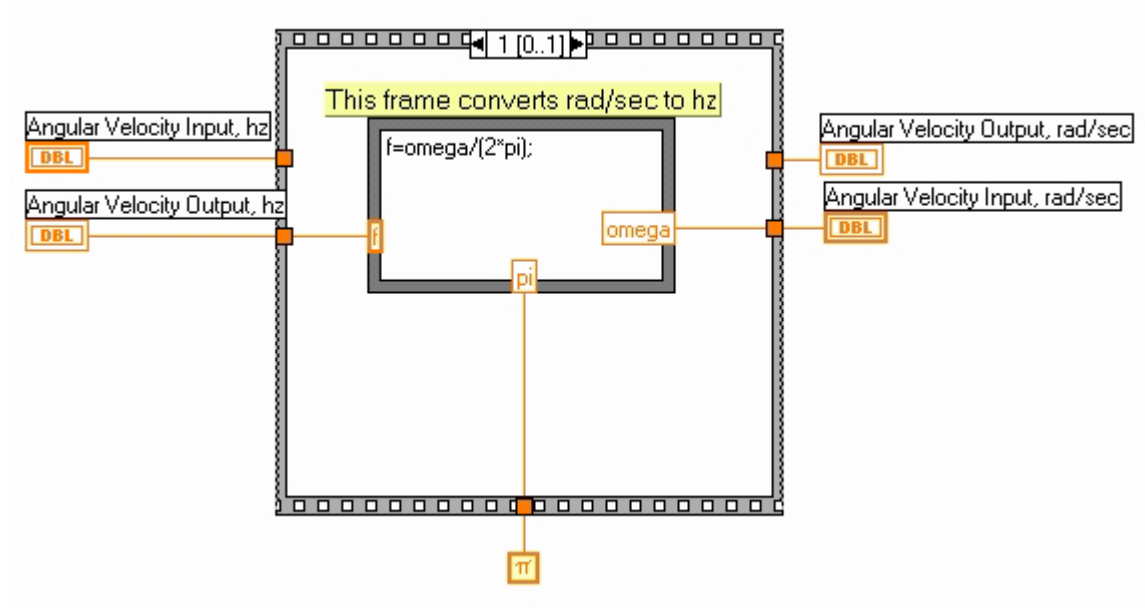
$$f = \frac{\omega}{2\pi} \tag{D.4}$$

Figure 68: Line Diagram of the Process to Convert Radians Per Second to Hertz

3.   Moment of Inertia Subroutines

Modeling the extrernal dynamics of a centrifuge required determining its mass and mass moment inertia.

As shown in Figure 69, the Annular Centrifuge modeled in this thesis consists of four main geometric components. A hollow-cylinder, or drum, is used to provide the floor the centrifuge's occupant would perceive. The drum is covered on each side by a pair of end-caps, or discs, that serve as walls for the astronaut. The centrifuge is then attached to its prime mover by a shaft, a long thin rod, which transmits the rotational force of the motor to the centrifuge. The sum of the masses and mass moment of inertias of each shape make up the total for the centrifuge.

Analytical Term	Meaning	Units
J_n	Mass Moment of Inertia of n-shape	kg·m²
l	Shaft Length	m
m	Mass	kg
r_{inner}	Centrifuge Inner Radius	m
r_{outer}	Centrifuge Outer Radius	m
r_{shaft}	Shaft Radius	m
t	End-cap (Disc) Thickness	m
V_n	Volume of n-shape	m³
π	Circular Constant, 3.1415…	Unitless
ρ	Material Density	kg/m³

Table 18: Terms Used in the Mass Moment of Inertia Subroutines
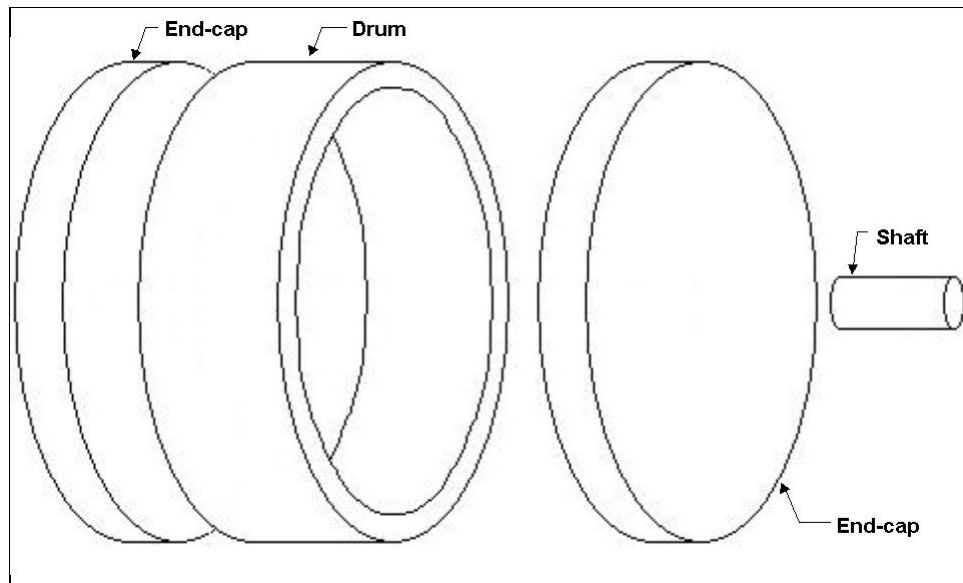
Figure 69: Geometric Decomposition of an Annular Centrifuge

a.   *Disc Mass Moment of Inertia*

This VI computes the mass and mass moment of inertia of a disc that rotates like a wheel.

Radius, m
0.00

Mass, kg
0.00

Thickness, m
0.00

Mass Moment of Inertia, kg m²
0.00
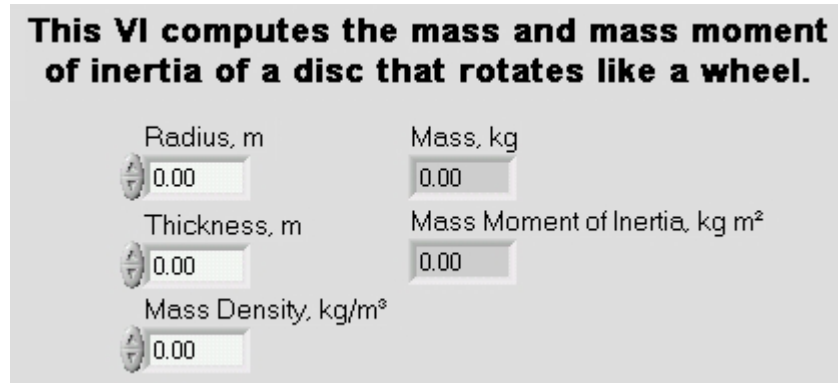
Mass Density, kg/m³
0.00

Figure 70: Disc Mass Moment of Inertia Front Panel

The front panel of the Disc Moment Of Inertia VI, shown in Figure 24, is not designed for direct user manipulation. Rather, this VI is designed to be a subordinate VI invoked whenever the mass and mass moment of inertia of a disc are required. The input controls, Radius, Thickness, and Mass Density, are linked from an outside source. The necessary computations are performed with the results passed to the mass and mass moment of inertia output indicators.

The computation used to determine mass of a disc shown in Figure 71 can be determined by multiplying its mass density (ρ) by its volume (V) as shown in Equation (D.5).[73]

$$m = \rho V_{disc} = \rho\left(\pi r^2 t\right) \tag{D.5}$$

The mass moment of inertia of a disc rotating like a wheel can then be computed, as shown in Figure 71, by using Equation (D.6).[74]

$$J_{disc} = \frac{1}{2}mr^2 \tag{D.6}$$

---

[73] Beyer, p. 129

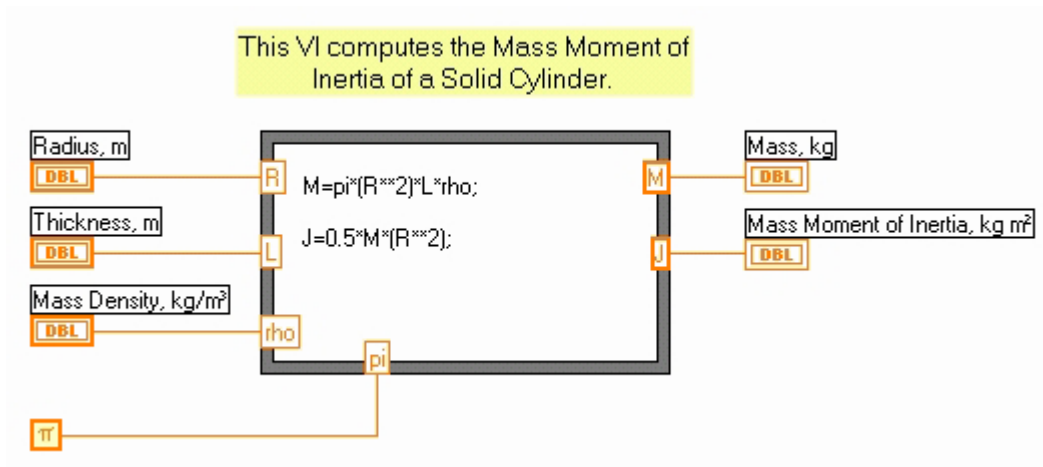[74] Meriam and Kraige, <u>Dynamics</u>, p. 630

Figure 71: Line Diagram of the Process to Calculate Disc Mass Moment of Inertia

b.   *Hollow-Cylinder Mass Moment of Inertia*

The front panel of the Hollow-Cylinder Moment Of Inertia VI, shown in Figure 72, is not designed for direct user manipulation. Rather, this VI is designed to be a subordinate VI invoked whenever the mass and mass moment of inertia of a hollow-cylinder are required. The input controls, Outer Radius, Inner Radius, Drum Length, and Mass Density, are linked from an outside source. The necessary computations are performed with the results passed to the mass and mass moment of inertia output indicators.

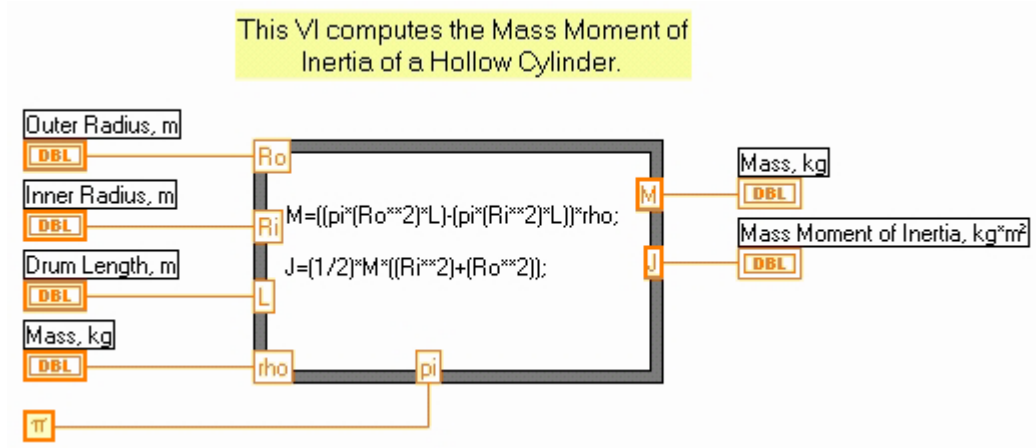**Figure 72: Hollow-Cylinder Mass Moment of Inertia Front Panel**

Figure 73: Line Diagram of the Process to Calculate Hollow-Cylinder Mass Moment of Inertia

The computation used to determine mass of a hollow cylinder in Figure 75 can be determined by multiplying ρ by V_{rod} as shown in Equation (D.7).[75] In this case, two volumes must be computed. The first volume is that of the overall cylinder from which is subtracted the volume of the hollow part of the cylinder.[76]

$$m_{drum} = \rho V_{drum} = \rho \left(\pi r_o^2 l - \pi r_i^2 l \right) \qquad (D.7)$$

The mass moment of inertia of a hollow cylinder (J_{drum}) is found in the same manner as its volume. Equation (D.8) is a modified form of the equation for Cylinder,[77] in this case the mass moment of inertia of the hollow interior has been subtrated.[78]

$$J_{drum} = \frac{1}{2} m \left(r_i^2 + r_o^2 \right) \qquad (D.8)$$

c.   Slender-Rod Mass Mass Moment of Inertia

The front panel of the Rod Moment Of Inertia VI, shown in Figure 74, is not designed for direct user manipulation. Rather, this VI is designed to be a subordinate

[75] Beyer, p. 129

[76] Meriam and Kraige, <u>Dynamics</u>, p. 593

[77] Meriam and Kraige, <u>Dynamics</u>, p. 630

[78] Meriam and Kraige, <u>Dynamics</u>, p. 593

123

VI invoked whenever the mass and mass moment of inertia of a rod are required. The input controls, Radius, Length, and Mass Density, are linked from an outside source. The necessary computations are performed with the results passed to the mass and mass moment of inertia output indicators.
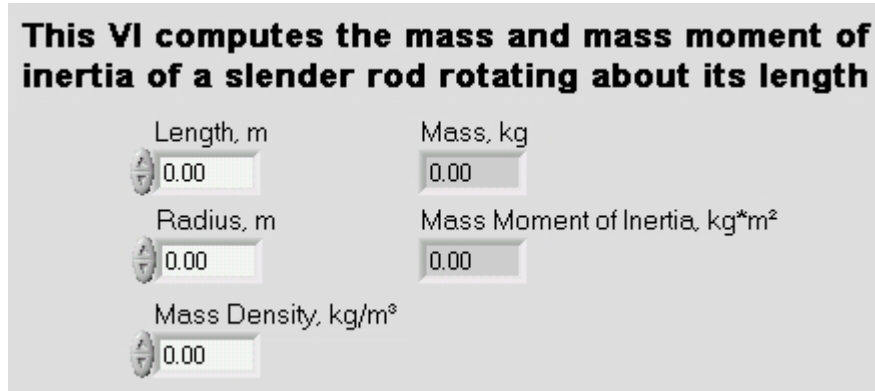

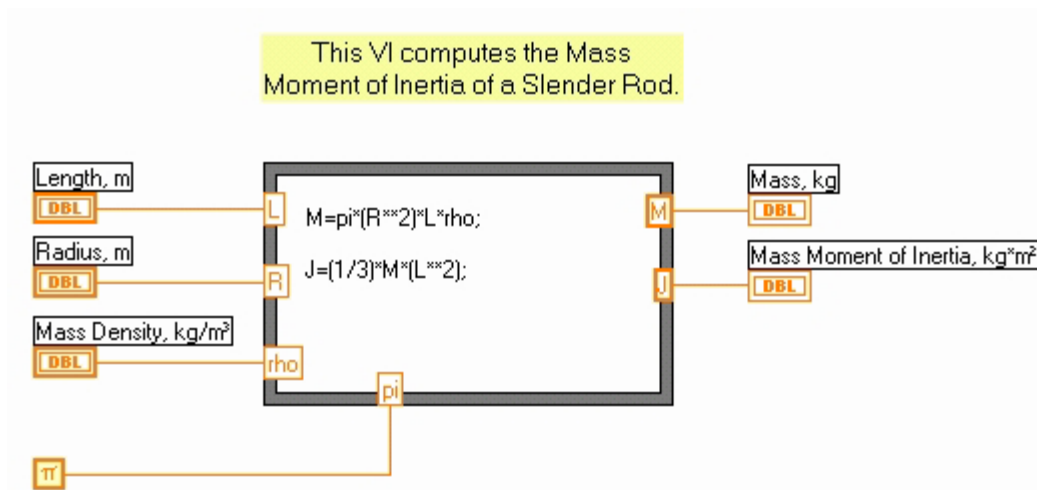**Figure 74: Slender-Rod Mass Moment of Inertia Front Panel**

Figure 75: Line Diagram of the Process to Calculate Slender-Rod Mass Moment of Inertia

The computation in Figure 75 used to determine mass of a slender rod can be determined by multiplying ρ by V_{rod} as shown in Equation (D.9).[79]

$$m_{rod} = \rho V_{rod} = \rho \pi r^2 l \qquad\qquad (D.9)$$

---

[79] Beyer, p. 129

The mass moment of inertia of a slender rod (J_{rod}) is determined using Equation (D.10)[80].

$$J_{rod} = \frac{1}{3}ml^2 \qquad \text{(D.10)}$$

d. *Centrifuge Total Mass Moment of Inertia*

The front panel of the Centrifuge Total Moment Of Inertia VI, shown in Figure 76, is not designed for direct user manipulation. Rather, this VI is designed to be a subordinate VI invoked whenever the total mass and mass moment of inertia of a cylindrical centrifuge is required. The input control cluster, Centrifuge Dimensions, is linked from an outside source. The necessary computations are performed within subordinate VIs with the sum of their results computed and passed to the mass and mass moment of inertia output indicators.
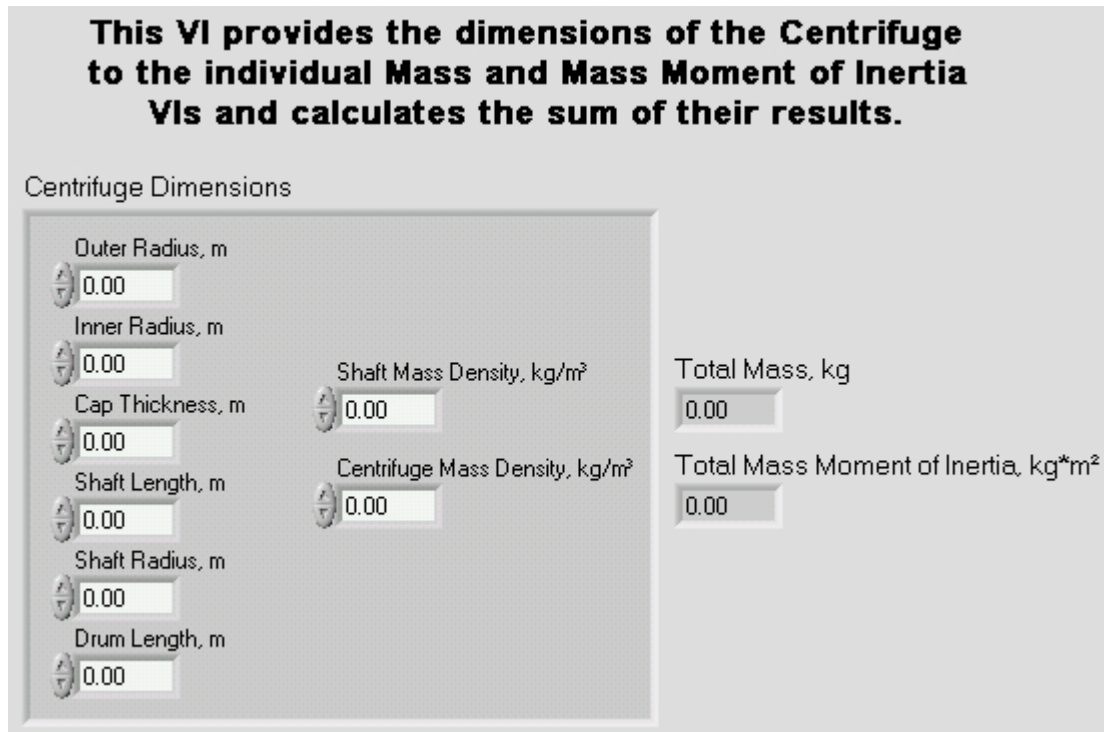

Figure 76: Centrifuge Total Mass Moment of Inertia Front Panel

---

[80] Meriam and Kraige, <u>Dynamics</u>, p. 631

The formulae used to compute the some of the results of the subordinate VIs, as shown in Figure 77 are imbedded into the wiring diagram. The equations upon which those computations were based are:[81]

$$J_{centrifuge} = \sum J_{components} = 2(J_{disc}) + J_{drum} + J_{rod} \tag{D.11}$$

By extension, the mass of the separate components is also additive:

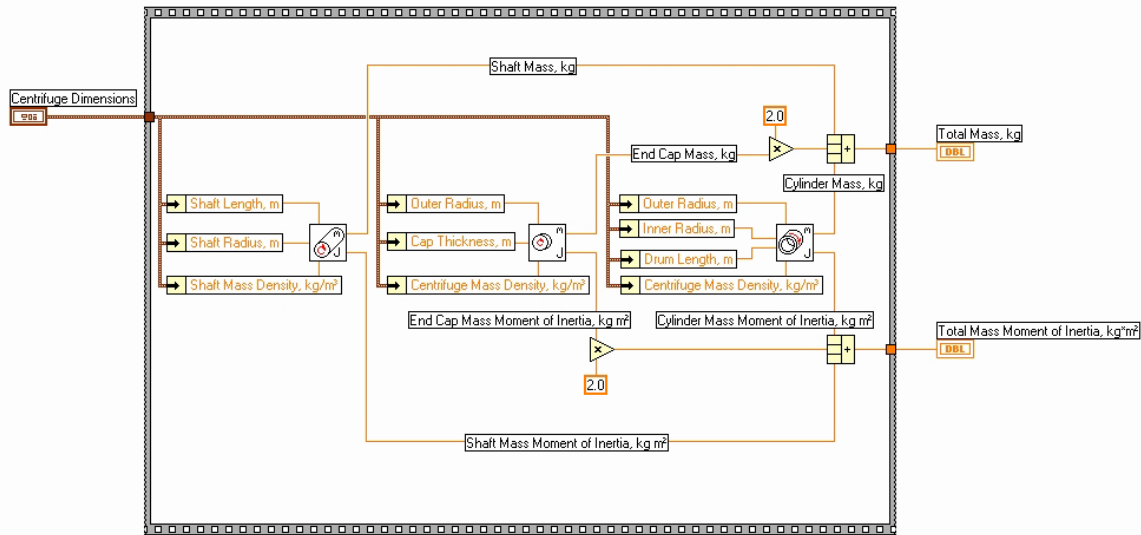$$m_{centrifuge} = \sum m_{components} = 2(m_{disc}) + m_{drum} + m_{rod} \tag{D.12}$$

Figure 77: Line Diagram of the Process To Calculate Total Mass Moment of Inertia

---

[81] Meriam and Kraige, <u>Dynamics</u>, p. 593

INITIAL DISTRIBUTION LIST

1.   Defense Technical Information Center
        Ft. Belvoir, VA

2.   Dudley Knox Library
        Naval Postgraduate School
        Monterey, CA

3.   Dr. Stephen A. Whitmore, PhD
        NASA Dryden Flight Research Center
        Edwards, CA

4.   CDR Percival McCormack USN (Ret), MD, PhD, ScD
        The University of Illinois at Chicago
        Department of Bioengineering (M/C 063)
        Science and Engineering Offices
        Chicago, IL

5.   Dr. Orlando Santos, PhD
        NASA Ames Research Center
        Moffett Field, CA

6.   Dr. Sherif Michael, PhD
        Associate Professor
        Department of Electrical and Computer Engineering (Code: EC/Mi)
        Naval Postgraduate School
        Monterey, CA

7.   Dr. Alan A. Ross, PhD
        Navy TENCAP Chair
        Naval Postgraduate School
        Space Systems Academic Group (Code: SP/RA)
        Monterey, CA

THIS PAGE INTENTIONALLY LEFT BLANK